

rajesh kumar

Experimental Investigation and Thermal Modeling of PCM based Latent Heat Thermal Energy Storage Syst

 Delhi Technological University

Document Details

Submission ID

trn:oid:::27535:105872565

Submission Date

Jul 26, 2025, 12:35 PM GMT+5:30

Download Date

Jul 26, 2025, 12:46 PM GMT+5:30

File Name

final Thesis jayesh 17th july 2025.pdf

File Size

4.4 MB

117 Pages

30,833 Words

167,205 Characters





10% Overall Similarity

The combined total of all matches, including overlapping sources, for each database.




Filtered from the Report

- Bibliography
- Quoted Text
- Cited Text
- Small Matches (less than 8 words)

Match Groups

-  **291** Not Cited or Quoted 10%
Matches with neither in-text citation nor quotation marks
-  **0** Missing Quotations 0%
Matches that are still very similar to source material
-  **0** Missing Citation 0%
Matches that have quotation marks, but no in-text citation
-  **0** Cited and Quoted 0%
Matches with in-text citation present, but no quotation marks

Top Sources

- 5%  Internet sources
- 8%  Publications
- 5%  Submitted works (Student Papers)

Integrity Flags

0 Integrity Flags for Review

No suspicious text manipulations found.

Our system's algorithms look deeply at a document for any inconsistencies that would set it apart from a normal submission. If we notice something strange, we flag it for you to review.

A Flag is not necessarily an indicator of a problem. However, we'd recommend you focus your attention there for further review.

Match Groups

- 291** Not Cited or Quoted 10%
Matches with neither in-text citation nor quotation marks
- 0** Missing Quotations 0%
Matches that are still very similar to source material
- 0** Missing Citation 0%
Matches that have quotation marks, but no in-text citation
- 0** Cited and Quoted 0%
Matches with in-text citation present, but no quotation marks

Top Sources

- 5% Internet sources
- 8% Publications
- 5% Submitted works (Student Papers)

Top Sources

The sources with the highest number of matches within the submission. Overlapping sources will not be displayed.

- 1

Publication

Piyush Rawat, Ashwni, Ahmad Faizan Sherwani. "A numerical study on the impac... <1%
- 2

Internet

scholarshare.temple.edu <1%
- 3

Publication

"Recent Advances in Mechanical Engineering", Springer Science and Business Me... <1%
- 4

Internet

nrl.northumbria.ac.uk <1%
- 5

Internet

www.researchgate.net <1%
- 6

Publication

Hameed B. Mahood, Mustafa S. Mahdi, Alireza Abbassi Monjezi, Anees A. Khadom... <1%
- 7

Internet

link.springer.com <1%
- 8

Publication

Lecture Notes in Energy, 2014. <1%
- 9

Internet

eprints.utas.edu.au <1%
- 10

Internet

acikerisim.atlas.edu.tr <1%

11	Internet	spectrum.library.concordia.ca	<1%
12	Publication	Jayesh Kumar, Pushpendra Singh, Rajesh Kumar. "Enhancement of the part-load t...	<1%
13	Internet	etheses.whiterose.ac.uk	<1%
14	Publication	ELSaeed Saad ELSihy, Haozhe Xie, Haitao Lin, Xiaoze Du, Zuyuan Wang. "Combine...	<1%
15	Publication	Lokesh Kalapala, Jaya Krishna Devanuri. "Energy and exergy analyses of latent he...	<1%
16	Publication	Saleh Chebaane, Saeid Pour Nemat, Hayder I. Mohammed, Sana Ben Khalifa et al....	<1%
17	Submitted works	University Of Tasmania on 2023-10-14	<1%
18	Publication	Jayesh Kumar, Pushpendra Singh, Rajesh Kumar. "Performance enhancement of I...	<1%
19	Publication	Manal Hariss, Ayoub Gounni, Mustapha El Alami. "A practical guide on numerical ...	<1%
20	Internet	gyan.iitg.ernet.in	<1%
21	Publication	Reza Babaei, Ardalan Shafiei Ghazani. "Numerical investigation of melting proces...	<1%
22	Internet	www.mdpi.com	<1%
23	Publication	Nazila Parsa, Babak Kamkari, Hossein Abolghasemi. "Experimental study on the i...	<1%
24	Submitted works	Staffordshire University on 2024-01-04	<1%

25	Internet	pure-oai.bham.ac.uk	<1%
26	Publication	Sandip Khobragade, Jaya Krishna Devanuri. "Impact of inclination on the thermal...	<1%
27	Submitted works	Loughborough University on 2020-09-06	<1%
28	Publication	Teather, Kyle. "Experimental Investigation of the Phase Change Process within Ci...	<1%
29	Internet	dokumen.pub	<1%
30	Publication	Ali Hammoodi Mahdi, Munther Abdullah Mussa. "Comprehensive review of optim...	<1%
31	Submitted works	Anna University on 2025-02-28	<1%
32	Publication	Shamseldin A. Mohamed, Fahad A. Al-Sulaiman, Nasiru I. Ibrahim, Md. Hasan Zah...	<1%
33	Publication	Vikas, Ankit Yadav, Sushant Samir. "Melting dynamics analysis of a multi-tube lat...	<1%
34	Submitted works	University of Pretoria on 2024-06-06	<1%
35	Publication	Xiaolong Li, Guolong Cui, Lingjiang Kong, Zhi Sun. "Radar High-Speed Target Dete...	<1%
36	Submitted works	University of Birmingham on 2025-05-02	<1%
37	Internet	atrium.lib.uoguelph.ca	<1%
38	Internet	gyan.iitg.ac.in	<1%

39	Submitted works	Khalifa University of Science Technology and Research on 2017-09-08	<1%
40	Submitted works	University Of Tasmania on 2021-10-23	<1%
41	Publication	Banumathi Munuswamy Swami Punniakodi, Ramalingam Senthil. "A review on co...	<1%
42	Submitted works	Anna University on 2025-05-29	<1%
43	Submitted works	City University on 2023-12-25	<1%
44	Submitted works	College of Engineering, Pune on 2022-08-10	<1%
45	Publication	Kaibao Liu, Chenhui Wu, Haolin Gan, Changhui Liu, Jiateng Zhao. "Latent heat the...	<1%
46	Publication	Lehar Asip Khan, Muhammad Mahabat Khan, Hassan Farooq Ahmed, Muhamma...	<1%
47	Publication	S. H. Chan. "Transport Phenomena In Combustion, Volume 1 - Proceedings of the ...	<1%
48	Publication	Yang Hu, Kun Zhang, Junqing Wang, Kewei Song, Liangbi Wang, Guangtian Shi. "T...	<1%
49	Submitted works	Coventry University on 2013-12-19	<1%
50	Submitted works	Glasgow Caledonian University on 2024-04-24	<1%
51	Publication	Ismail, Abdulmalik Bamidele. "Low-Cost Cenosphere Microencapsulation Technol...	<1%
52	Submitted works	City University on 2023-08-29	<1%

53	Publication	Kulkarni, Rituja. "Parametric Study of a Thermal Energy Storage Module Coupled ..."	<1%
54	Submitted works	University of Ulster on 2022-06-17	<1%
55	Internet	ore.exeter.ac.uk	<1%
56	Publication	Shubham Jain, K. Ravi Kumar, Dibakar Rakshit, B. Premachandran, K.S. Reddy. "St..."	<1%
57	Submitted works	University Of Tasmania on 2023-05-24	<1%
58	Submitted works	University of Birmingham on 2024-07-29	<1%
59	Publication	Zhi Li, Yiji Lu, Rui Huang, Jinwei Chang, Xiaonan Yu, Ruicheng Jiang, Xiaoli Yu, Ant...	<1%
60	Submitted works	Loughborough University on 2020-05-10	<1%
61	Submitted works	University of Sannio on 2022-06-27	<1%
62	Submitted works	National Institute Of Technology, Tiruchirappalli on 2018-05-01	<1%
63	Submitted works	University of Hull on 2018-08-11	<1%
64	Submitted works	University of Technology on 2024-05-22	<1%
65	Submitted works	The University of Manchester on 2025-05-02	<1%
66	Publication	Mohamed A. Alnakeeb, Mohamed A. Abdel Salam, Mohamed A. Hassab. "Numeric..."	<1%

67	Internet	repositories.nust.edu.pk	<1%
68	Publication	Berihu Gebreyohannes Abreha, Pinakeswar Mahanta, Gaurav Trivedi. "Thermal p...	<1%
69	Submitted works	Indian Institute of Technology Patna on 2021-06-16	<1%
70	Publication	Lascano, Armando Enrique Fontalvo. "Integration of Accurate Thermo-Mechanica...	<1%
71	Publication	Mashhour A. Alazwari, Mohammed Algarni, Mohammad Reza Safaei. "Effects of v...	<1%
72	Publication	Mohsen Izadi, Ioan Pop, Sabir Ali Shehzad, Faris Alqurashi, Mohamed H. Mohame...	<1%
73	Submitted works	University of Sheffield on 2019-09-25	<1%
74	Publication	Abdul Rahim, Wan Khairul Khairul. "Numerical Analysis of Phase Change Material...	<1%
75	Submitted works	Coventry University on 2015-08-27	<1%
76	Submitted works	Coventry University on 2020-03-17	<1%
77	Publication	International Journal of Numerical Methods for Heat & Fluid Flow, Volume 10, Iss...	<1%
78	Publication	Mahboobe Mahdavi, Saeed Tiari, Vivek Pawar. "A numerical study on the combine...	<1%
79	Publication	Maziar Dehghan, Mahsa Ghasemizadeh, Saeed Rahgozar, Abolfazl Pourrajabian, ...	<1%
80	Publication	Muhammad Shahid Shafiq, Muhammad Mahabat Khan, Muhammad Irfan. "Perfo...	<1%

81	Publication	Mustafa S. Mahdi, Hameed B. Mahood, Ahmed A. Alammam, Anees A. Khadom. "N...	<1%
82	Publication	Nabeel S. Dhaidan, J. M. Khodadadi. "Improved performance of latent heat energ...	<1%
83	Publication	Saber Abdollahzadeh Bonab, Ardalan Shafiei Ghazani. "Accelerating heat storage ...	<1%
84	Publication	Teng Xiong, Long Zheng, Kwok Wei Shah. "Nano-enhanced phase change materia...	<1%
85	Publication	Thiago Torres Martins Rocha, Paulo Vinicius Trevizoli, Raphael Nunes de Oliveira. ...	<1%
86	Publication	Vikas ., Ankit Yadav, Sushant Samir, Müslüm Arıcı. "A comprehensive study on me...	<1%
87	Internet	www.dspace.dtu.ac.in:8080	<1%
88	Publication	"Advances in Mechanical and Materials Technology", Springer Science and Busine...	<1%
89	Publication	Abdulhammed K. Hamzat, Adewale Hamed Pasanaje, Mayowa I. Omisanya, Ah...	<1%
90	Submitted works	Anna University on 2024-03-22	<1%
91	Publication	Anto Zacharias, Rajesh Baby, Hanna J. Maria, Sabu Thomas. "Preparation, charact...	<1%
92	Publication	Burak İzgi, Hüseyin Zahit Demirağ. "Multi-objective optimization of fin shape in a ...	<1%
93	Submitted works	CSU, San Diego State University on 2021-12-28	<1%
94	Publication	Faisal Hassan, Furqan Jamil, Abid Hussain, Hafiz Muhammad Ali et al. "Recent adv...	<1%

95	Publication	Farhan Lafta Rashid, Alireza Rahbari, Raed Khalid Ibrahim, Pouyan Talebizadehs...	<1%
96	Publication	Ghulam Rasool, Ali B.M. Ali, Yahia Said, Mohammed Jameel et al. "Transforming t...	<1%
97	Publication	Hamza Faraji, Ayman Benkaddour, Kenza Oudaoui, Mustapha El Alami, Mustapha...	<1%
98	Publication	Hua-Yang Liu, Li Zhang, Chun-Mei Wu, You-Rong Li. "Comprehensive investigatio...	<1%
99	Submitted works	IIT Delhi on 2022-11-06	<1%
100	Submitted works	Indian Institute of Technology, Bombay on 2016-05-22	<1%
101	Publication	Ioan Sarbu. "Advances in Building Services Engineering", Springer Science and Bu...	<1%
102	Publication	Lanka Sandeep Raj, Kongari Yashwanth, Chinnam Madan, Avula Anusha, Godha S...	<1%
103	Publication	Liu Yang, Jia-nan Huang, Fengjiao Zhou. "Thermophysical properties and applicati...	<1%
104	Submitted works	Loughborough University on 2020-03-17	<1%
105	Submitted works	Loughborough University on 2021-05-08	<1%
106	Publication	Mohamed A. Alnakeeb, Mohamed Shatarah, M.K. Hamza, M.A. Abdel Salam, H.M. ...	<1%
107	Publication	Mostafa Kamal Fahad, Salim Subah, Nowroze Farhan Ifraj, Sharzil Huda Tahsin, T...	<1%
108	Submitted works	National Institute of Technology, Silchar on 2024-01-12	<1%

109	Publication	Nosrati, Mehrdad. "Methods for the Next Generation of Contactless Doppler Rad...	<1%
110	Publication	Piyush Rawat, Ashwni Goyal, Ahmad Faizan Sherwani. "A comparative numerical ...	<1%
111	Submitted works	University Of Tasmania on 2015-06-01	<1%
112	Submitted works	University Of Tasmania on 2024-06-10	<1%
113	Submitted works	University of Anbar on 2023-05-23	<1%
114	Submitted works	University of Northumbria at Newcastle on 2022-02-09	<1%
115	Publication	Yongxue Zhang, Bohui Lu, Zixi Wang, Jianjun Zhu, Jinya Zhang, Cong Wang. "Expe...	<1%
116	Publication	Zeyu Wang, Yanhua Diao, Yaohua Zhao, Chuanqi Chen, Tengyue Wang, Lin Liang. ...	<1%
117	Publication	Zhenyu, Wang. "High-Performance Vanadium Redox Flow Battery for Large-Scale ...	<1%
118	Internet	coek.info	<1%
119	Internet	pmc.ncbi.nlm.nih.gov	<1%
120	Internet	tel.archives-ouvertes.fr	<1%
121	Internet	thesis.cust.edu.pk	<1%

Chapter 1

Introduction

1. Introduction

The escalating reliance on conventional energy sources has sparked significant concern due to their swift exhaustion and the environmental damage caused by rising CO₂ emissions. As a result, attention has shifted toward alternative renewable energy solutions such as solar, wind, tidal, and geothermal power [1]. These sustainable energy sources are expected to play a crucial role in meeting future global energy demands. Among them, solar energy holds immense promise for applications like water heating, space heating and cooling, cooking, and greenhouse temperature regulation. However, its intermittent availability poses challenges for efficient and economical usage. Similar difficulties exist in harnessing waste heat and recovering surplus thermal energy from industrial exhausts. To mitigate these issues, storing thermal energy has emerged as a highly viable strategy, offering a practical approach to energy conservation across both domestic and industrial sectors. In this context, thermal energy storage systems act as essential intermediaries, ensuring a balance between energy supply and demand. Moreover, they help improve the reliability and thermal performance of energy systems by capturing excess energy and releasing it when needed, thereby optimizing overall system efficiency.

1.1 Thermal energy storage

Generally, heat from a thermal source is transferred to a storage material, where it is converted into internal energy. This energy is then retained in the form of thermo-chemical energy, sensible heat, latent heat, or a hybrid of sensible and latent forms. Accordingly, thermal energy storage (TES) technologies are primarily classified into three major categories [2] :

Thermo-chemical thermal storage systems

Sensible heat storage systems

Latent heat or phase change material (PCM) storage systems

Among these, thermo-chemical storage involves the accumulation of thermal energy through reversible chemical reactions, enabling efficient energy retention and release during endothermic and exothermic processes [3]. It utilises endothermic and exothermic reactions to store and release energy efficiently. The process involves two key steps: during charging, heat energy breaks chemical bonds, creating separate products and storing energy in chemical form. When needed, the stored products recombine in an exothermic reaction, releasing the stored heat. This mechanism allows for energy storage over long periods without significant losses. In sensible heat storage (SHS) systems [4], thermal energy is accumulated by elevating the temperature of a storage medium, which may be a liquid or a solid. The energy retained relies on the medium's specific heat capacity, the amount of material used, and the temperature range over which heating or cooling occurs. During the phases of thermal accumulation and extraction, the thermal energy exchange is governed by changes in the medium's internal energy without any phase change. Among commonly used liquids, water is considered one of the most effective due to its low cost and relatively high specific heat capacity. However, for applications requiring functional temperature range exceeding 100°C, other fluids such as molten salts, thermal oils, and liquid metals are preferred [5]. In air-based heat-driven operations, materials like packed rock beds are widely adopted to facilitate effective heat retention and transfer.

1.1.1 Latent heat thermal energy storage systems

Latent heat thermal storage (LHTS) systems preserve heat primarily through phase change processes, where a material absorbs or releases energy during transitions between different physical states [6]. During the charging process, as the temperature of the PCM rises, it absorbs thermal energy and begins to melt, storing energy in the form of latent heat along with some sensible heat. Conversely, during cooling or discharging, the material solidifies, gradually releasing the absorbed latent energy back to the surrounding environment. These phase transitions may include solid–liquid, liquid–gas, solid–gas, or solid–solid transformations [3], depending on the application and material used. Among these, Thermal conversions from liquid to vapor and solid to vapor boast elevated phase change enthalpy but pose challenges due to significant

volume changes, making container design complex and impractical. While solid-solid phase change avoids container design issues, its economic feasibility suffers due to a smaller latent heat value. In contrast, the change of state from solid to liquid emerges as a more favourable option. In spite of its comparatively low latent heat than liquid-gas or solid-gas cases, the volume change during phase transition is minimal, not exceeding 10%, making it a practical and efficient choice [7].

The substance experiencing a phase change during the process of storing or releasing energy is known as a PCM. PCM stores heat by transitioning from a solid to a liquid phase and liberates this stored heat by reverting to the solid state (freezing). The specific term for the heat absorbed and stored per unit mass by the medium during the phase transition is referred to as latent heat. Across the three TES categories systems, LHTS is recognized as a highly efficient and attractive method for thermal energy management. This approach employs PCMs, which have the capacity to store 5 to 14 times more thermal energy compared to conventional sensible heat storage substances [3]. A key advantage of LHTS systems is their thermal retention capacity and release energy at nearly constant temperatures, aligning with the PCM's phase transition point. This feature allows for enhanced efficiency in both energy absorption and discharge processes. Its superiority lies in the superior energy storage per unit of space, leading to significant space savings. As a result, latent heat storage is an ideal choice in situations where space is limited or highly valued. Each LHTESS is composed of three fundamental elements at minimum:

1. A suitable PCM with a melting point within the target temperature span [3].
2. An efficient heat exchange surface to facilitate heat transfer [8].
3. A compatible container designed to securely hold the PCM without degradation or leakage [9].

To efficiently store energy with PCMs, the PCM must exhibit suitable thermophysical, chemical, and kinetic characteristics to perform effectively in TES systems [3] [10].

➤ **Thermal Properties:**

1. The PCM should melt within the acceptable temperature limits for its intended application and have a high latent heat of enthalpy per unit volume to minimise the amount of material needed for a given energy storage capacity [11].

2. It should also possess an elevated specific heat to increase its sensible heat capacity.
3. Both phases of the PCM should exhibit high thermal conductivity to reduce required temperature gradients during charging and discharging of TES.
4. Reversible phase change throughout multiple thermal cycles without significant degradation. Thermal reliability and stability are crucial factors to consider [12].

➤ **Physical Properties:**

1. The PCM should exhibit limited volumetric variation during the phase transition to facilitate simpler and more reliable heat exchanger design.
2. A higher density is desirable in the PCM to minimize the size of the thermal storage unit required for holding a specific amount of thermal energy
3. Congruent melting is preferred, where the liquid formed after melting has the same composition as the solid. Incongruent melting results in the formation of both a saturated hydrous phase coexisting with a solid phase, leading to settling of the solid phase at the bottom of the container caused by density gradients [13] [14]. Since the solid phase is unavailable throughout the container for recombination with the saturated solution during the reverse process of melting to form the original salt hydrate. This can hinder recombination during the reverse melting process. Methods to address this include stirring, encapsulating the PCM, adding thickening agents, using rolling cylinders, and adding extra water to supersaturated salt solutions [3] [14] [15]. Air-tight containers are essential for salt hydrate PCMs to prevent water loss through evaporation, which can significantly impact their performance [14].

➤ **Kinetic Properties:**

1. Supercooling: Supercooling occurs when the PCM solidifies below its intended melting temperature, typically by 10 to 20 °C, due to poor nucleation properties and slow crystallisation rates [13]. This can affect heat transfer rates from the TES system to the application, as temperature gradients decrease. Adding nucleating agents, using rough metallic heat exchange surfaces in contact with the PCM, and incorporating cold fingers can help reduce supercooling effects [3][14].

➤ **Chemical Properties:**

1. The phase change material should possess chemical stability and be safe to handle, meaning it must not be corrosive, toxic, flammable, or prone to explosion.

It is significant to recognize that no single material can meet all the desired characteristics and criteria of a TES system. Therefore, a balanced approach is necessary when selecting a candidate heat storage material.

1.1.2 Classification of the PCM

PCMs are largely organized into three essential categories: organic compounds, inorganic substances, and eutectic mixtures [16]. The subdivisions within these groups are illustrated in Fig.1.1.

➤ Organic PCM

Organic PCMs are compounds that contain carbon atoms within their molecular structure and are extensively utilized in TES applications due to their favourable thermal characteristics. These materials generally exhibit low thermal conductivity, typically ranging from 0.1 to 0.7 W/m·K, [13][17], which may limit their heat transfer rate. Despite this, they offer notable advantages such as freezing without significant supercooling or subcooling, making them highly stable during phase transitions. Organic PCMs are known for their ability to be incorporated directly into

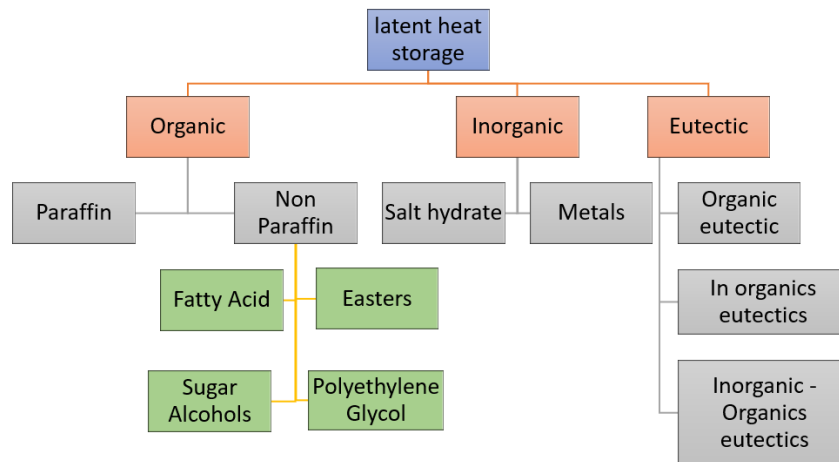


Fig. 1.1 Classification of PCM

thermal systems and possess low vapour pressure during the phase change process, which enhances their safety and operational stability. They melt congruently, meaning they maintain their chemical composition during melting and solidification cycles, and they possess self-nucleating properties, reducing the need for external nucleating

agents. Additionally, they demonstrate excellent compatibility with conventional construction materials, are chemically stable, non-reactive, and recyclable, making them environmentally friendly and sustainable for long-term use [14]. Organic PCMs are available across a wide temperature range and offer high fusion enthalpy with latent heat storage capacities ranging from 125 to 200 kJ/dm³, [14], making them effective for various thermal storage needs without risk of segregation or component separation. However, organic PCMs also present certain limitations. Due to their low solid-state thermal conductivity, heat transfer enhancement methods must be incorporated to boost the overall efficiency of the system. Some organic PCMs are insoluble in water and possess low phase change enthalpy compared to other PCM types. They tend to have low density, necessitating larger volumes for equivalent energy storage, and require large surface areas and high heat transfer rates during the freezing cycle to achieve effective thermal regulation. Their volumetric latent heat storage capacity is relatively low, and some types are flammable, although this risk can be mitigated through the use of proper containment and safety measures. Additionally, organic PCMs may be more expensive compared to other materials, and they exhibit high volumetric expansion during phase change, which must be considered in system design. Furthermore, they generally have low specific heat capacity, which limits their ability to store sensible heat.

➤ Paraffins as PCM

Paraffins are made up of long, straight-chain alkanes like CH₃–(CH₂)–CH₃. The fusion temperature and the related phase change enthalpy of paraffin are influenced by the length of its hydrocarbon chains [3][15]. Paraffins with melting points between 6 to 80 °C usually have 14-40 carbon atoms in their structure [14]. Main Challenges include poor thermal conductivity and moderate flammability [15]. These materials are commonly employed in cooling or low-heat systems because of their relatively modest phase change temperatures. However, they are cost-effective, non-corrosive, chemically inert, undergo minimal volume changes when melting, freeze without supercooling, and have low vapour pressure in their molten form [13]. Paraffins also exhibit congruent melting, good nucleating properties, and moderate latent heat of enthalpy [3][14].

➤ Non-paraffins as PCM

Non-paraffins include a variety of materials such as esters, fatty acids, alcohols, and glycols, all of which have diverse thermophysical properties. They are considered for energy storage systems but often face challenges such as flammability, corrosion and poor thermal conductivity [15]. Fatty acids, for example, can cause corrosion in storage system containers, but they possess superior heat absorption capacity during melting than paraffins and lower supercooling [18]. However, they are also more expensive [3]. Sugar alcohols like erythritol and xylitol can have high volumetric storage densities up to 450MJ/m³ [19], but they are not suitable for thermal energy storage due to issues like wide melting temperature ranges, high supercooling and high cost. Galactitol shows poor cycling stability, while D-mannitol reacts with oxygen in the atmosphere [12], reducing its storage capacity.

➤ Inorganic PCM

Inorganic PCMs are thermal storage substances that are composed primarily of metallic compounds, salts, or hydrated salts, which do not contain carbon in their molecular structure. They are broadly adopted in TES systems due to their high latent heat of fusion and improved thermal conduction in contrast to organic PCMs [20]. Inorganic PCMs generally exhibit higher energy storage densities and have the capability to operate at a broad range of temperatures, making them suitable for medium to high-temperature applications such as solar power systems, industrial heat recovery, and building energy management. A major benefit of inorganic phase change materials is their superior ability to conduct heat [6], which enables faster charging and discharging rates during the phase change process. Additionally, they typically have non-flammable properties and lower material costs, enhancing their economic feasibility for large-scale thermal storage systems. However, inorganic PCMs also face certain challenges, including the tendency to undergo phase segregation or supercooling during melting and solidification cycles, which can affect their long-term reliability. Some inorganic PCMs, such as salt hydrates, may also cause corrosion in storage containers due to their chemical reactivity, necessitating the use of protective coatings or compatible materials. Moreover, many inorganic PCMs exhibit volume

changes during phase transitions, which must be carefully managed in the design of storage systems. Despite these drawbacks, inorganic PCMs remain a strong candidate for thermal energy storage solutions, particularly where high thermal conductivity, low flammability, and cost-effectiveness are prioritized.

➤ Salt hydrate as PCM

The inorganic group encompasses salt hydrates and metallic materials. Inorganic PCMs, like salt hydrates of the general formula $AB \cdot nH_2O$ [3], form when water is added to an anhydrous salt at room temperature, causing the water molecules to become part of the salt's crystal structure. While transitioning from a solid form to a liquid form, the salt hydrate either loses some water molecules or becomes anhydrous. The bond strength of water molecules and salt decides the latent heat of phase change [13]. Popular salt hydrates studied include calcium chloride hexahydrate, magnesium chloride hexahydrate, sodium sulfate decahydrate, and sodium phosphate dodecahydrate [21]. Salt hydrates offer moderately higher thermal conductivity (0.4 and 0.7 W/mK) [17] compared to paraffins, are cost-effective, and generally safe. However, they may decompose, corrode container materials like Aluminum, stainless steel and copper [13] [22], and suffer from incongruent melting and segregation after repeated cycles [23][3]. Despite having higher volumetric thermal energy density than organic PCMs, salt hydrates also face the challenge of supercooling due to poor nucleating properties[3] during fusion.

➤ Metal as PCM

Metals and metal-based alloys are increasingly being explored as PCMs for LHTES, particularly under elevated temperature conditions. Pure metals such as aluminum (Al) and zinc (Zn) exhibit high melting points along with high energy storage density and high volumetric heat of fusion, making them attractive for thermal storage systems where compactness and high heat absorption are required. Additionally, molten metals such as lithium (Li) and sodium (Na) have shown superior thermal performance compared to conventional molten heat transfer salts, offering better heat storage and transfer characteristics. Research studies have demonstrated that metals like zinc and tin exhibit [16] excellent thermal behavior in high-temperature applications (up to

approximately 445°C), outperforming traditional molten salts in terms of thermal transport and storage efficiency. This category of PCMs also includes metals with low fusion temperatures and metallic eutectic alloys. Although these materials have not been widely adopted in PCM technologies, mainly due to their high density and associated weight penalties, they are considered promising candidates in systems where volume constraints are more critical than weight, as they offer very high heat of fusion per unit volume. A unique advantage of metallic PCMs is their high thermal conductivity, eliminating the need for additional heat transfer augmentation methods such as fins or fillers, which are often necessary in organic or inorganic salt-based PCMs. However, their use also introduces specific engineering challenges, such as handling, containment, and material compatibility at high temperatures. Metallic PCMs are characterized by several unique properties, such as: (i) a comparatively low latent heat per unit mass but a high energy retention per unit volume, (ii) excellent thermal conductivity, enabling rapid charging and discharging, (iii) low specific heat capacity, and (iv) subdued vapor pressure characteristics, which contributes to safer high-temperature operations. These features make metals and metal alloys potential candidates for specialized thermal storage applications, especially in scenarios requiring compact storage, high heat transfer rates, and reliable high-temperature performance.

➤ Eutectics PCM

It is defined as a mixture of two or more components which usually do not form a new chemical compound by interaction, but maintain consistent phase transition temperature that is lower than the melting point of either of the components [24]. It is usually done to diminish the temperature required for melting of the material to achieve the operating range of temp of application temperature or enhance the desirable properties of PCM [3]. For example, Magnesium chloride hexahydrate ($\text{MgCl}_2 \cdot 6\text{H}_2\text{O}$) has a melting temp 117°C with an enthalpy of 150 kJ/kg, which is not suitable for a low-temperature water heating system [25]. However, $\text{NH}_4\text{Al}(\text{SO}_4)_2 \cdot 12\text{H}_2\text{O}$ has high supercooling with the good latent heat of enthalpy (260 kJ/kg) with melting temp 93 °C [25]. The addition of 30% mass fraction of $\text{MgCl}_2 \cdot 6\text{H}_2\text{O}$ in the eutectic mixture $\text{MgCl}_2 \cdot 6\text{H}_2\text{O} - \text{NH}_4\text{Al}(\text{SO}_4)_2 \cdot 12\text{H}_2\text{O}$ reduces the

melting temp up to 64.15 °C with a very low supercooling degree (0.74 °C)[25]. Similarly, $\text{MgCl}_2 \cdot 6\text{H}_2\text{O}$ (30% mass ratio) is added to the $\text{KAl}(\text{SO}_4)_2 \cdot 12\text{H}_2\text{O}$ and gains a new melting temp of 60.93 °C [25]. Shaolin Xie et al. investigated the binary eutectic mixture of oxalic acid dihydrate (88 wt%) and boric acid (12 wt%) for thermal stability. It is found that the eutectic mixture is thermally stable for 1000 cycles [26].

Various potential applications have been explored in relation to PCM utilization, including [27][28]:

- Regulating thermal comfort in textile clothing
- Storing cold thermal energy in refrigerators/air conditioners
- Recovering and preheating exhaust waste heat in internal combustion engines
- Enhancing thermal comfort in buildings
- Managing thermal conditions in portable electronic devices
- Optimizing thermal performance in photovoltaics
- Utilizing in solar thermal power plants

This list provides examples and is not exhaustive. Choosing a suitable PCM largely relies on its transition temperature, and a variety of PCMs with diverse melting points have been investigated to suit different applications.

1.1.3 Challenges in latent heat TES

Despite its elevated energy density and ability to accumulate thermal energy at nearly invariant temperatures, LHTES faces several critical challenges that limit its large-scale implementation. One of the most significant barriers is the inherently low thermal conductivity of PCMs, typically distributed between 0.1 to 0.7 W/m·K in many commonly used organic and inorganic PCMs [3] [25]. This poor thermal conductivity drastically slows down the thermal heat transport process during both melting (charging) and solidification (discharging), resulting in prolonged charging times and lower system efficiency. Therefore, enhancing the heat transfer rate remains a major research focus in the development of advanced LHTES systems.

Another critical issue is supercooling, which refers to the solidification of PCM at a temperature significantly below its normal melting point, typically ranging from 10°C

to 20°C below the melting temperature [4]. Supercooling occurs due to poor nucleation behavior and insufficient crystallization rates, delaying the solidification process and potentially compromising the reliability of the energy release process during discharging cycles.

Corrosion is another important concern, as certain PCMs—especially inorganic salts—can react with the materials used for storage containers or heat exchangers, leading to degradation, leakage, or mechanical failure of the system components over time [6]. This poses serious risks to the durability and safety of LHTES systems, particularly under high-temperature operating conditions.

Incongruent melting or phase separation also presents a significant challenge, especially for salt-based PCMs. In an ideal case of congruent melting, the composition of the liquid phase after melting remains identical to that of the solid phase, allowing for stable and repeatable phase change cycles [3]. However, many PCMs exhibit incongruent melting, where phase separation occurs, leading to uneven melting and non-uniform energy storage behavior over repeated cycles.

Lastly, limited thermal cycling stability restricts the performance over an extended period of many PCMs. Frequent thermal cycling—the repeated process of charging and discharging—can cause material degradation, phase separation, or chemical instability, thereby reducing the effective lifespan of the PCM [11] [13]. Ensuring stable thermal behavior over a high number of cycles remains a crucial requirement for commercial LHTES applications.

Given these challenges, particularly the issue of poor thermal conductivity, current research—including the focus of this study—is directed toward developing innovative heat transfer enhancement strategies. These include techniques such as integrating heat pipes, fins, advanced geometries, and high-conductivity additives to expedite the thermal response and improve the overall performance of LHTES systems.

1.1.4 Heat transfer enhancement techniques

A predominant share of the organic and salt hydrate PCMs exhibit low thermal conductivity [13] as shown in Table 1.1. The rate of heat transport to and from the PCM relies on factors such as the surface area for heat convey, the temperature

difference, and the thermal conductivity of the PCM. Increasing the thermal gradient can lead to higher irreversible thermal losses in the system. As a result, researchers aim to increase the heat exchange region and boost the thermal conductivity of PCMs to achieve the desired heat transfer performance for targeted applications. Techniques such as adding thermally conductive materials, mixing of nano particles, integration of the heat pipe, addition of metal mesh, encapsulation of PCM and increasing the thermal exchange interface by using metallic fins, etc, as depicted in Fig. 1.2, are commonly employed for this purpose.

Nanoparticles such as copper oxide (CuO), nanowires, silica, alumina, titania, exfoliated graphite nanoplatelets [29] (xGnP), multilayer graphene nanoplatelets (MLG) [30], graphite nanofibers [31], multiwalled carbon nanotubes (MWCNTs) [32], silver nanowires, carbon black nano powder, CuO nanoparticles [33] and manganese dioxide nanowires [34] and nanotubes [35] have been investigated for this purpose. Encapsulation is a method where PCM materials are enclosed within an impermeable shell, providing thermal insulation and structural integrity. Encapsulation sizes are categorized based on shell dimensions and classified as macro (greater than 1 mm), micro (0–1000 μm), and nano (0–1000 nm) [36].

Table 1.1 Thermal properties of PCM

PCM	Melting Temp. ($^{\circ}\text{C}$)	Latent Heat (kJ/kg K)	Thermal Conductivity (W/m K)	
			Solid	Liquid
Formic acid	8	277	0.30	0.27
Acetic acid	17	192	0.26	0.19
Palmitic acid	61	222	0.21	0.17
Paraffin wax	0-90	150-250	0.2	-
Erythritol	117	340	0.73	0.33
Urea	134	250	0.80	0.60
d-Mannitol	165	300	0.19	0.11
Water	0	333	1.60	0.61
Calcium chloride hexahydrate	30	125	1.09	0.53
Barium hydroxide octahydrate	78	280	1.26	0.66
Oxalic acid dihydrate	105	264	0.9	0.70

Carbon fibres exhibit exceptionally Intensified thermal conductivity ($900 \text{ W/m}\cdot\text{K}$) [28], low density, and require only a minimal volume fraction to significantly improve the heat conduction capability of PCMs [37]. Aluminum, magnesium, and zinc powder are effective materials for enhancing the thermal conductivity of paraffin, whereas copper and nickel are incompatible with paraffin [22][38]. Similarly, certain salt hydrates are incompatible with aluminum and copper [22].

Straight longitudinal finned tubes and straight circular finned tubes are commonly employed in PCM systems to enhance the heat transfer surface area [39]. Some researchers have also stated that the impact of heat pipe in the PCM is effective than that of nanoparticles [40].

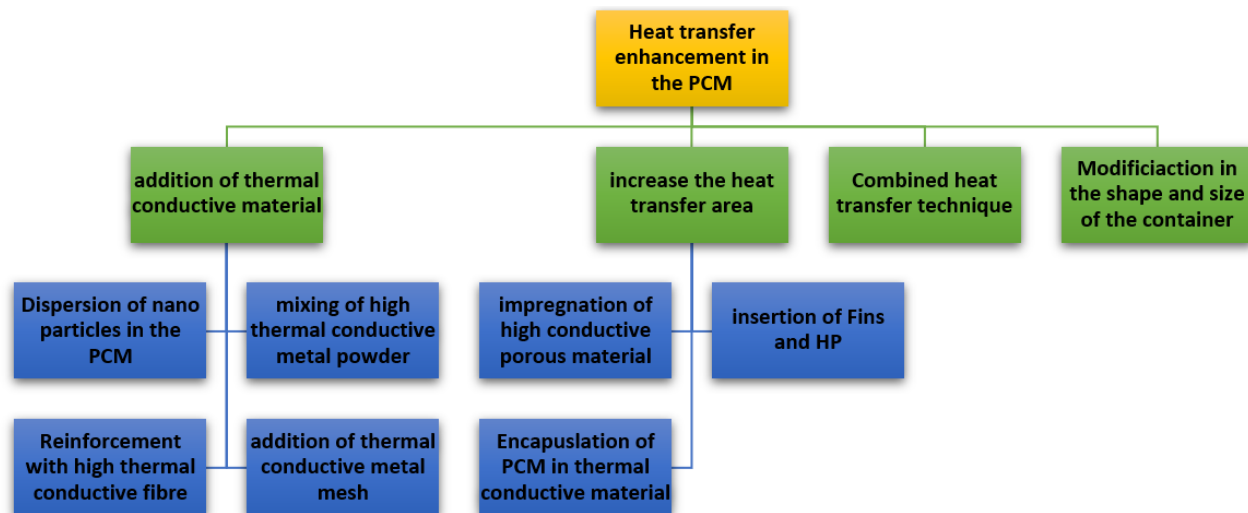


Fig. 1.2 Heat transfer enhancement techniques

1.1.5 Heat Pipe

Heat pipes (HPs) are highly effective, passive heat convey devices known for their exceptional capability to transport heat efficiently over considerable distances with minimal temperature gradients. Unlike conventional heat transfer methods that rely solely on sensible heat transfer through conduction or convection, heat pipes employ the latent heat of vaporization to achieve superior thermal performance. This phase-change-based mechanism allows them to deliver exceptionally high heat transfer rates

and maintain nearly isothermal conditions along their length, making them ideal for applications where uniform temperature distribution is critical.

The fundamental working principle of a heat pipe revolves around the cyclic evaporation and condensation of a working fluid encapsulated within a sealed enclosure. A typical heat pipe comprises three key sections:

Evaporator Section: This is the region where external heat is introduced to the HP, causing the working fluid to absorb thermal energy and vaporize.

Adiabatic Section: The vaporized fluid then travels through this region, which acts as a conduit with negligible heat loss, ensuring the thermal energy is efficiently transported from the evaporator to the condenser.

Condenser Section: In this section, the vapor releases its latent heat to the surrounding environment or working medium, condensing back into liquid form. The condensed fluid then returns to the evaporator via capillary action (using a wick structure) or gravity, completing the cycle.

This continuous phase-change cycle enables heat pipes to offer thermal conductivities several orders of magnitude higher than those of solid conductive materials like copper or aluminum. Consequently, they are extensively implemented in a variety of thermal management applications, including electronic cooling systems, renewable energy systems, HVAC systems, and LHTESS systems.

In the context of PCM-based TES systems, heat pipes have demonstrated significant potential in accelerating the liquefaction and solidification stages of the PCM. Their ability to rapidly absorb and redistribute thermal energy leads to faster charging and discharging cycles, improved energy storage density, and enhanced system efficiency. Several studies have confirmed that the integration of heat pipes within LHTESS markedly enhances the thermal response of the system. In fact, researchers have noted that the effectiveness of heat pipes in amplifying PCM melting performance often surpasses that of other techniques such as the incorporation of nanoparticles into the PCM matrix [40]. While nanoparticles enhance thermal conductivity via conduction, heat pipes dominate through phase-change-driven convection, leading to far superior heat transfer enhancement.

Moreover, heat pipes offer the additional advantages of reliable, maintenance-free operation and design flexibility, as they can be oriented and shaped to suit different configurations, making them highly adaptable for various thermal energy storage applications. Their integration into PCM systems represents a promising approach for optimizing both charging speed and thermal uniformity, making them a key focus area for ongoing and future research in thermal energy management technologies.

Chapter 2

Literature Review

2. Literature Review

Commercially viable PCM used in LHTESS have poor thermal conductivity [13], [41], resulting in significantly longer thermal charging (THC) times and rendering the system economically unviable. Furthermore, the large temperature gradient in the PCM can induce excessive heat and material breakdown [42] due to the sensible THC process. To mitigate these issues, several techniques have been developed to reduce THC time, including the (1) integration of materials with elevated thermal conductivity such as metal powder (e.g., Al, Cu, Fe) [43], [44] and nanoparticles (e.g., C), [30], [45]–[47] (2) the insertion of fins (e.g., Al, Cu,), metal matrix [48] and heat pipe (HP) [42], [49]–[52], modification of the configuration and dimensions of the PCM enclosure [53]–[56], changing the slope of the PCM enclosure [57]–[59], altering the relative position of the PCM and heat source [60], and continuous rotation of the PCM enclosure.

Modifying the shape of the PCM's enclosure unit has emerged as the most cost-effective solution compared to adding expensive, high thermal conductive materials to the PCM. Therefore, researchers have dedicated considerable efforts to analysing the melting behaviour of PCM in diverse PCM shapes of the system, such as rectangular, conical, cylindrical, trapezoidal, spherical, and shell and tube, in various orientations.

2.1 LHTESS container/ heat exchanger

Researchers have explored a wide range of design configurations for PCM enclosures, as illustrated in Fig. 2.1. These include tube-in-shell systems, spherical shapes, triplex tubes, rectangular layouts, multi-tube arrangements, and cavities with conical or trapezoidal profiles [61]. Among the various approaches, geometry-based enhancement techniques have shown significant potential. Such modifications in container design have been reported to strengthen the thermal charging performance

of LHES systems by as much as 80%. The cylindrical container used in LHES systems can be oriented vertically, horizontally, or at an inclination—each configuration significantly influencing the system’s thermal charging rate [62]. This rate can be further enhanced through structural modifications of the tube and shell within the heat exchanger. Tube-side improvements include the use of multiple tubes, integration of internal fins, incorporation of heat pipes, and design transformations such as helical or conical geometries, as well as altering the relative positioning between the tube and shell, etc. On the shell side, performance can be improved by modifying its shape to conical or trapezoidal forms [63] , which enhance natural convection and thermal distribution within the PCM.

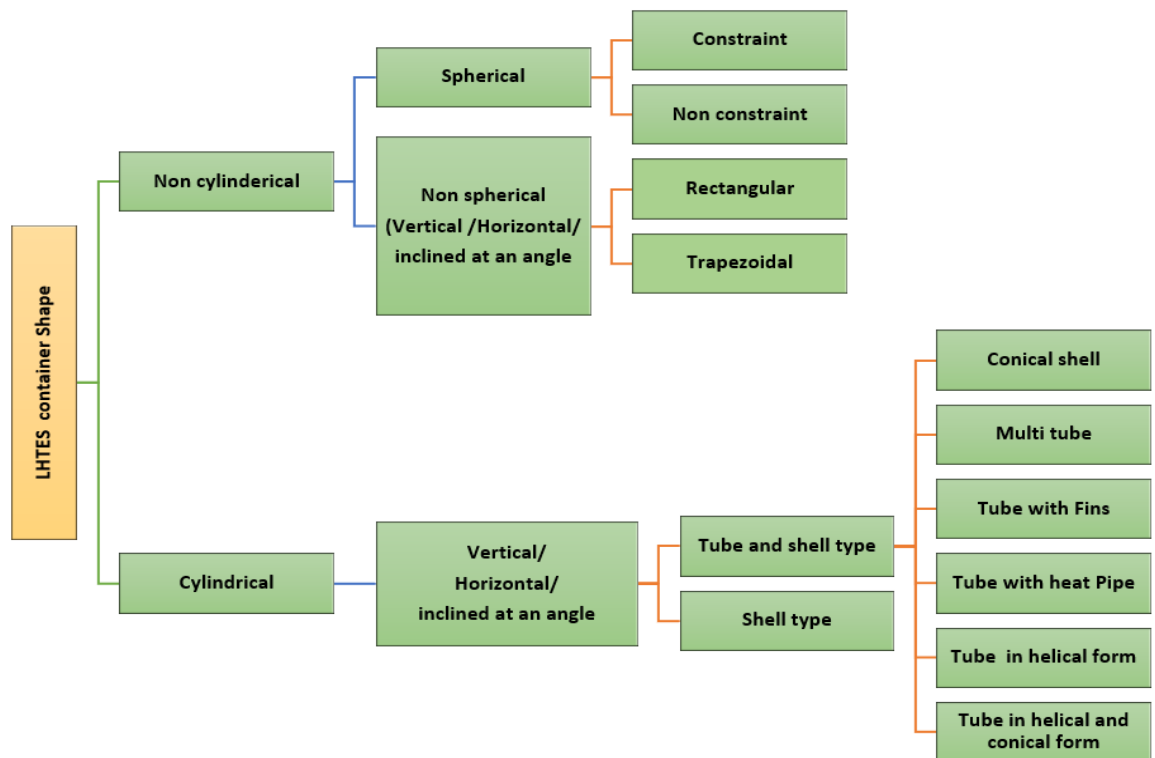


Fig. 2.1 LHES containers/heat exchangers

➤ Melting behaviour of PCM in a spherical vessel

F.L. Tan et al. (2008) [64] executed an experimental assessment into the melting behavior of PCM by immersing a spherical container in a heated fluid bath. The study compared constrained and unconstrained melting scenarios. Following the onset of

melting, buoyancy-driven convection became the prevailing heat convey mechanism in the upper region of the PCM, resulting in an improved rate of thermal energy transfer. Total thermal charging time was less in unconstrained melting (80 mins) than that of constrained melting (130 mins). H. Sattari et al. (2016) [56] also stated a similar result. They concluded that a 27% enhancement of diameters results in an 80% increase in the melting time of PCM. Researchers clearly stated that the total thermal charging time is less in unconstrained melting than that of constrained melting [64]. Spherical containers possess a lower volume per unit surface area, which offers a larger effective area for heat transfer compared to non-spherical designs. This geometry also makes them well-suited for compact arrangement within a LHTES bed system [65].

➤ Melting behaviour of PCM in a non-cylindrical and non-spherical Configuration

Babak Kamkari et al. (2014) [59] evaluated an experimental exploration to analyze the melting behavior of PCM inside a rectangular container positioned at various inclination angles—90°, 45°, and 0° relative to the horizontal axis. The findings revealed that containers inclined at 0° and 45° melted 53% and 35% faster, respectively, compared to the vertically oriented configuration. The study also demonstrated that lowering the height of the container further contributes to reducing the overall melting duration, particularly in the 90° and 45° inclined setups. Mohamed Fadl et al. (2019) [66] implemented an experimental probe to inquiry the melting dynamics of PCM within a rectangular container, where thermal energy was supplied from both the left and right boundaries. The results showed that the melting front advanced more rapidly in the upper region of the container in contrast to the bottom section, primarily due to the influence of natural convection occurring in the liquid phase of the PCM [66]. Farida Iachachene et al. (2019) [55] through computational evaluation probed the melting of PCM accumulated in a trapezoidal vessel as shown in Fig. 2.2.

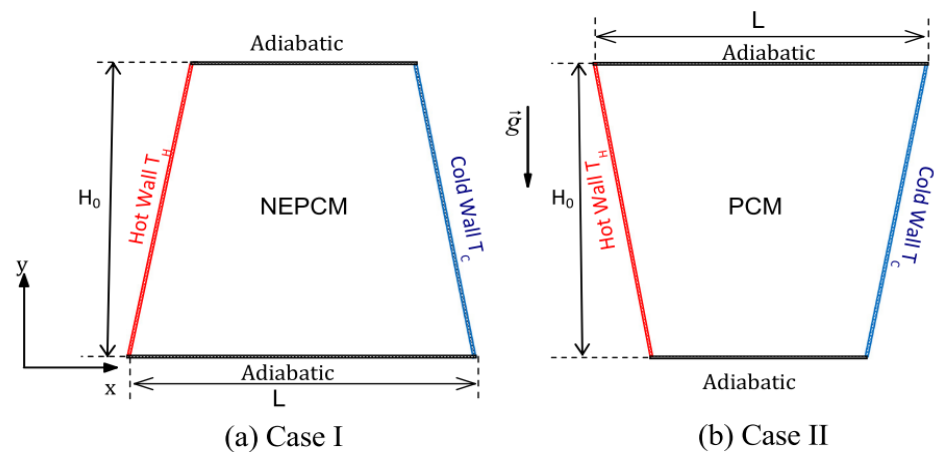


Fig. 2.2 Trapezoidal container

It was stated that the melting occurs more quickly in case II due to the melted PCM moving further in the top region, which has a relatively higher surface area compared to case I. It was found that Case II exhibited a 53% shorter melting duration for the PCM in comparison to Case I. Zivkovic et al. [67] established that a rectangular enclosure consumes 50% less melting time than a cylinder enclosure when the largest dimension is placed horizontally for equal heat transfer region and PCM mass.

➤ **Melting Behaviour of PCM in the cylindrical container**

Ajay Kumar Yadav et al. (2019) [68] experimentally examined and numerically studied unconstrained and constrained melting of Paraffin in a horizontally positioned cylindrical vessel. Melting was higher in the bottom half in constrained melting due to conduction, while the top half melted faster in unconstrained melting due to natural convection in the liquid PCM.

Mohammed Bechiri et al. (2019) [69] accomplished a numerical assessment on the melting behavior of partially filled PCM within a vertically oriented cylindrical tube. The study indicated that during the initial phase, the vertical length of the PCM layer had minimal consequence on the melting operation since heat was primarily transferred through thermal conduction. However, as the container height increased, the overall melting duration also increased. In a more recent study, Mustafa S. Mahdi et al. (2019) [60] employing numerical techniques examined the influence of PCM placement on thermal efficiency in a concentric pipe system using ANSYS Fluent. The PCM was positioned in the annular region in one case and inside the inner pipe in

another. The findings revealed that placing the PCM in the inner tube reduced the melting time by approximately 50% compared to the configuration with PCM in the annular space.

➤ **Melting of PCM in the shell and tube type heat exchanger (HX)**

In terms of LHTESS design development, multiple approaches have been considered by the researchers which three techniques are most popular: (1) alteration in PCM packing location either in shell or tube [60] (2) modification in relative position between shell and tube [70] (3) change in the shape and size of shell and tube [71]. Park et al. [72] explored numerically the consequences of the tube count and configuration in the horizontally oriented shell and tube container. They found the interesting result that two tubes in the shell case demonstrate less melting time than the eight tubes for the equal amount of PCM packing in the shell. They also stated that tube insertion at the base of the horizontal enclosure enhances the PCM liquefaction rate. Kumar et al. [73] successfully managed the more uniform PCM temperature by using the funnel shape shell in the vertical orientation. The thermal charging rate was found to be lowest for the cylindrical shape, followed by conical, and the highest for the funnel shape.

Recently, Ghazani et al. [74] examined and compared the vertical cylindrical shell TES system with a conical shell with a tube (diffuser and nozzle shapes). Their findings indicate that the most influential factor is the cross-section area proportion of the PCM at the pinnacle of the system to that at the beneath. Augmenting this ratio reduces the impact of conductive heat exchange while enhancing natural convection. [75]

Mustafa S. Mahdi et al. (2019) [75] experimentally scrutinized the melting behavior of paraffin wax within a conical coil LHTES unit housed in a cylindrical reservoir. Their findings demonstrated that the melting rate in the conical coil configuration was approximately 22% higher compared to that of a conventional coil design [75]. This enhancement was primarily attributed to the extended surface domain of the heat transfer fluid (HTF) piping in the lower region of the cylinder, where the solid PCM naturally settled due to its higher density [75]. Sodhi et al. [54] also considered the conical geometry but in a horizontal orientation. They found a result which favours the conical shell for reducing the THC time. They stated the optimized angle of about 3.4

degrees for 54- and 98.6-mm front and rear diameters of the conical shell. The shifting of more PCM in the upper zone of the storage unit promotes the natural convection process in the larger domain and drastically reduces the THC time [54].

According to the literature survey, it is apparent that repositioning the PCM towards the upper portion of a vertically oriented container yields significant benefits in reducing THC time. Therefore, the use of trapezoidal or conical containers with a wider top is a preferable approach to decrease the overall liquid fraction time. Additionally, integrating HP with fins (HP-Fins) in a trapezoidal LHTESS unit may further enhance THC performance.

To improve the thermal charging design of a horizontal tube and shell LHTESS, the easiest approach would involve modifying the relative positions of the inner tube and shell. Zheng et al. [70] undertook numerical optimization to specify the optimal location of the circular inner tube in a horizontally oriented system. They found that vertically moving the interior tube downwards from the centre of the outer shell led to a reduction of the total melting duration. However, they also noted that there is an optimum degree of eccentricity that can achieve better melting performance. This happens as the process of natural convection involves a crucial contribution during the melting mechanism, causing the PCM to melt more promptly in the upper regions of the LHTESS than in the lower regions [70]. To address this, redistributing the PCM from the lower regions to the upper regions can decrease the total liquefaction time. This can be achieved by lowering the inner tube, which effectively shifts the PCM from the base to the summit of the system. Cao et al. [76] explored an analysis of the consequences of eccentricity in the horizontal tube and shell of an LHTESS. The probe revealed that the area driven mainly by buoyancy-induced flow is increased by the downward shifting of the inner tube in the horizontal shell, resulting in higher thermal charging rates. Moreover, the study found that tube eccentricity also enhances heat transfer efficiency. Demirkiran et al. [77] examined the consequence of eccentricity on multiple circular tubes in a rectangular horizontal shell. The findings demonstrated that a 70% advancement in system performance can be accomplished through the use of eccentricity in the four tubes within the rectangular container. Recently, Safari et al. [78] explored an examination to analyze the impact of the eccentricity of the heat

exchange tube on the liquefaction behaviour of PCM in a shell and tube LHTESS. They found that the circular shell with an eccentricity factor of 0.5 showed a maximum suppression of 50.4% in thermal charging time in comparison to the circular shell with the concentric tube [78]. According to previous research, it has been observed that in a shell-and-tube (horizontal) LHTESS, it is possible to lessen the time needed for melting by vertically descending the inner tubes from the centre of the shell.

Saeid Seddegh et al. (2017) [79] implemented a research effort to evaluate the thermal performance of vertical conical and cylindrical shells. Their outcomes indicated that the conical geometry was capable of storing thermal energy more rapidly than the cylindrical configuration under identical operating conditions. Subsequently, Qianjun Mao et al. (2019) [80] carried out a quantitative assessment focusing on the heat transport behavior during PCM melting within a similar conical vessel. Their findings exposed that the total melting period was mitigated by approximately 30.69% compared to that of a traditional cylindrical shell. Sodhi et al. [54] declared that the horizontal conical shell is more efficient than the cylindrical one in terms of thermal charging of LHTESS by using the numerical technique. The concept of accumulating more PCM in the top zone (convection governed) and less amount in the lower zone (conduction governed) would employ natural convection more efficiently.

Rupinder Pal Singh et al. (2019) [81] investigated the thermal charging performance of PCMs in shell-and-tube storage systems featuring both conical and cylindrical geometries, enhanced with the use of fins. Conical LHTES makes use of the natural convection advantageously by packing more PCM quantity in the upper region. A mitigation of 16% in the melting span is observed with conical LHTES. Employing fins in the conical LHTES provides enhanced heat transport augmentation than the nanoparticle dispersion. Lokesh Kalapala et al. 2019 [82] investigated numerically the impact of non-dimensional attributes on the melting behaviour of PCM in a shell and tube model. The last 10% unmelted portion was melted in about 30% total span of melting time, and this is a significant period. They observed that by enhancing the “length to diameter ratio” four times, the total melting duration increased 1.75 times. Hameed B. Mahood et al. (2020) [83] explored the effect of fin placement on the melting performance of PCM in a horizontal shell-and-tube heat exchanger. The data

obtained indicated that positioning the fins beneath the horizontal axis, particularly at a 15-degree spacing, was the most efficient configuration for reducing the melting duration of the PCM. In a related numerical investigation, Gurpreet Singh Sodhi et al. (2019) [54] analyzed the phase transition behavior of PCM in a horizontal conical shell-and-tube configuration where air, acting as the HTF, was introduced through the wider end of the conical shell. The study concluded that a cone angle of 3.4 degrees, along with inlet and outlet diameters of 98.6 mm and 54 mm respectively, yielded the most favorable performance, achieving 96% melting in reduced charging time [54]. It was also noted that fins significantly enhanced conduction-based heat transfer near the inlet region, while their effect became negligible toward the outer regions of the conical shell. Vyshak et al. [84] further contrasted the shell and tube enclosures with rectangular and cylindrical for the same PCM mass and equal heat diffusion region. Shell and tube enclosure demonstrated the best THC performance among all, and THC impact is further enhanced by increasing the mass quantity.

➤ Integration of Heat Pipe in PCM

The use of HPs is a widely adopted approach to amplify heat transfer in PCM-based LHTESS. HPs have the capability to transmit substantial quantities of heat over extended dimensions with minimal temperature loss through a small cross-sectional area [85]. Numerous physical and computational simulations have been performed to probe the influence of HP integration in LHTESS during the melting mechanism of PCM. One of the commonly used approaches to enhance THC in PCM is by incorporating HP and fins, which can be easily installed and integrated with PCM. It maintains low-temperature gradients and almost isothermal heat sources for integrated fins. HPs can also be employed as a diode [49] to operate unidirectionally. Similarly, in comparison to other heat transfer enhancement techniques, fins are less expensive and simpler to fabricate. In a study conducted by Abhat [49], the effectiveness of vertical fins integrated with a single HP in a PCM enclosure was examined. The HP was placed horizontally, and the fins were added in a vertical direction. Abhat identified that the dimensions of the fins and the heat source's temperature are the most significant variables affecting the system's performance. The work by Tiari et al. [85] investigated the use of vertically positioned HPs integrated with multiple horizontally

aligned fins of varying lengths in a rectangular enclosure. By augmenting the number of HPs from 1 to 3, they observed a reduction in THC time of approximately 10%. However, the improvement in performance was not significant with a further increase in the number of HPs, thus warranting the determination of the optimal number of HPs based on PCM mass. Moreover, amplifying the length of the fins reduced the temperature gradient in the PCM regions, which led to improved performance. Amit Saraswat et al. (2016) [86] explored the melting behavior of paraffin housed within a semi-cylindrical container, where a heating element (heat pipe) was positioned axially along the central axis of the vessel. It was determined that the Integration of transverse heat pipes in the PCM mass reduces the overall time of melting to just 5.5 hours, as compared to 12 hours, which takes place without the heat pipes.

In a probe executed by Tiari et al. [87], the employ of vertically embedded finned HPs in LHTESS was investigated for thermal charging performance. The observations indicated that the addition of more HPs led to an appreciable augmentation in the rate of phase transition of the PCM. The influence of HPs in vertical LHTESS units was experimentally studied by Motahar et al. [88]. It was observed that a 15°C augmentation in the heat input temperature led to a remarkable 53% minimization in the thermal charging period. Mahdavi et al. [40] performed an examination of the aftermath of the horizontal placement of HPs and nanoparticles in vertical shells and tube LHTESS. Their findings demonstrated that the integration of four HPs diminished the melting period by 83%, with only a 14% reduction in stored heat. Moreover, they concluded that the presence of embedded HPs had greater consequences on the system performance compared to nanoparticle inclusion. The numerical examination performed by Zhang et al. [89] inspected the effectiveness of HP, copper foam (CF), and fins on the thermal charging capabilities of a vertically placed single HP in a vertical LHTESS cylinder. The observations demonstrated that elevating the height of the PCM enclosure in HP without CF and Fins significantly reduced the melting times. Furthermore, the combination of HP, fins, and CF was discovered to be the most efficient method for enhancing heat transport. In the investigation carried out by Yang et al. [90], the aftermath of a horizontally placed single HP in a horizontally oriented cylinder was analysed. The results indicated that the integration of an HP could

diminish the overall charging period by 11.26%. Furthermore, the study found that extending the length of the condenser did not have a substantial impact on the charging period of LHTESS.

The key insights derived from the reviewed literature are summarized as follows:

- The thermal charging rate is significantly higher when the shell-and-tube LHTESS system is oriented horizontally [91].
- In cases where a vertical orientation is necessary due to space constraints, using a conical shell can substantially reduce the thermal charging time [53].
- Positioning the inner tube eccentrically—shifted downward from the centre of the shell—markedly enhances the thermal charging performance [70].
- The final 10% of the solid PCM requires over 25% of the total melting time, making it more efficient to begin thermal discharging after 90% of the PCM has melted.

2.2 Gaps in existing research

The opportunities of developing a TES system with a shell and tube type heat exchanger (HX), which enables boosting the heat transport and melting rate as follows:

1. Natural convection plays a vital contribution in accelerating the melting rate of PCM during thermal charging. But no sufficient research work has been found to investigate and augment the natural convection in the lower portion of the TES system in a shell and tube type HX.
2. The effect of the heat pipe in a conical shell to enhance the melting rate has not been explored fully yet. The effect of numbers, pitch, length, diameter, zone location and inclination of the heat pipe in the tube and conical shell HX on thermal characteristics like melting rate, solid-liquid front movement, liquid melting fraction, temperature profile and total thermal charging time of PCM is not understood fully.
3. Research lacks detailed comparative studies of thermal characteristics of a TES system in a conical vertical shell and tube type HX for diverse PCM materials.
4. The effect of height, maximum and minimum shell diameters ratio, semi angle of the cone, the maximum and minimum diameter of a cone for conical shell and tube type HX with a heat pipe to intensify the thermal charging performance of a system has not been studied fully yet.

5. Lack of research findings for comparative studies to understand the loss of thermal energy capacity (storage) of PCM by the insertion of the heat pipe, fins, and copper foam, etc., in the same volume in a shell and tube type HX.

2.3 Research Objectives

1. Mathematical Modelling of PCM-based TES heat exchanger system integrated with augmentation of heat transfer techniques by employing heat pipe or others will be performed.
2. Numerical simulation of different thermal characteristics of the TES heat exchanger system integrated with augmentation of heat transfer techniques by employing heat pipe or others will be performed for different operating and geometric conditions.
3. Experimental investigation of thermal characteristics for the TES heat exchanger system integrated with heat transfer enhancement techniques by using a heat pipe or other methods will be performed.
4. Comparative analysis of experimental results for different PCM materials in the TES heat exchanger system.

2.4 Research Methodology

- A detailed mathematical model was developed based on the fundamental conservation laws of mass, momentum, and energy to evaluate the heat convey behavior and assess the thermal effectiveness of the LHTES system using PCM.
- The solution of the developed mathematical model was carried out using ANSYS Fluent, a widely used computational fluid dynamics (CFD) software that provides built-in modules for thermodynamic and fluid flow analysis. This tool was employed to numerically solve the coupled mass, momentum, and energy equations, enabling an accurate simulation of the melting behaviour and heat transport processes within the PCM storage container.
- In addition to the numerical analysis, a comprehensive experimental setup for the LHTES system was designed and examine the system's effectiveness under practical conditions. The experimental arrangement consisted of key components such as a

PCM selected for its suitable thermal properties, an LHTES container or heat exchanger for PCM encapsulation, and temperature sensors placed at various strategic points to monitor the temperature distribution within the PCM during thermal loading and unloading. A fluid pump was integrated to circulate the HTF throughout the system. A hot water bath maintained the desired inlet temperature of the HTF, providing consistent thermal input. Additionally, a data acquisition system or data logger was integrated to continuously record temperature and flow data during the experiments. The system was tested under a range of operating conditions and geometrical configurations to comprehensively evaluate its thermal response and energy storage characteristics, providing valuable experimental insights.

Chapter 3

Mathematically Modelling and Simulation Technique

3. Mathematically modelling for phase transition

In this study, the thermal diffusion within LHTESS is investigated by employing a coupled conduction–convection heat transfer mechanism. The phase change phenomenon is captured using the enthalpy–porosity method, wherein the mushy zone model is implemented to accurately describe the interface between solid and liquid phases as the material undergoes melting. The computational fluid dynamics (CFD) simulations are performed using ANSYS Workbench, which is utilized for geometry creation, meshing, and solution setup. The following assumptions are adopted to simplify and optimize the numerical analysis [91]:

- A two-dimensional (2D) model is employed to evaluate the thermal charging performance of the LHTESS, based on the premise that it provides a reasonable approximation while reducing computational cost.
- Viscous dissipation effects within the PCM are considered negligible due to the low flow velocities involved in the phase change process.
- The Boussinesq approximation is integrated to model the buoyancy effects resulting from density variations in the molten phase of the PCM, assuming these changes are sufficiently small.
- The PCM is considered to exhibit homogeneous and isotropic thermal properties in both liquidus and solidus phases, ensuring uniform behaviour across the domain.
- The molten PCM is modelled as a Newtonian fluid with laminar flow behavior, and its compressibility is neglected, assuming constant density except for buoyancy-driven flow.
- Volume changes of the PCM during phase transition, as well as any movement or deformation of the solid phase, are ignored to simplify the computational model.
- Heat transfer by radiation is considered negligible in comparison to conduction and convection, and is therefore excluded from the analysis.

- Thermal contact resistance at interfaces between different components or materials is disregarded, assuming ideal thermal continuity.

In line with the adopted assumptions, the governing equations are formulated as follows:

The equations that govern the continuity or mass conservation are expressed as:

$$\triangleright \quad \frac{\partial u}{\partial x} + \frac{\partial v}{\partial y} = 0 \quad (3.1)$$

This ensures mass conservation in a two-dimensional incompressible flow. It implies that the mass entering and exiting a control volume is balanced, with no accumulation.

The equation describing momentum conservation in the x-direction

$$\triangleright \quad \rho \left(\frac{\partial u}{\partial t} + u \frac{\partial u}{\partial x} + v \frac{\partial u}{\partial y} \right) = \mu \left(\frac{\partial^2 u}{\partial x^2} + \frac{\partial^2 u}{\partial y^2} \right) - \frac{\partial p}{\partial x} + S_x \quad (3.2)$$

The governing equation used in this analysis is a modified form of the Navier–Stokes equation, adapted to established for the phase change behaviour of the PCM within the LHTESS. This equation encompasses several critical physical phenomena contributing to fluid motion and heat transfer. These components include:

- Convective acceleration (appearing on the left-hand side of the equation) represents the inertial transport of momentum within the fluid due to its motion. This term accounts for the nonlinear advection of velocity and is essential in capturing flow dynamics, particularly in regions where natural convection is dominant.
- Viscous diffusion which models the internal friction within the fluid as a result of viscosity. This term governs the momentum dissipation due to shear stresses and is critical for describing laminar flow behavior in the molten PCM.
- The pressure gradient term, which drives the fluid flow in response to differences in pressure across the domain. It reflects how pressure variations influence the velocity field and help establish hydrostatic and dynamic pressure distributions in the system.
- A source term (denoted as S_x, S_y), which may include additional physical effects such as flow resistance due to porous media (e.g., the mushy zone during phase transition),

momentum sinks, or buoyancy forces arising from density variations. In phase change modelling, this source term often incorporates a Darcy-like damping force to suppress velocity in the solid and partially solidified regions of the PCM.

The equation describing momentum conservation in the y-direction

$$\rho \left(\frac{\partial v}{\partial t} + u \frac{\partial v}{\partial x} + v \frac{\partial v}{\partial y} \right) = \mu \left(\frac{\partial^2 v}{\partial x^2} + \frac{\partial^2 v}{\partial y^2} \right) - \frac{\partial p}{\partial y} + S_y + \rho g \beta (T - T_m) \quad (3.3)$$

In the given equation, μ represents the viscosity of the PCM. The enthalpy-porosity method considers the mushy zone as a porous domain, with the porosity of each element estimated to be equivalent to the liquid fraction within that element [92].

An additional term incorporated into the momentum equation is the buoyancy force, expressed as $\rho g \beta (T - T_m)$. This term plays a pivotal role in accurately modelling natural convection within the molten phase of the PCM.

- Here, ρ represents the density of the fluid, g is the gravitational acceleration, β is the thermal expansion coefficient, T is the local fluid temperature, and T_m is the reference or mean fusion temperature of the PCM [62].
- This buoyancy-driven source term arises from the application of the Boussinesq approximation, which simplifies the density variation in the Navier–Stokes equations by assuming that density changes are only significant in the body force term and negligible elsewhere in the flow field.
- The presence of a temperature gradient within the PCM leads to localized density differences. As a result, warmer (less dense) fluid rises while cooler (denser) fluid sinks, setting up convective currents. This mechanism of heat transfer—natural convection—is crucial during the melting process, as it significantly accelerates thermal distribution in the liquid PCM.
- Accurately capturing this buoyancy effect is essential in phase change simulations, particularly in LHTESS, where the heat transport performance is strongly influenced by convection in the molten region.

The momentum dissipation components S_x and S_y , which account for the diminished porosity within the mushy zone, are articulated as follows:

$$\triangleright S_x = - \frac{(1-\lambda)^2}{(\lambda^3 + \varepsilon)} A_{mushy} u \quad (3.4)$$

$$\triangleright S_y = - \frac{(1-\lambda)^2}{(\lambda^3 + \varepsilon)} A_{mushy} v \quad (3.5)$$

To prevent divisions by zero, the parameter ε [93] is introduced in the equation. The mushy zone constant, denoted as A_{mushy} , decides the magnitude of the damping effect, with higher values resulting in a more rapid velocity transition to zero during solidification. Previous numerical studies have reported a range of mushy zone constants from 10^3 to 10^{10} [94]–[96]. In this study, A_{mushy} is set to 10^5 , which aligns well with previous findings. The liquid volume fraction λ is derived in relation to the PCM temperature [97].

Inside the partially solidified zone —characterized by a mixture of solid and liquid PCM—the material exhibits a porous-like behavior due to the coexistence of both phases. As a result, the movement of fluid within this region is partially restricted by the presence of solid structures. To model this phenomenon numerically, momentum-damping terms are introduced into the Navier–Stokes equations in both the x and y directions, denoted as S_x and S_y , respectively.

These source terms are essential in representing the gradual transition from solid to liquid. They act to suppress fluid motion in regions dominated by the solid phase, while allowing free movement where the material has fully melted. Thus, they enable the model to simulate the realistic behaviour of PCM during the phase change process.

- When $\lambda \rightarrow 0$ (mostly solid): The denominator $\lambda^3 + \varepsilon$ becomes very small, causing the source term S_x or S_y to grow very large in magnitude. This effectively dampens the velocity, simulating the resistance to motion in solid regions.
- When $\lambda \rightarrow 1$ (fully liquid): The numerator $(1 - \lambda)^2$ approaches zero, rendering the entire source term negligible. As a result, fluid is allowed to move freely without resistance in the fully melted regions.

These source terms are derived from a Darcy's law-based porous media approach, a technique commonly employed in the enthalpy–porosity method for modelling melting and solidification in CFD. This approach effectively treats the mushy region as a porous medium, where the permeability varies with the liquid fraction, thereby simulating the progressive unblocking of flow paths as the material transitions from solid to liquid.

This section describes the method used to calculate the liquid fraction (λ) of a PCM as a function of temperature. The liquid fraction is a critical parameter in modeling phase change phenomena, particularly when using the enthalpy–porosity technique, as it governs both the energy absorption during the phase transition and the momentum damping in the semi-solid (mushy) region.

The liquid fraction λ is determined using a piecewise linear function that relates the material's phase state to its temperature:

$$\lambda = \begin{cases} 0 & \text{if } T < T_{Solidus} \\ \frac{T - T_{Solidus}}{T_{Liquidus} - T_{Solidus}} & \text{if } T_{Solidus} < T < T_{Liquidus} \\ 1 & \text{if } T > T_{Liquidus} \end{cases} \quad (3.6)$$

Where:

- TTT is the local temperature of the PCM,
- $T_{Solidus}$ is the solidus temperature, below which the PCM is entirely freeze.
- $T_{Liquidus}$ is the liquidus temperature, above which the PCM is entirely fluid.

The use of a continuous, piecewise-linear function for λ is essential for accurately resolving the phase transition region in computational models. Specifically:

It enables a smooth and realistic transition of thermophysical features (such as heat capacity and thermal conductivity) between solid and liquid states. In the enthalpy–porosity method, λ directly influences the latent heat source term in the energy equation, ensuring that thermal energy is appropriately captured or emitted during melting and solidification. Furthermore, λ is a key input in the momentum source terms, which regulate the suppression of fluid motion in the mushy zone, thereby capturing the solid–liquid resistance realistically.

This modelling approach ensures robust and physically consistent simulation of melting and solidification in LHTESS, making it a foundational concept in phase change computational analysis.

The generalized form of the transient energy conservation equation, incorporating convective, conductive, and phase change effects, is expressed as:

$$\rho \left(\frac{\partial H}{\partial t} + \frac{\partial(uH)}{\partial x} + \frac{\partial(vH)}{\partial y} \right) = \frac{\partial}{\partial x} \left(k \frac{\partial T}{\partial x} \right) + \frac{\partial}{\partial y} \left(k \frac{\partial T}{\partial y} \right) \quad (3.7)$$

The left-hand side of the equation symbolizes the rate of change of enthalpy due to time and advection (movement of energy with the flow). The right-hand side denotes thermal diffusion via conduction in both spatial directions.

The overall thermal energy of the PCM can be described as the combination of the sensible (h) and latent (Δh) heat elements, which are characterized as the enthalpy (H) [56].

$$H = h + \Delta h \quad (3.8)$$

where the heat contribution from temperature change is delineated as

$$h = h_0 + \int_{T_{ref}}^{T_m} C_p dT \quad (3.9)$$

The alteration in enthalpy resulting from the phase transition is characterized as

$$\Delta h = \lambda L \quad (3.10)$$

The latent heat of the PCM, denoted by L , contributes to the overall heat content, while the λ , ranges from 0 to 1.

The equation for energy conservation for fins:

$$(\rho c_p)_{fins} \frac{\partial T}{\partial t} = k_{fins} \left[\frac{\partial^2 T}{\partial x^2} + \frac{\partial^2 T}{\partial y^2} \right] \quad (3.11)$$

E_s represents the aggregate energy stored within the PCM and fins upon the conclusion of the melting phenomena.

$$E_s = E_{PCM} + E_{fins} \quad (3.12)$$

E_{PCM} denotes the total energy accumulated in PCM after the melting process is finished.

$$\triangleright E_{PCM} = m_{PCM} \lambda L + m_{PCM} C_{p,PCM} (T_{avg,PCM} - T_0) \quad (3.13)$$

$$\triangleright E_{fin} = m_{fin} C_{p,fin} (T_{Avg,fin} - T_0) \quad (3.14)$$

Whereas, T_{avg} denotes the mean temperature, m represents the mass, C_p is the specific heat capacity, and the subscript PCM signifies the energy storage material.

t_m signifies a point in time when the fraction of PCM in the liquid state reaches one, indicating complete melting. The mean power (P_m) is determined as the ratio of total energy (E_s) accumulated in the PCM and the time (t_m) taken for the melting process [98]

$$\triangleright P_m = \frac{E_s}{t_m} \quad (3.15)$$

C_{cp} (Cost per mean power) is delineated as the quotient of the total cost (C_{tt}) and the P_m .

$$\triangleright C_{cp} = \frac{C_{tt}}{P_m} \quad (3.16)$$

The overall system cost (C_{tt}) is determined through the computation outlined in Eqn. (17)

$$\triangleright C_{tt} = m_{PCM} \cdot C_{PCM} + m_{fin} \cdot C_{fin} \quad (3.17)$$

Herein, C_{PCM} and C_{fin} denote the costs associated with the PCM and fin material, respectively.

➤ HP

HPs represent a category of passive heat transfer devices leveraging the liquid-vapour phase change of their working fluid to enhance thermal energy transfer rates, surpassing those achievable by conventional conductors. However, comprehending the intricate hydrodynamics and thermal dynamics within HPs poses a formidable challenge. The simulation of all phenomena within HPs is prohibitively expensive due to substantial computational costs, surpassing the scope of this investigation. Therefore, this study prioritizes the THC of the PCM and simplifies the modelling of HPs.

Conventionally, HPs have been viewed as tools with consistently high thermal conductivity, with reported values ranging from 30 kW/mK to 100 kW/mK [87], [94], [95]. In this study, HPs are treated in the simulation as highly thermally conductive elements with thermal conductivity of 38000 W/m K [94], [95] to address the computational challenges outlined earlier. The thermal characteristics of the HPs are encapsulated by the energy equation provided below:

$$\triangleright (\rho c_p)_{eff} \frac{\partial T}{\partial t} = k_{eff} \left[\frac{\partial^2 T}{\partial x^2} + \frac{\partial^2 T}{\partial y^2} \right] \quad (3.18)$$

Where the term *eff* signifies the effective thermal property of the HP.

3.1 Modelling of PCM Numerical Simulations

The simulation is conducted using the ANSYS Fluent 2022 software package, a widely adopted commercial software solution. The SIMPLE algorithm [80], [99], [100] is employed for the resolution of the pressure-velocity coupling. The second-order upwind method [98], [101] is employed to solve the momentum equations, while the pressure equations [102] are tackled with the PRESTO! scheme. To achieve accurate results, suitable under relaxation factors are applied, specifically 0.3 for pressure, 0.7 for velocity components, 0.9 for liquid fraction, and 1 for energy [80]. The attainment of solution convergence is monitored meticulously at each time step, ensuring that the residuals of the energy, velocity components, and continuity equations fall below the specified thresholds of 10^{-7} , 10^{-5} , and 10^{-4} , respectively.

➤ Phase Change Modeling Using the Enthalpy–Porosity strategy

To accurately capture the fusion and freezing behavior of the PCM, the enthalpy–porosity technique was employed. This method is widely embedded in CFD for modeling solid–liquid phase transitions within thermal systems. The approach was implemented in the present study using the finite volume strategy within ANSYS Fluent.

Key Features of the Enthalpy–Porosity Method:

Rather than explicitly tracking the moving solid–liquid interface (also known as the melting front), the enthalpy–porosity method treats the mushy zone—a mixture of solid and liquid phases—as a porous medium with variable permeability.

The liquid fraction (λ) is used as a continuous scalar field, varying from 0 (fully solid) to 1 (fully liquid), to describe the state of the PCM at each computational cell.

The method incorporates both sensible heat and latent heat contributions into a single enthalpy term, allowing for a smooth and continuous transition between solid and liquid phases.

Momentum source terms are added to the Navier–Stokes equations to dampen fluid velocities in regions with partial solid content, simulating the mechanical resistance of the mushy zone to flow [103].

This modeling strategy significantly simplifies the numerical simulation by eliminating the need for interface-tracking algorithms, such as front-tracking, volume-of-fluid (VOF), or level-set methods, thereby enhancing computational stability and efficiency.

Advantages in PCM Simulation:

Effectively captures the heat accumulation during melting and the heat emitting during solidification.

Accurately resolves the influence of natural convection within the liquid phase, which dominates the heat transport process during melting.

Suitable for complex geometries and widely validated in LHTEs applications.

➤ Buoyancy Effects Modelled Using the Boussinesq Approximation

To account for buoyancy-driven natural convection in the molten PCM, the Boussinesq approximation was applied in the momentum equations [104]. This approximation simplifies the treatment of density variation by assuming that:

Density ρ is treated as constant in all terms of the governing equations, except in the body force (buoyancy) term, where it varies linearly with temperature.

The fluid is incompressible, and the variation in density is small enough that it does not significantly affect the continuity or momentum equations, except as a source of buoyancy.

Mathematical Formulation:

The buoyancy force per unit volume is given by:

$$F_{buoyancy} = \rho g \beta (T - T_{Ref}) \quad (3.19)$$

Where:

ρ is the reference fluid density,

g is the gravitational acceleration,

β is the thermal expansion coefficient,

T is the local temperature,

T_{Ref} is the reference temperature, typically taken as the liquification temperature of the PCM.

In the molten region, temperature gradients result in localized density differences. Hotter, lighter fluid rises, and cooler, denser fluid sinks, establishing natural convective currents that boost the heat convey rate and accelerate the melting phenomena. The Boussinesq approximation provides a computationally efficient means to capture these buoyancy effects without solving a fully compressible flow model.

Chapter 4

Investigation of Eccentric Tube Shapes and Heat Pipes on PCM's Thermal Charging

4. Introduction

Thermal energy storage (TES) is getting attention worldwide due to its capability of solving the problem of an energy shortage, air pollution, and better utilization of sustainable energy sources. TES techniques store thermal energy, such as low-temperature heat, industrial unused heat, and solar heat energy, by utilizing heat storage material. TES techniques can be arranged into sensible heat TES technique, latent heat TES technique and thermos-chemical TES technique [105]. The latent heat TES system (LHTESS) has an advantage over the sensible system in terms of higher heat of enthalpy and constant phase change temperature [11], [106] by the phase change of the material (PCM). Heat storage and release in the material are considered as thermal loading and unloading of the LHTESS, respectively. However, PCM thermal conductivity is a serious drawback in the practical application of the system due to its low value, which worsens the thermal charging performance drastically.

In the techniques of LHTESS, the shape and size of the enclosure or container utilized for the accumulation of PCM have a remarkable contribution to the thermal loading and unloading behaviours of the unit [41]. There are mainly three common PCM containers, such as cylindrical, rectangular, and annular geometrical structures designs. Researchers have done a significant amount of work to understand how container shape influences thermal charging and discharging performance. Zivkovic and Fujii [67] evaluated the performance of the rectangular and cylindrical enclosures by computational techniques. They exhibited that the rectangular enclosure took nearly 50% less time than the other enclosure for the equivalent heat exchange area and volume. Seddegh et al. [91] compared the thermal charging properties between horizontally and vertically maintained shell and tube enclosures by heat transfer computational technique. They stated that the thermal charging performance of LHTESS in horizontal orientation is more augmented than that of the other case [91].

LHTESS should be established horizontally rather than vertically as a result. Consequently, the horizontal shell and tube LHTESS has emerged as one of the most well-liked LHTESS due to its exceptional performance [91].

However, the thermal charging time of (horizontal) shell and tube LHTESS can be augmented owing to the low thermal value of PCM thermal conductivity. Consequently, three techniques for improving heat transfer may be used in this LHTESS: (1) enhance the heat transfer area for example by including fins, heat pipes (HPs) and porous materials inside the PCM [107], [108] (2) improve the design of LHTESS, mainly shape and size of the enclosure [109] (3) boost the thermal conductivity (PCM) by integrating nano-particles or metal powder inside the PCM [40]. In comparison to the other two techniques, the second one is more rational and considerably less expensive. Because the second way neither diminishes the LHTESS's ability to store heat nor uses pricey materials with high thermal conductivity.

In terms of LHTESS design development, multiple approaches have been considered by the researchers of which three techniques are most popular: (1) alteration in PCM packing location either in shell or tube [60] (2) modification in relative position between shell and tube [70] (3) change in the shape and size of shell and tube [71]. Hasan and Suffer [110] demonstrated that a spiral tube enhances the thermal charging rate by about 21% to a straight tube. Ghasemi and Ranjbar [111] declared that two tubes instead of one are more beneficial for reducing the melting span, and the distance between the two tubes should be 1.5 times the diameter of the tube. Guo et al. [16] welded varying lengths of annular fins with tubes to boost the thermal charging effectiveness of the LHTESS. Sodhi et al. [54] declared that the conical shell is more efficient than the cylindrical one in terms of thermal loading of LHTESS by using the numerical technique. Park et al. [72] explored numerically the consequences of the tube count and configuration in the horizontally oriented shell and tube container. They found the interesting result that two tubes in the shell case demonstrate less melting time than the eight tubes for the equal amount of PCM packing in the shell. They also stated that tube insertion at the base of the enclosure enhances the melting rate of PCM. Kumar and Saha [73] successfully managed the more uniform PCM temperature by

using the funnel-shaped shell in the vertical orientation. The thermal charging rate was found to be lowest for the cylindrical shape, followed by conical, and the highest for the funnel shape.

Recently, Shafiei Ghazani and Gholamzadeh [74] examined and compared the vertical cylindrical shell TES system with a conical shell with a tube (diffuser and nozzle shapes). Their findings indicate that the most influential factor is the cross-sectional area ratio of the PCM at the pinnacle of the system to that at the beneath. Augmenting this ratio reduces the impact of conductive heat exchange while enhancing natural convection.

To improve the thermal charging design of a horizontal tube and shell LHTESS, the easiest approach would involve modifying the relative positions of the inner tube and shell. Zheng et al. [70] explored numerical optimization to check the optimal location of the circular inner tube in a horizontally oriented system. They found that vertically moving the interior tube downwards from the centre of the outer shell led to a diminishing of the total melting duration. However, they also noted that there is an optimum degree of eccentricity that can achieve better melting performance. This happens as the process of natural convection involves a crucial contribution during the melting mechanism, causing the PCM to melt more rapidly in the upper regions of the LHTESS than in the lower regions. To address this, redistributing the PCM from the lower regions to the upper regions can decrease the total liquefaction time. This can be achieved by lowering the inner tube, which effectively shifts the PCM from the base to the summit of the system. Cao et al. [76] explored an analysis of the consequences of eccentricity in the horizontal tube and shell of an LHTESS. The probe revealed that the area dominated by natural convection is increased by the downward shifting of the inner tube in the shell, resulting in higher thermal charging rates. Moreover, the study found that tube eccentricity also enhances heat transfer efficiency. Demirkıran and Cetkin [77] examined the consequence of eccentricity on multiple circular tubes in a rectangular horizontal shell. The findings demonstrated that a 70% betterment in system performance can be achieved through the use of eccentricity in the four tubes within the rectangular container. Recently, Safari et al. [78] explored an examination to analyze the impact of the eccentricity of the heat exchange tube on the liquefaction

behaviour of PCM in a shell and tube's LHTESS. They found that the circular shell with an eccentricity factor of 0.5 showed a maximum mitigation of 50.4% in thermal charging time in comparison to the circular shell with the concentric tube.

The use of HPs is a widely adopted approach to amplify heat transfer in PCM-based LHTESS. HPs have the capability to transmit substantial quantities of heat over extended dimensions with minimal temperature loss through a small cross-sectional area [85]. Numerous physical and computational simulations have been performed to probe the influence of HP integration in LHTESS during the melting mechanism of PCM. In a probe conducted by Tiari and Qiu [87], vertically embedded finned HPs in LHTESS were investigated for thermal charging performance. The observations indicated that the addition of more HPs led to an appreciable augmentation in the rate of phase transition of the PCM. The influence of HPs in vertical LHTESS units was experimentally studied by Motahar and Khodabandeh [88]. It was observed that a 15°C augmentation in the heat input temperature led to a remarkable 53% minimization in the thermal charging period. Mahdavi et al. [40] performed an examination of the aftermath of the horizontal placement of HPs and nanoparticles in vertical shells and tube LHTESS. Their findings demonstrated that the integration of four HPs diminished the melting period by 83%, with only a 14% reduction in stored heat. Moreover, they concluded that the presence of embedded HPs had greater consequences on the system performance in contrast to nanoparticle distribution. The numerical examination performed by Zhang et al. [89] scrutinized the effectiveness of HP, copper foam (CF), and fins on the thermal charging capabilities of a vertically placed single HP in a vertical LHTESS cylinder. The observations demonstrated that elevating the height of the PCM enclosure in HP without CF and Fins significantly reduced the melting times. Furthermore, the combination of HP, fins, and CF was discovered to be the most efficient method for enhancing heat transport. In the investigation carried out by Yang et al. [90], the consequences of a horizontally placed single HP in a horizontally oriented cylinder was analysed. The results indicated that the integration of an HP could diminish the overall charging period by 11.26%. Furthermore, the study found that extending the length of the condenser did not have a substantial impact on the charging period of LHTESS.

According to previous research, it has been observed that in a shell-and-tube (horizontal) LHTESS, it is possible to lessen the time needed for melting by vertically descending the inner tubes from the centre of the shell. However, it is still unknown what the effectiveness of the eccentric inner tube with varying shapes is on the thermal charging rate. In order to determine the consequences of the eccentric inner tube with different shapes on the thermal charging rate, it is necessary to obtain the melting characteristics for a range of inner tube shapes. The objective of this manuscript is to explore the influences of varying shapes of eccentric inner tubes on the thermal charging rate in a tube and shell enclosure. Various physical models are constructed with eccentric inner tube shapes such as circular, semi-circular, square, triangular, inverted (Inv.) triangular, and C-Shape. The optimal shape of the eccentric inner tube is determined by analysing the selected cases based on several performance indicators, including thermal charging time, TES, PCM temperature, and mean power of energy storage. In addition, HPs are utilized as a heat transfer boosting strategy to reduce the melting duration of the system in the optimal case. Furthermore, the aftermaths of the quantity of HPs on the thermal charging of the enclosure are also examined.

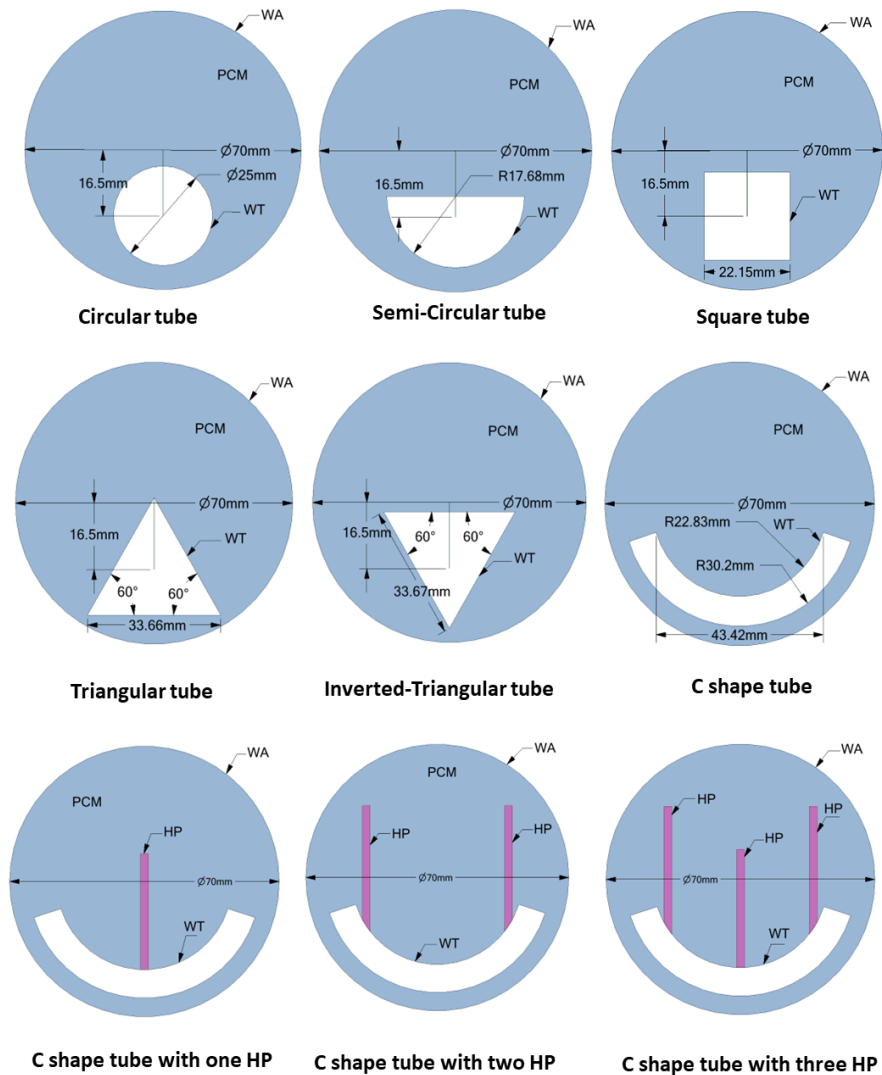
4.1 Physical model

In this examination, a horizontal tube and shell LHTESS is selected for investigation, with six equal eccentric tube shapes including circular, semi-circular, square, triangular, Inv. triangular, and C-shape as shown in Fig. 4.1.

Table 4.1 All considered cases

Case No.	Case	Shape of the tube	No. of HP
1	Circular	Circular	-
2	Semi-circular	Semi-circular	-
3	Square	Square	-
4	Triangular	Triangular	-
5	Inv. triangular	Inverted triangular	-
6	C-shape	C-shape	-

7	C-shape-1HP	C-shape	1
8	C-shape-2HP	C-shape	2
9	C-shape-3HP	C-shape	3



WA —————> Wall at adiabatic condition

WT —————> Wall at constant temperature

Fig.4.1 Physical model of 6 different shapes of tube cases with 3 cases of HPs

Aluminium is assumed material for tubes during simulation. Additionally, a C-shaped tube with vertically embedded one, two, and three HPs is also analysed to further improve the system's thermal performance. All nine considered cases are also demonstrated in Table 4.1.

The HP's dimensions are 30 mm by 2 mm in length and thickness, respectively. As depicted in Fig. 4.1, the inner tube wall is regarded as a heat source with a constant temperature, while PCM is discovered outside of the inner tube. All cases with three-dimensional structures are assumed to be made of identical materials and are depicted in Fig. 4.2.

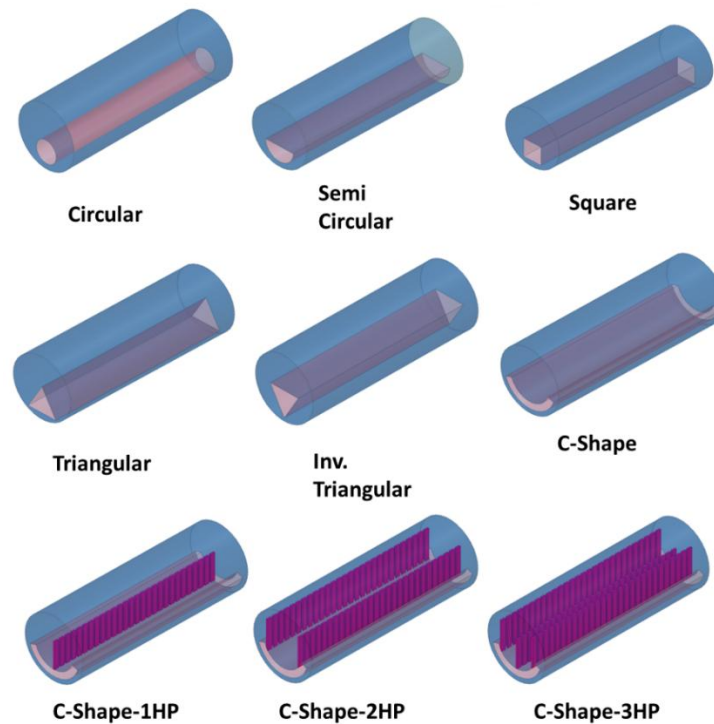


Fig. 4.2 Schematic 3-dimensional diagram of all considered cases

A fixed outer shell diameter of 70mm is established, and the entire volume of PCM between the shell and tube is equal in all six varying tube cases. Additionally, the eccentricity of the tube from the geometric centre of the shell is held constant across all cases. The eccentric circular tube case is chosen as the baseline case for comparison with other tube shapes in terms of performance evaluation. PCM employed in the

present investigation was RT-50 paraffin [60], and thermophysical characteristics of PCM, HP and Aluminium are outlined in Table 4.2 [60], [83], [87], [94], [95], [112].

Table 4.2 Thermophysical characteristics of materials

	PCM	HP	Aluminium
h (J/kg K)	2000	381	871
$T_{\text{solidus}}, T_{\text{liquidus}}$ (K)	318.15-324.15	-	-
ρ (kg / m ³)	800	8978	2719
β (1/K)	0.0006	-	-
L (J /kg)	168,000	-	-
μ (kg/m s)	0.004	-	-
k (W/m K)	0.2	38000	202.4

4.2 Numerical model

This research paper utilizes the enthalpy-porosity strategy [94] to emulate phase change phenomena in a finite volume technique. The Boussinesq approximation [113] is executed to account for buoyancy effects. The tracking of the phase change boundary front is not performed explicitly in this method. The liquid fraction is determined within every cell of the computational domain, rather than explicitly tracking the solid-liquid interface front, with the porous media representing the liquid phase within each cell. The porosity is assumed to vary from zero to one as the PCM melts within the cell. The characteristics of PCM are considered to be temperature-independent and identical for both phases. The melted PCM is approximated as being Newtonian, having a laminar flow, and incompressible properties. During the phase change process, volume variations of PCM and the motion of solid PCM are neglected. Radiation heat transfer and viscous dissipation are considered negligible. The models are simplified to two-dimensional structures with the orthogonal coordinate system for the PCM region and HPs. Because the PCM area, tube wall perimeter, and width and length of HP are in the same vertical flat plane. The LHTES system's length can be

segmented into these vertical parallel flat planes, allowing the 2D plane simulation to be extrapolated across the entire length of the system. Many researchers have adopted this approach to optimize simulation cost and time [72], [85], [114]. A constant density assumption is employed in all equations except the buoyancy expression in the momentum conservation equations, where density fluctuation is taken into account linearly with temperature. Based on the assumptions mentioned above, the equations that dictate the system are used as explained in Chapter 3.

HPs are a type of passive heat transfer device that employs the liquid-vapour phase change of their working fluid to facilitate thermal energy transfer at an enhanced rate, surpassing that of conventional conductors. However, the detailed hydrodynamics and thermal dynamics inside HPs are intricate. It is prohibitively expensive to simulate all phenomena inside HPs due to the substantial computational costs involved, and is beyond the scale of this investigation. The key concern of this study is the phase change of the PCM, which simplifies the HP modelling. Heat pipes have traditionally been seen as instruments with elevated and invariant thermal conductivity, with reported values ranging from 30 kW/m K to 100 kW/m K [85], [87], [94], [95]. Here, HPs are assumed during the simulation as a highly thermal conductive element to tackle the issue mentioned above. Consequently, researchers commonly assume the effective thermal conductivity of HPs to be 38000 W/m K [94], [95].

For the numerical simulation of the governing equations in the TES system, the CFD software Ansys Fluent 2022 R2 was employed. The numerical solution of the energy and momentum equation was obtained by implementing a second-order upwind algorithm [98]. The pressure equation [98], [101], [102] was solved using the PRESTO! scheme. The SIMPLE algorithm [80], [92], [99] was applied to couple the velocity and pressure in the computational zone. Time discretization was achieved by considering the first-order implicit technique.

To improve convergence stability, an under-relaxation ingredient was applied to density, velocity, fractional melting, pressure, body force, and energy, with values of 1, 0.7, 0.9, 0.3, 1, and 1, correspondingly. The residual of the convergence indicator of the momentum, energy, and continuity equations was settled to 10^{-5} , 10^{-7} , and 10^{-4} ,

correspondingly. This numerical approach and setting are commonly used in TES research to obtain accurate and reliable results [80], [92], [98], [99], [101], [102].

The inception temperature of the entire PCM in the TES is set to 303.15 K in all cases, which is 15 K below the liquidus temperature of the PCM. This indicates that the PCM is entirely in the solid phase at the start of the heat charging. The model assumes that the exterior surface of the shell is well insulated, preventing any heat leakage to the ambient environment. The entire walls of the tube in all cases are considered at the constant temperature of 353.15 K.

To ensure accurate numerical simulations, a grid independence test was conducted using three mesh arrangements (coarse-grid, medium-grid, and fine-grid) with 75,00, 10,680, and 14,000 elements, respectively, for the concentric circular tube in the shell. A mesh with 10,680 elements is demonstrated in Fig. 4.3 (a).

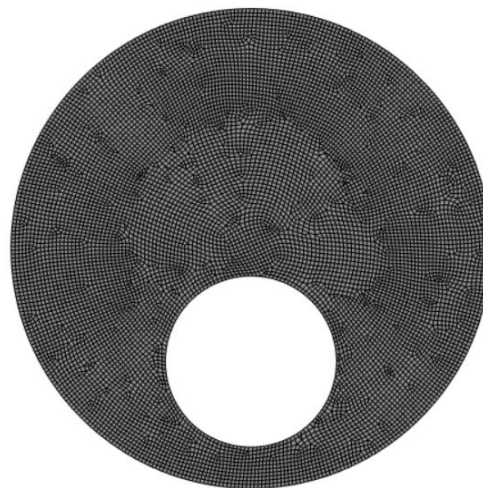


Fig. 4.3 (a) Generated mesh in eccentric circular tube case

The PCM liquid fraction for each grid was compared, and it was observed that the medium grid was adequate for the calculations. The conclusions of the grid dependency analysis are presented in Fig. 4.3 (b). The simulation used a time step of 0.1 seconds while the PCM was in the solid condition, which was then decreased to 0.02 seconds after the beginning of the solid-to-liquid transition. The time step dependency test findings revealed that a further reduction in the time step did not significantly influence the accuracy of the results. As a result, a mesh with 10,680

elements and a time step of 0.02 seconds was used to investigate the thermal performance of the PCM in all situations.

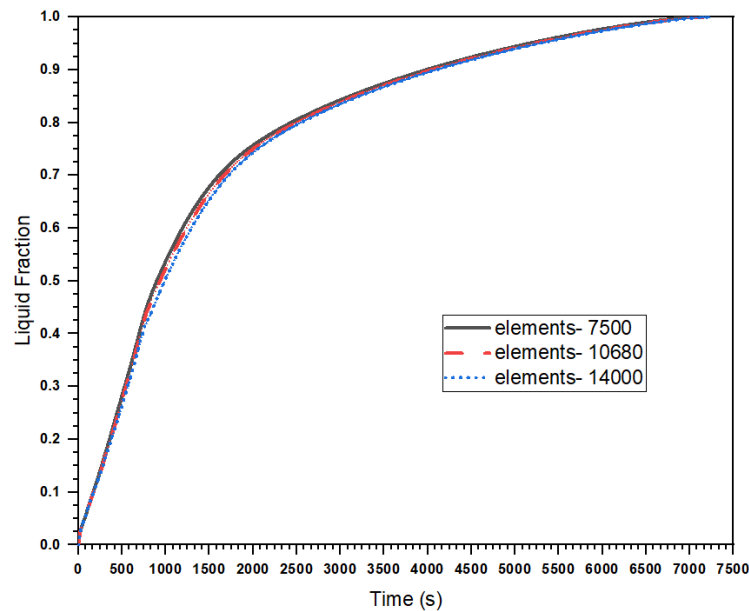


Fig. 4.3 (b) Mesh independent investigation

4.3 Model validation

In order to ascertain the validity and credibility of the developed numerical model, a comparative analysis was conducted between the current study and previously published numerical results by Mahdi et al. [60]. The PCM melt fraction history and liquid fraction patterns at various time intervals are depicted in Fig.4.4 (a) and Fig.4.4 (b), correspondingly.

The comparison reveals an outstanding level of agreement between the current study and published results, with a negligible difference of 0.36 % in total melting time. For experimental validation of the present model, we also evaluated the position of the solid-liquid interface of Gallium at specific time intervals and compared it with the experimental findings of Gau and Viskanta [115], the numerical analysis conducted by Brent and colleagues [92], and the numerical analysis performed by Khodadadi and Hosseinzadeh [45], as illustrated in Fig. 4.5.

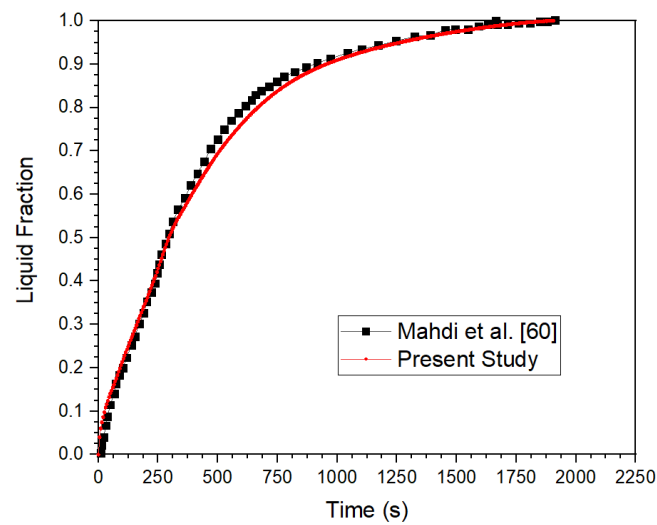


Fig. 4.4(a) Comparison of the present study liquid fraction time history to that of Mahdi et al. [60]

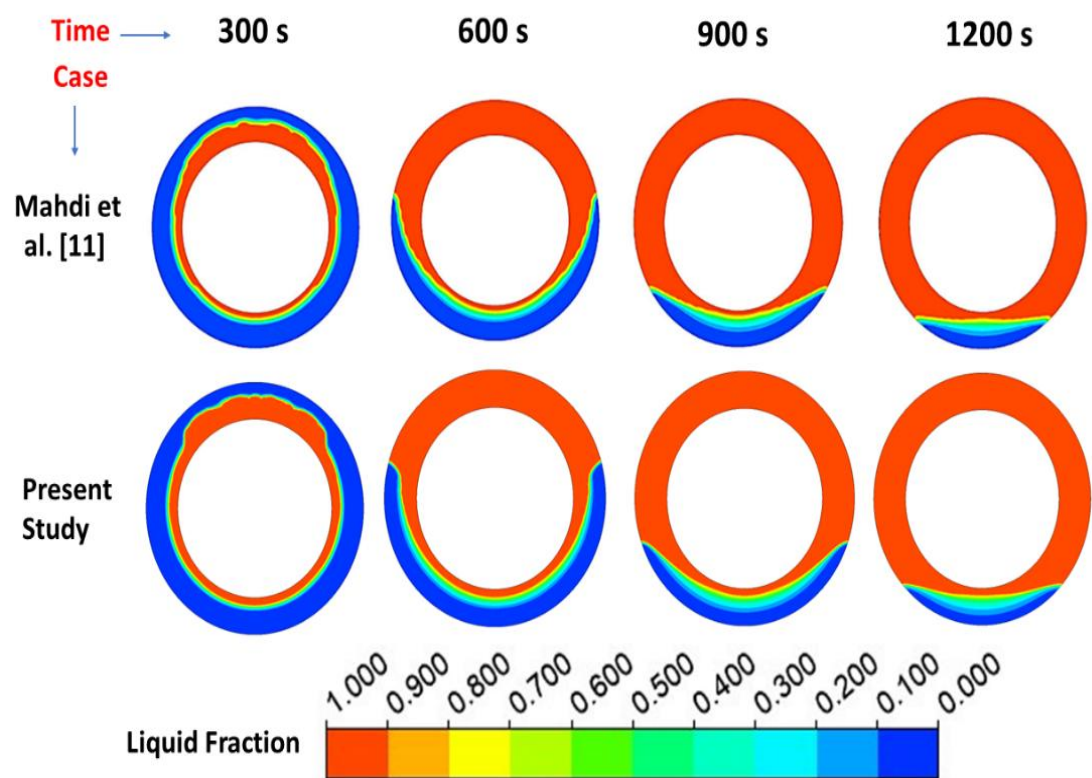


Fig. 4.4 (b) Comparison of liquid distribution patterns to those reported by Mahdi et al. [60]

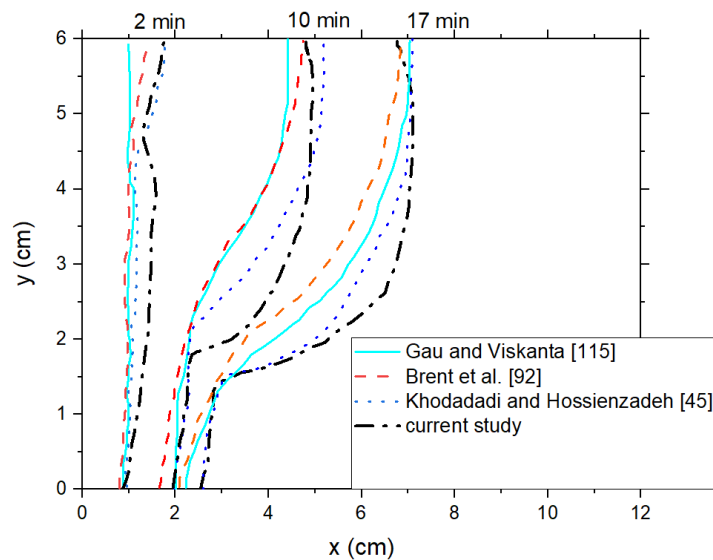


Fig. 4.5 Comparative analysis between the current study and prior research conducted by Gau and Viskanta [115], Brent et al. [92], and Khodadadi and Hosseinizadeh [45]

The slight disparity observed between the anticipated melting interface in our current model and the experimental findings can be attributed to two potential factors. Firstly, maintaining precise temperature control of the heat and cold walls during the experimental setup can be challenging. Secondly, the model does not account for three-dimensional effects, which could contribute to the observed variation. Remarkably, a strong agreement is evident between the results obtained from these prior studies and our current simulation. This demonstrates the high accuracy and effectiveness of the numerical model in simulating the thermal behaviour of the PCM in the LHTSS, thereby providing a robust foundation for further research in this case.

4.4 Results and Discussion

The molten fraction of PCM was analysed over time for various cases, as illustrated in the accompanying Fig. 4.6. The C-shape tube case exhibited the steepest curve slope among all the considered cases, up to a molten fraction of 0.94, indicating the fastest thermal charging. At a liquid fraction of 0.5, the C-shape tube case demonstrated a thermal charging rate that surpassed that of the circular, triangular, square, semi-circular, and Inv. triangular cases by 43.9%, 41.0%, 36.11%, 30.30%, and 28.2%, respectively. This can be attributed to the fact that the walls of the C-shaped tube

possess a greater length spread in the PCM, thereby facilitating heat transfer in the PCM more effectively.

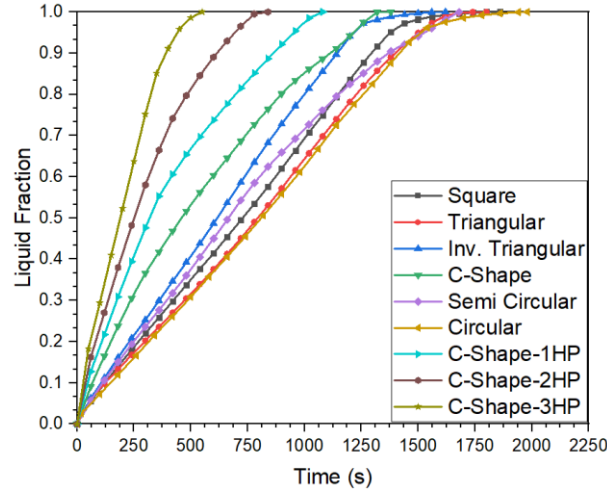


Fig. 4.6 Molten fraction time history for the different shapes of tube and HPs cases

To gain further insight into the rate of phase change in PCM, an enhancement ratio (e_r) parameter was introduced by Eq. (4.2) as given below [98].

$$e_r = \left[\frac{\lambda}{\lambda_c} - 1 \right] \times 100\% \quad (4.2)$$

Where λ and λ_c are the liquid fractions of non-circular and circular tube cases for the same instant of time. This parameter reflects the influence of the tube's shape on the rate of PCM melting, with the circular tube serving as the benchmark case. The outcomes are shown in Fig. 4.7, that the C-shaped tube had the highest e_r value, with a mean value of 54.34% over the entire melting period, followed by the Inv. triangular, semi-circular, square, and triangular tubes, with an average e_r values of 24.33%, 14.03%, 9.34%, and 3.73%, respectively. Among all the tube shapes, the square tube exhibited the most consistent superior performance over the largest time span during melting. However, as the melting progressed and approached 0.85 liquid fraction, the e_r values decreased sharply and approached zero due to the PCM's sensible heating. This implies that non-circular tube shapes are advantageous for partial thermal charging or 90% thermal charging of the system.

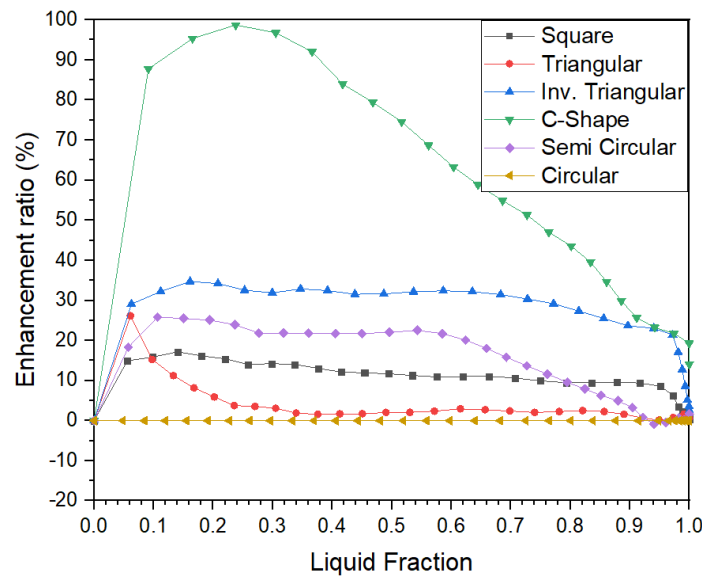


Fig. 4.7 Enhancement ratio time history for the different shapes of tube cases

The enhancement ratio of the non-circular tube shows a sharp decline, converging towards zero value post the 90% thermal charging phase as depicted in Fig. 4.7. This behavior is mainly due to the prevalence of conductive heat transfer in the bottom region of the container, along with the sensible heating of the melted PCM, which is affected by its inherently low thermal conductivity.

Fig. 4.8 demonstrates the e_r achieved by the insertion of HPs in the C-shape tube, which is considered the optimal case for comparison. The results indicate that C-shape-3HP (C-shape tube with three HP) exhibits the highest enhancement ratio, with a mean value of 103.50% for the entire melting period span. The performance of HPs in terms of enhancement ratio is found to be more consistent and uniform compared to different tube cases. This happens as the activation of natural convection mechanisms starts from the lower region around the tube wall in the PCM. After that, its natural convection is activated in the middle portion of the shell around the heat pipe. At last, natural convection is activated around the upper portion of the heat pipe. The first stage of natural convection promotes the later stages of natural convection in the PCM because it is above it. The temperature variation of molten PCM is in a decreasing trend from the bottom to the upper region, which continuously promotes natural convection as the solid PCM is further melted. It maintains the consistency in the

enhancement ratio when using different numbers of HPs from liquid fraction 0.15 to 0.90, as shown in Fig. 4.8. The drop in e_r performance at the end of melting in HP cases is also minimal. Furthermore, C-shape-1HP and C-shape-2HP have e_r values of approximately 23.5% and 52.84%, respectively, indicating that e_r performance is continuously maintained after the addition of HP.

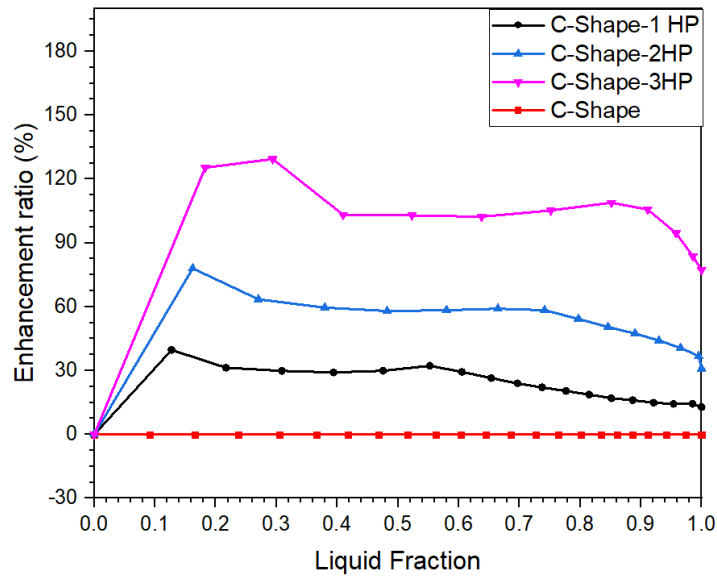


Fig. 4.8 Enhancement ratio time history for the C-Shape and HPs cases

The total melting time of various tube geometries was presented in a graphical form in Fig. 4.9. It was observed that the non-circular cases exhibited a shorter melting time than the circular tube case. Specifically, the Inv. triangular case had half the percentage reduction time compared to the triangular case. This can be attributed to the increased tube area exposed in an upward direction, which facilitates the convection mechanism in the PCM. The C-shaped tube demonstrated the shortest melting time in all tube cases. Moreover, the utilization of HPs elevated the thermal charging performance of the C-shaped tube. Upon enhancing the count of HPs from one to two, the thermal charging performance increased by 12%, and with an increase from two to three, the performance increased by 14.7%. The melting time, e_r , and heat storage values of all cases considered here are also presented in Table 4.3.

The study revealed that non-circular tube geometries, particularly the C-shaped tube, and the insertion of HPs can appreciably augment the thermal charging effectiveness of PCMs.

Table 4.3

Melting time, Heat storage, and Avg. Enhancement ratio (%) of all cases

Case	Melting time (s)	Heat storage (kJ)	Avg. Enhancement ratio (%)
Circular	1980	686	base case
Semi-circular	1680	648	14 (w.r.t circular tube)
Square	1860	688	9.34 (w.r.t circular tube)
Triangular	1800	691	3.7 (w.r.t circular tube)
Inv. Triangular	1620	693	24.3 (w.r.t circular tube)
C-shape	1380	664	54.3 (w.r.t circular tube)
C-shape-1HP	1080	617	22.3 (w.r.t C-shape tube)
C-shape-2HP	840	675	49.3 (w.r.t C-shape tube)
C-shape-3HP	550	650	94.8 (w.r.t C-shape tube)

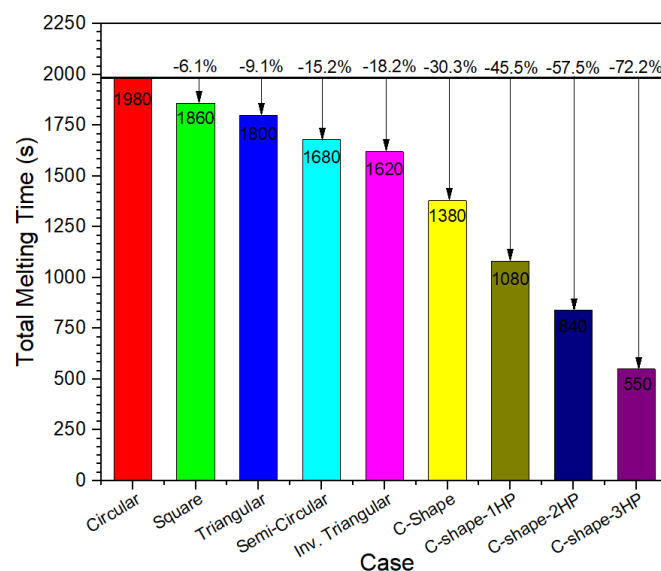


Fig. 4.9 Total melting times for all considered cases of the tube and HPs

Fig. 4.10 presents colour maps of the liquid fraction during the melting of PCM for different tube cases. It is evident that the melting phenomenon for all scenarios is more pronounced near the upper end of the tubes, i.e., in the top portion of the horizontal storage shell and near the tube wall surface. The convective flow is most vigorous in the upper part of the container as the liquefied PCM is carried upward and displaced from the heat exchange surface. As the PCM continues to melt, the natural convection becomes more intense, and it becomes dominant in the upper part of the LHTESS due to buoyancy.

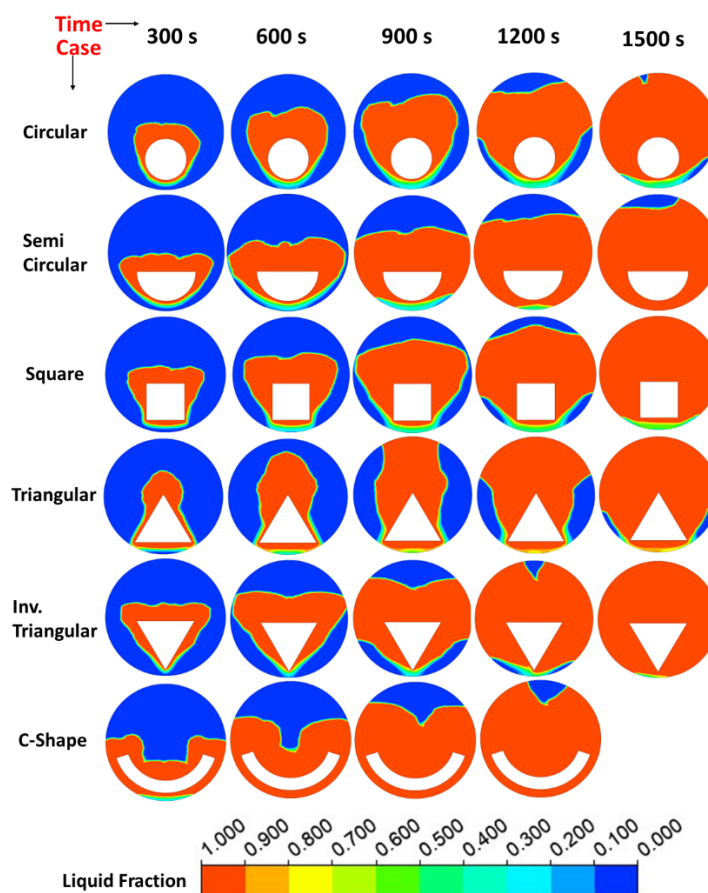


Fig. 4.10 Contours of liquid fraction for the various shapes of tube cases

In all cases, except for the triangular case, a wider liquid PCM region is observed at the top of the tube compared to the circular case. This facilitates the convection mechanism within a larger PCM region. At 900 seconds, the liquid PCM domain in the triangular case reaches the top of the shell. However, the side-wise PCM region of the tube remains un-melted due to a larger portion of the tube perimeter being located

towards the bottom of the shell. At 1500 seconds, a significant amount of PCM is found at the bottom of the shell, except for the C-shaped and semi-circular cases, where heat is transferred through the conduction mode. Consequently, it takes a longer time to melt the remaining frozen PCM at the bottom, particularly in the circular and triangular tube cases. Therefore, the PCM requires more time to completely melt. Among the two, the Inv. triangular tube is more efficient than the triangular tube in promoting the convection mode within a larger region. In the Inv. triangular case, the flat horizontal base of the triangle is at the upper side of the shell. A larger amount of PCM is also available above the flat horizontal base of the tube, which can be melted through convection because density variation after melting favours the natural convection current above the tube. Hence, a larger heat diffusion area, which enhances the natural convection current, is available for a larger amount of PCM region.

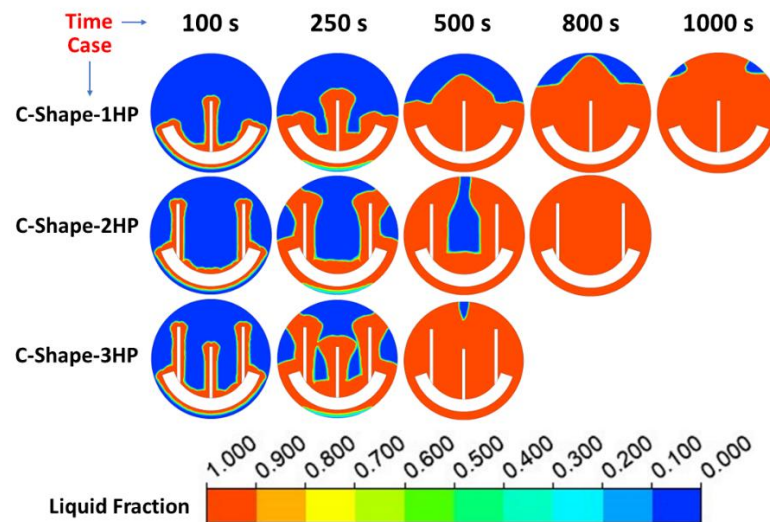


Fig. 4.11 Liquid fraction contours for the C-shape tube and embedded HPs cases

The liquid fraction contours with time for HPs insertion with the C-shape tube are depicted in Fig. 4.11. In the case of C-Shape-1HP, the insertion of one HP in the centre of the shell increased the melting rate of the middle portion of the PCM in the shell. This was due to the extended diffusion of heat into the PCM by the HP, which has a high capacity for heat transfer. However, some PCM remained un-melted after 1000 seconds on the sides of the HP in the shell. The addition of two HPs on the sides of the C-Shape tube further enhanced the liquid fraction rate but also increased the non-uniformity of melting, as shown in the C-Shape-2HP case. At 500 seconds, an un-

melted portion was observed in the middle of the HPs. After adding three HPs, the thermal charging time was reduced drastically, and the uniformity of melting in the PCM domain was enhanced.

Fig. 4.12 displays the mean temperature evolution of the PCM during the phase transformation across all cases considered in the study. The C-Shape-2HP case exhibits the highest PCM temperature of approximately 350K, while the semi-circular tube case shows the lowest PCM temperature of about 340K after the complete phase transition of the PCM. The C-Shape-1HP and C-Shape-3HP cases exhibit lower PCM temperatures than C-Shape-2HP, with a difference of approximately 5K and 4K, respectively. The higher PCM temperature observed in the C-Shape-2HP case is attributed to the placement of HPs closer to the shell wall, which promotes non-uniform melting within the PCM domain. Notably, the curve for the circular tube case shows a sudden surge after the liquid fraction reaches 0.95, which is due to slow LH transfer and a higher rate of sensible heat (SH) transfer. This curve also exhibits the lowest mean temperature until the molten fraction reaches 0.9 of the PCM zone.

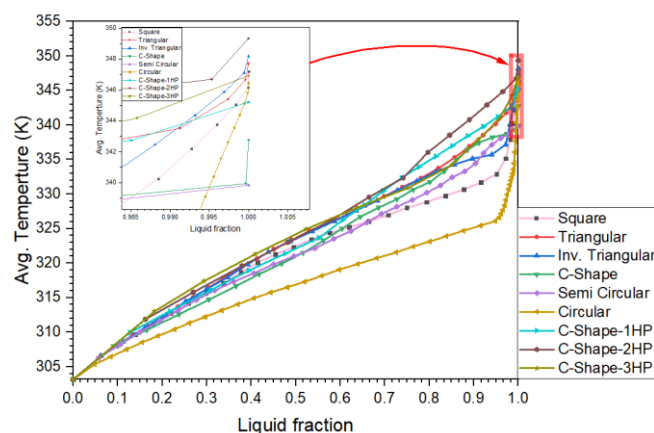


Fig. 4.12 Time history for the different shapes of tube and HPs cases

The temperature profiles of the PCM zone during the phase transformation exhibit similar behaviour, as depicted in Fig. 4.13. Notably, in the triangular and Inv. triangular tube cases, there is significant sensible heating of the liquid PCM after 1200 seconds, instead of the phase transformation of the remaining frozen PCM located at the bottom. This is attributed to the PCM at the bottom of the shell, which is melted by the conduction regime of heat transfer, but the heat transfer rate is elevated in the upper half due to the convection mode of heat transfer. The circular tube case exhibits the

lowest sensible heating of the PCM, indicating that a major portion of the heat diffusion is utilized as LH for PCM melting. However, a larger solid PCM region is found below the tube, which enhances the total melting time. The temperature distribution is most uniform in the circular, semi-circular, and square tube cases.

The temperature profile of PCM in the C-Shape tube with HPs is depicted in Fig. 4.14. The C-shaped tube is located at a considerable depth at the bottom of the shell, requiring heat to penetrate a significant distance from beneath to above in the PCM. Therefore, the insertion of HP in the middle of the C-shape tube can reduce the sensible heating of PCM and augment the thermal charging rate of the unit, as demonstrated in the case of C-Shape-1HP. It can be observed that in the C-Shape-2HP case, there is

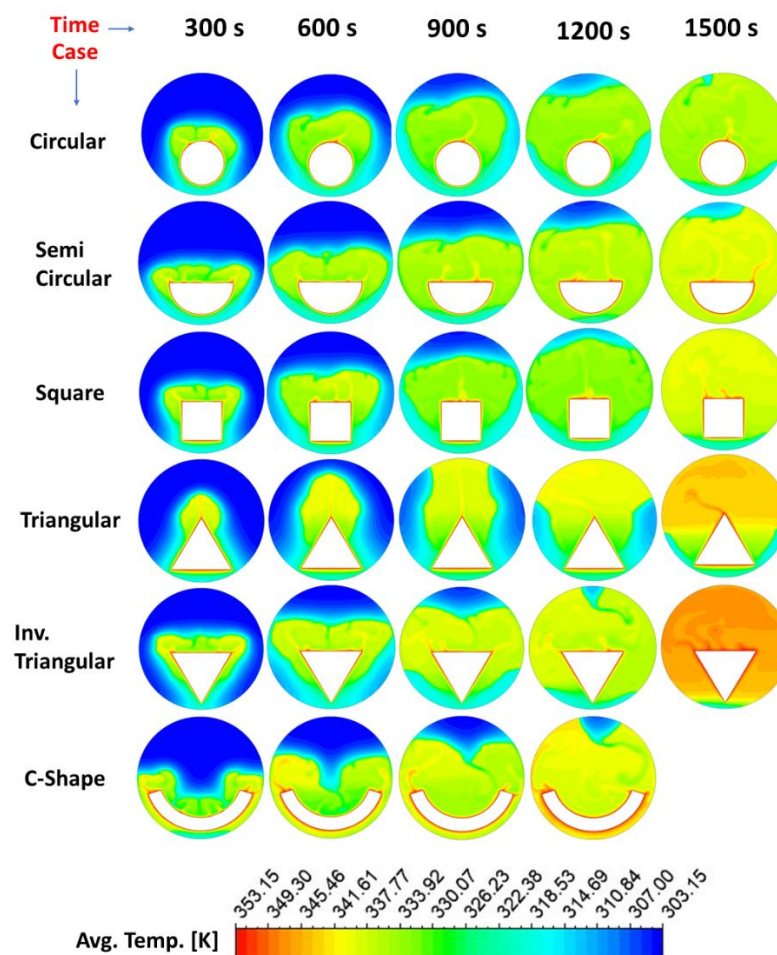


Fig. 4.13 Avg. temperature contours for the different shapes of tube cases significant sensible heating of PCM after 500 s, indicating that the addition of heat by two HPs is high but not absorbed by solid PCM at the same rate as LH, owing to the

inadequate thermal conductivity of the PCM. Furthermore, the case C-Shape-3HP results demonstrate a more homogenous temperature profile and reduce the sensible heating of the PCM due to the uniform insertion of three HP in the PCM domain. It implies that the location of HPs in the PCM region influences the temperature profile and sensible heating pattern.

To evaluate the overall energy accumulated in the LHTESS, the heat retention capacity of the PCM is evaluated in Fig. 4.15 while neglecting the energy absorbed by the HPs, as it is comparatively negligible. The circular tube case absorbs less energy than all other cases, except for the C-shape and semi-circular cases, where the difference is

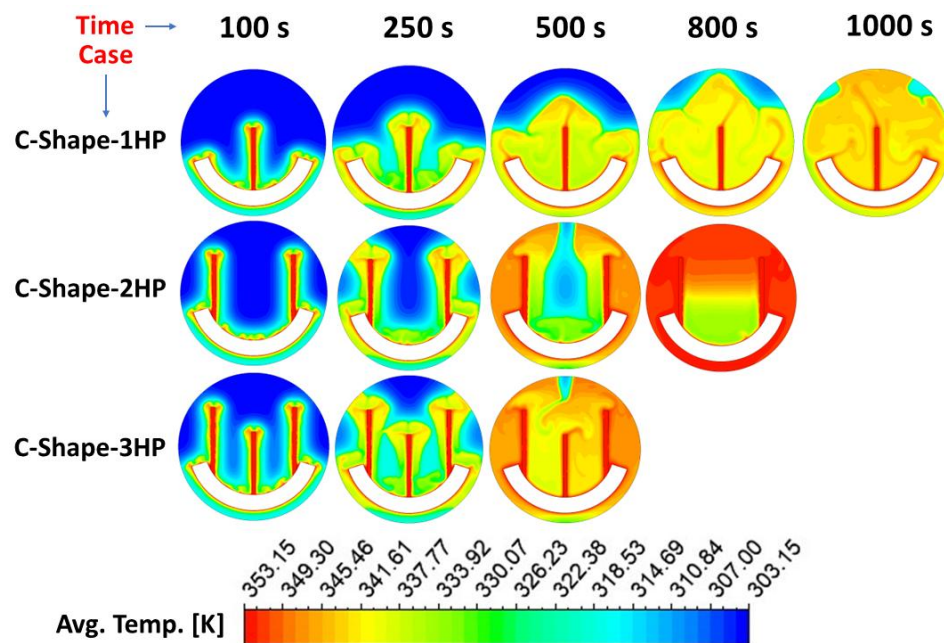


Fig. 4.14 Avg. temperature contours for the C-shape tube and embedded HPs cases are insignificant. The C-Shape-1HP and semi-circular tube cases exhibit the lowest energy storage, with 10% and 5.5% lower values than the circular tube case, respectively. In contrast, the Inv. triangular, triangular, and square tubes exhibit higher energy storage values of about 1.1%, 0.7%, and 0.3%, respectively, compared to the circular tube.

The presence of HPs reduces the amount of PCM in the LHTESS, leading to a diminish in the energy absorbed by the system. However, the C-shape-2HP case accumulates only 1.6% less energy than the circular tube case but exhibits a substantial decrease in melting period by 57.5%. Likewise, the C-shape-3HP case accumulates only 5.2% less

energy than the circular tube case but exhibits a considerable reduction in melting time by 72.2%. Notably, the Inv. triangle case stores the maximum energy of 693 kJ, which is 1.1% more than that of the circular case and reduces the melting time by about 18%.

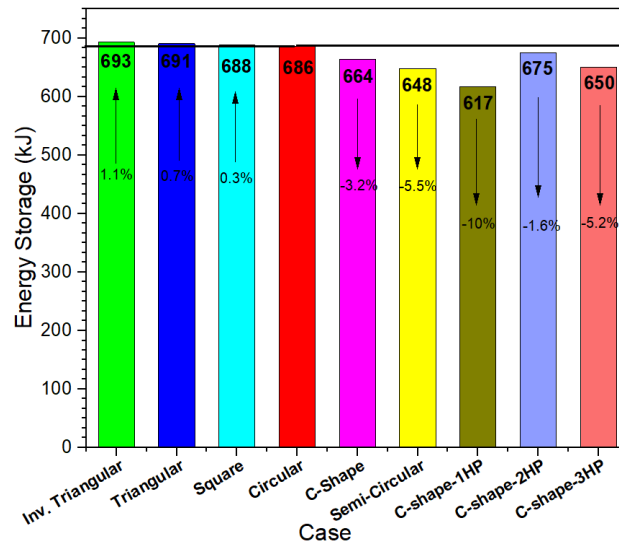


Fig. 4.15 Total energy storage for all considered cases of tube and HPs

The energy accumulated in PCM is a considerable component of the total stored energy in a container, which comprises both the LH and SH absorbed by the PCM. The SH is directly proportional to the average temperature of the PCM, whereas the LH is related to the phase transition phenomena, specifically the molten fraction of the PCM. Hence, it is crucial to analyse the rate of energy accumulation in the PCM, as illustrated in the accompanying Fig. 4.16. Initially, the solid PCM undergoes sensible heating when the temperature is below the liquefaction temperature. Subsequently, the PCM near the tube wall reaches the melting temperature, and melting begins, leading to energy storage as LH. As the thermal conductivity of the PCM is low, heat diffusion from the wall to the PCM's core is slow, resulting in simultaneous sensible heating of the remaining solid PCM and melted PCM. After 1250 seconds, the liquefaction rate of the solid PCM furthest from the tube wall becomes exceedingly sluggish, leading to a near-flat LH curve. However, the accumulation rate of SH increases significantly during this phase, resulting in a steep slope of the SH curve. Among all tube cases, the C-shaped case has the highest LH and SH accumulation rates, which further increase

substantially with the addition of an HP due to its elevated heat transfer capacity within the PCM. The C-shaped-3HP case exhibits the highest LH and SH accumulation rates in all the considered cases.

The mean power of a system, which is the total accumulated energy divided by the entire phase transition time of the PCM, is a crucial factor in TES research. Fig. 4.17 presented in this study demonstrates that non-circular tubes exhibit higher mean power than circular tube due to improved heat transfer in the PCM. Among the non-circular tubes, the C-shaped tube yields the highest mean power of 481 W, which is 65% greater

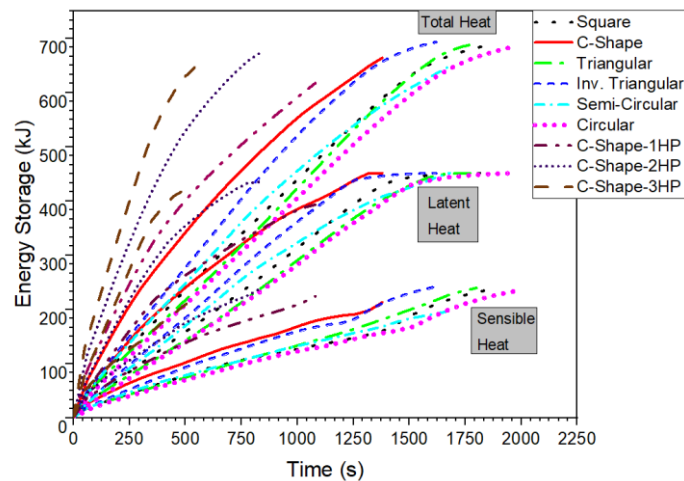


Fig. 4.16 Variation of energy stored for all considered cases of the tube and HPs than that of the circular tube. Additionally, the inclusion of an HP significantly enhances the mean power of the C-shaped tube. The C-shape-3HP case shows the highest increase in mean power, with a 241% improvement over the circular tube case. The C-shape-1HP and C-shape-2HP cases exhibit mean power increases of 65% and 132%, respectively, due to the worthier heat transfer capability of HP deep within the PCM.

The non-circular tubes outperform circular tubes in terms of mean power, showcasing their superior efficiency. While comparing energy storage capacities, the marginal differences within 1.1% are observed between circular and non-circular tube cases, as illustrated in Fig. 4.15. However, a substantial variation emerges in the melting time, with a maximum difference of 30%, as depicted in Fig. 4.9.

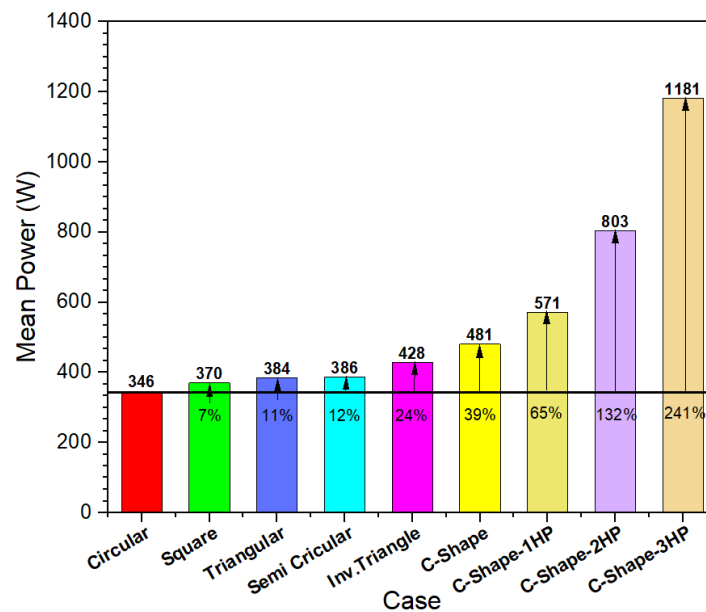


Fig. 4.17 Mean power for all considered cases of tube and HPs

This happens due to the following reasons. First, non-circular tubes feature a larger wall boundary perimeter compared to circular tubes. This expansion results in an enlarged heat transfer region within the PCM. Second, the non-circular tube occupies a larger area near the bottom of the shell, ensuring that more PCM is situated above it. This strategic positioning encourages natural convection over a broader region, thereby enhancing the melting rate [70], [76], [77], as vividly presented in Fig. 4.10. These findings demonstrate that tube shape and the incorporation of HP play critical roles in determining mean power, which is a crucial factor to consider when designing TES systems.

Chapter 5

A numerical study on the influence of fin numbers and material embedded with a heat pipe for thermal charging in a trapezoidal container

5.1 Introduction

Solar energy systems often face the issue of interrupted energy production during cloudy and non-sunlit hours. Thermal energy storage systems (TESS) can impart a practical resolution to this challenge. Among different types of TESS, LHTES is preferred because of its capacity to accumulate roughly 5-10 times extra energy per unit mass compared to sensible heating-based TESS. LHTESS exhibits extensive applicability across diverse domains, including solar water heating [116], solar cooking [117], drying systems, refrigeration, air conditioning [118], temperature management systems, buildings [119], distillation, waste heat recovery systems [120], and more. However, commercially viable PCM used in LHTES have poor thermal conductivity [41], [121], resulting in significantly longer thermal charging (THC) times and rendering the system economically unviable. Furthermore, the large temperature gradient in the PCM can induce excessive heat and material breakdown [42] due to the sensible THC process. To mitigate these issues, several techniques have been developed to reduce THC time, including the (1) integration of materials with elevated thermal conductivity such as metal powder (e.g., Al, Cu, Fe) [43], [44] and nanoparticles (For example Carbon), [46], [47] (2) the insertion of fins (e.g., Al, Cu) [111], metal matrix and foam [48], [122], heat pipe (HP) [42], [52], modification of the configuration and dimensions of the PCM enclosure [53], [54], changing the slope of the PCM enclosure [57], [58], altering the relative position of the PCM and heat source [60], continuous rotation of the PCM enclosure [101] and gravity variation [123].

Modifying the shape of the PCM's enclosure unit has emerged as the most cost-effective solution compared to adding expensive high thermal conductive materials to the PCM. Therefore, researchers have dedicated considerable efforts to identify

optimized shapes of the system, such as rectangular, conical, cylindrical, trapezoidal, spherical, and shell and tube, in various orientations. Zivkovic and Fujii [67] established that a rectangular enclosure consumes 50% less melting time than a cylinder enclosure when the largest dimension is placed horizontally for equal heat transfer region and PCM mass. Vyshak and Jilani [84] further contrasted the shell and tube enclosure with rectangular and cylinder for the same PCM mass and equal heat diffusion region. Shell and tube enclosure demonstrated the best THC performance among all, and THC impact is further enhanced by increasing the mass quantity. Seddegh et al. [79] further minimized the THC time by about 12% by giving the conical shape to the cylindrical shell in a vertical orientation. This happens due to the taper configuration promotes natural convection in a greater proportion of PCM at the upper part of the container. Similarly, Sodhi et al. [54] also considered the same geometry but in a horizontal orientation. They found a similar result, which favours the conical shell for reducing the THC time. They stated the optimized angle of about 3.4 degrees for 54, and 98.6 mm front and rear diameter of the conical shell. The shifting of more PCM in the upper region of the container promotes the natural convection process in the larger domain and drastically reduces the THC time. This strategy was also successfully approved by Iachachene et al. [55] by considering the trapezoidal enclosures. By taking a wider PCM trapezoidal enclosure at the upper region and heat transfer by the side wall, THC time was reduced by about 53% as opposed to the wider region at the bottom of the trapezoidal enclosure.

One of the commonly used approaches to enhance THC in PCM is by incorporating HP and fins, which can be easily installed and integrated with PCM. HPs possess the capability to convey substantial heat across extended distances with minimal cross-sectional area while maintaining low-temperature gradients and almost isothermal heat sources for integrated fins. HPs can also be employed as a thermal diode [49] to operate unidirectionally. In comparison to other heat transfer enhancement techniques, fins are less expensive and simpler to fabricate. In a study conducted by Abhat [49], the effectiveness of vertical fins integrated with a single HP in a PCM enclosure was examined. The HP was placed horizontally, and the fins were added in a vertical direction. Abhat identified that the fins' dimensions and the heat source's temperature

are the most significant variables affecting the system's performance. The work by Tiari et al. [85] investigated the employment of vertically positioned HPs integrated with multiple horizontally aligned fins of varying lengths in a rectangular enclosure. By augmenting the number of HPs from 1 to 3, they observed a reduction in THC time of approximately 10%. However, the improvement in performance was not significant with a further increase in the number of HPs, thus warranting the determination of the optimal number of HPs based on PCM mass. Moreover, increasing the length of the fins reduced the temperature gradient in the PCM regions, which led to improved performance. Zhang et al. [89] established that the integration of fins and HPs improved the THC performance significantly, surpassing the foam(Cu)-fins-HP combinations in the TESS unit. Similarly, Sharif et al. [124] showed that using a single HP in a vertically placed PCM enclosure led to enhanced THC impact, which was further increased by raising the height of the container while keeping the PCM mass constant. Yang et al. [90] horizontally incorporated HP in cylindrical-shaped encapsulated PCM to reduce the total THC time by approximately 11.2% compared to the case without HP. Li and colleagues [125] conducted experimental investigations to assess the impact of integrating HP into the PCM. Their findings revealed a significant enhancement in heat transfer within the PCM due to the incorporation of HPs, resulting in a vertical temperature gradient of less than 1.5 °C.

According to the literature survey, it is apparent that repositioning the PCM towards the upper portion of a vertically oriented container yields significant benefits in reducing THC time. Therefore, the use of trapezoidal or conical containers with a wider top is a preferable approach to decrease the overall liquid fraction time. Additionally, integrating HP with fins (HP-Fins) in a trapezoidal LHTESS unit may further enhance THC performance. While most studies have focused on implementing HP-Fin in rectangular and cylindrical enclosures, additional investigation is required on the incorporation of HP-Fins in trapezoidal systems. There is a lack of studies for HP-Fin embedded PCM trapezoidal systems with variable length fins and different fin materials. Thus, to assure commercial viability, the THC performance of the system should be comparable to its cost.

To develop efficient LHTES, this study seeks to explore the effects of HP-Fins in trapezoidal containers through numerical analysis. The first objective is to assess the THC aftermath of the number and length of fins with a single HP in a trapezoidal enclosure. The fins' Al material (as a base case) is later replaced with Cu and Steel of the same dimensions. The second objective is to make a comparative examination between Al, Cu and steel fins integrated with HP in a trapezoidal container using various THC performance benchmarks such as liquid fraction rate, average (avg.) temperature time history, contours of liquid fraction and avg. Temperature, total THC time, total energy storage, energy storage rate, enhancement ratio, mean power, and cost per mean power.

5.2 Thermal model

Fig. 5.1 depicts a two-dimensional trapezoidal enclosure characterized by a height of 250 mm and a bottom width of 150 mm. The inclined side wall, with an inclination of 76 degrees from the horizontal base, forms an integral part of the enclosure. Rubitherm 55 (RT55) [40], [126], possessing properties detailed in Table 5.1, has been chosen as PCM and is securely enclosed within the trapezoidal structure. HP are strategically inserted vertically along the central axis of the trapezoidal enclosure, serving as conduits for efficient THC from the bottom wall into the PCM and fins.

Table 5.1 Thermophysical characteristics of materials

	PCM	HP	Al	Cu	Steel
C_p (J/kg K)	2000	381	871	381	502.4
$T_{\text{solidus}}, T_{\text{liquidus}}$ (K)	324-330	-	-	-	-
ρ (kg / m ³)	880	8978	2719	8978	8030
β (1/K)	0.00011	-	-	-	-
L (J/kg)	170000	-	-	-	-
μ (kg/m s)	0.03	-	-	-	-
k (W/m K)	0.2	38000	202.4	387.6	16.27
Cost (\$/kg)	22.34	-	2.57	4.46	1.91

The HP features a diameter of 10 mm and a length of 230 mm. Variable-length fins have been horizontally inserted on both sides of the HP to elevate heat diffusion

uniformly throughout the PCM by extracting heat from the HP. These variable-length fins are uniformly spaced within the PCM. The physical models under analysis consist of six sets, each containing a single HP, as detailed in Table 5.2, and illustrated in Fig. 5.2.

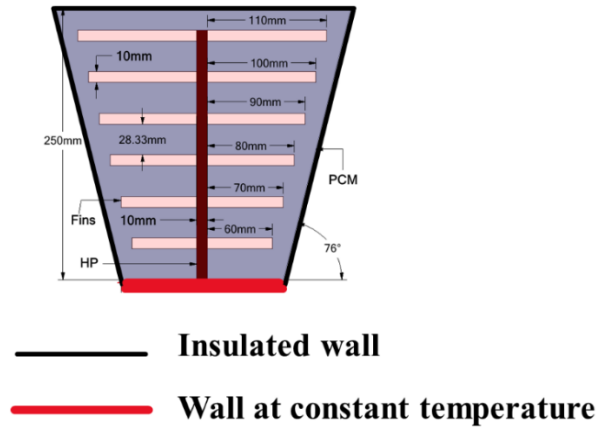


Fig. 5.1. 2D representation of the physical model for the trapezoidal container and its wall conditions.

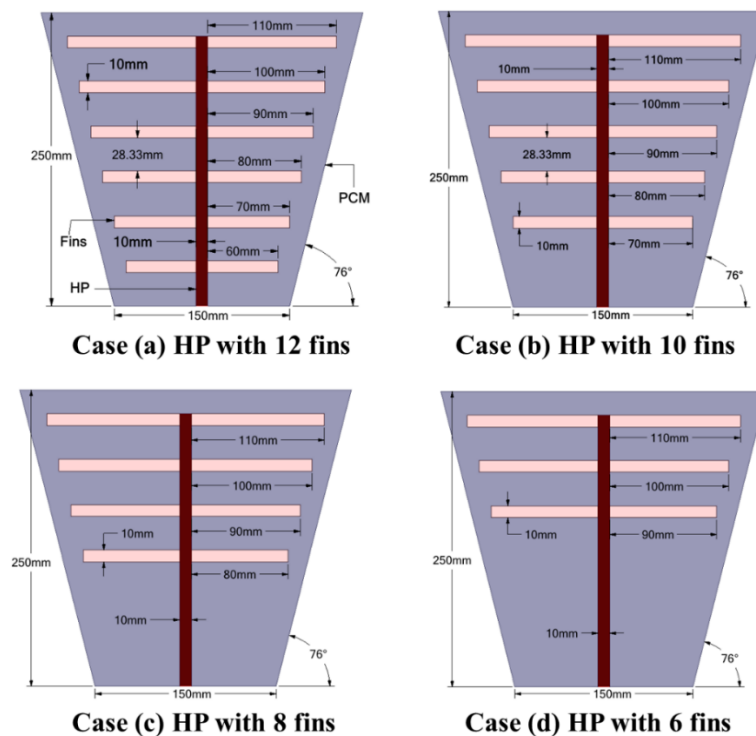


Fig. 5.2. Physical model illustrating the arrangement of 12, 10, 8, and 6 fins embedded with HP in the trapezoidal container.

Notably, the shortest length of fins is consistently located at the bottom side of the PCM's unit in all models. Taking the model "12-Al-fins" as an example, the shortest fin length is 60 mm, with the upper fin length progressively increased by 10 mm. This consistent progression is maintained across all six models, ensuring a maximum fin length of 110 mm. The thermophysical properties of both the HP [94] and the fin materials (Al, Cu, and Steel) [98], [127] have been integrated into Table 5.1 for comprehensive reference.

Table 5.2 Physical model analysed

Model Name	No. of HP	No. of fins	Fin's material
12-Al-fins	1	12	Al
10-Al-fins	1	10	Al
8-Al-fins	1	08	Al
6-Al-fins	1	06	Al
12-Cu-fins	1	12	Cu
12-Steel-fins	1	12	Steel

5.3 Numerical Model

To simulate the THC of PCM in the LHTESS, the enthalpy-porosity [128] procedure is utilized. The merged conduction and convection process is employed to investigate the thermal diffusion within the LHTESS. The mushy zone explicitly defines the solid-liquid interface. ANSYS Workbench is employed to generate the geometry and mesh. During the CFD analysis, the following presumptions are considered.

- A 2D model is adopted to evaluate the THC productivity of the LHTESS.
- Viscous dissipation effects are negligible.
- The Boussinesq approximation [113] is valid for the density alteration in the fluid.

- The liquidus and solidus phases of the PCM are employed to be homogeneous and isotropic throughout the system.
- The molten PCM is assumed to exhibit Newtonian behaviour, with a laminar flow regime and incompressible characteristics.
- Throughout the phase transition phenomenon, any changes in the PCM's volume and the movement of solid PCM are disregarded.
- The contribution of heat transfer through radiation is insignificant.
- Thermal interface resistances are neglected in the analysis.

Based on the previously stated assumptions, the governing equations are formulated as explained in Chapter 3.

The simulation is conducted using the ANSYS Fluent 2022 software package, a widely adopted commercial software solution. The SIMPLE algorithm [80], [99], [100] is employed for the resolution of the pressure-velocity coupling. The second-order upwind discretization approach is applied to resolve the momentum equations, while the pressure equations are tackled with the PRESTO! scheme [98], [101], [102]. To achieve accurate results, suitable under relaxation factors are applied, specifically 0.3 for pressure, 0.7 for velocity components, 0.9 for liquid fraction, and 1 for energy. The attainment of solution convergence is monitored meticulously at each time step, ensuring that the residuals of the energy, velocity components, and continuity equations fall below the specified thresholds of 10^{-7} , 10^{-5} , and 10^{-4} , respectively.

➤ HP

Heat pipes (HPs) are a class of passive thermal management devices that utilise the liquid-vapour phase change of an internal working fluid to achieve exceptionally high heat transfer rates, often far exceeding those attainable with conventional solid conductors. However, accurately modeling the complex hydrodynamic and thermodynamic phenomena occurring within HPs—such as evaporation, condensation, capillary action, and vapor flow—presents significant challenges due to their intricate multi-phase interactions. Capturing these detailed processes requires highly sophisticated numerical models, which impose substantial computational costs that exceed the practical limits of this study.

To focus the investigation on the thermal charging characteristics of the PCM, a simplified approach is adopted for modeling HPs in the simulation. In line with widely accepted practices in the literature, HPs are approximated as highly thermally conductive components with a constant and uniform thermal conductivity. Previous studies have reported equivalent thermal conductivity values for HPs ranging from 30 kW/m·K to 100 kW/m·K [75], [79]. For the purposes of this analysis, HPs are modeled with an assigned thermal conductivity of 38,000 W/m·K [94], [95] which effectively replicates their high heat transfer capability while significantly reducing computational complexity. This simplification enables efficient simulation of the PCM melting behavior without compromising the key thermal effects imparted by the presence of heat pipes.

5.4 Boundary conditions and Model validation

For simulating the LHTESS, we consider specific initial and boundary status. At the simulation onset ($t = 0$), all constituents are presumed to be at a consistent temperature of 315 K. The enclosure's walls, excluding the bottom wall, are set to adiabatic conditions, while the lower surface is upheld at a consistent temperature of 360 K, as depicted in Fig. 5.1.

The accuracy of unsteady numerical solutions should be independent of both mesh size and time step size. To verify mesh independence, Fig. 5.3 illustrates the melt fraction variation with different cell numbers considered in this study. Three different element numbers—19000, 24000, and 30000—were investigated for mesh independence analysis. From Fig. 5.3, it is manifest that the melt fraction results for element numbers 24000 and 30000 are very close, with a deviation of less than 2%. To expedite the simulation process, an element number of 24000 was selected for the subsequent investigation. Similarly, a time step of 1 s was employed in the solid PCM domain, reducing to 0.05 s following the initiation of the phase transition. Further time step refinement did not improve computational accuracy. Hence, a time step size of 0.05 s was selected for the remaining part of the study to optimize computational efficiency. For numerical model validation, the results accomplished in this investigation were compared with those reported in prior published experimental and numerical outcomes. Fig. 5.4(a) and Fig. 5.4(b) illustrate the melt front locations at various time

points and liquid friction time history in the current study alongside published simulation results by Mahdavi et al. [40]. The liquid fraction front exhibits substantial

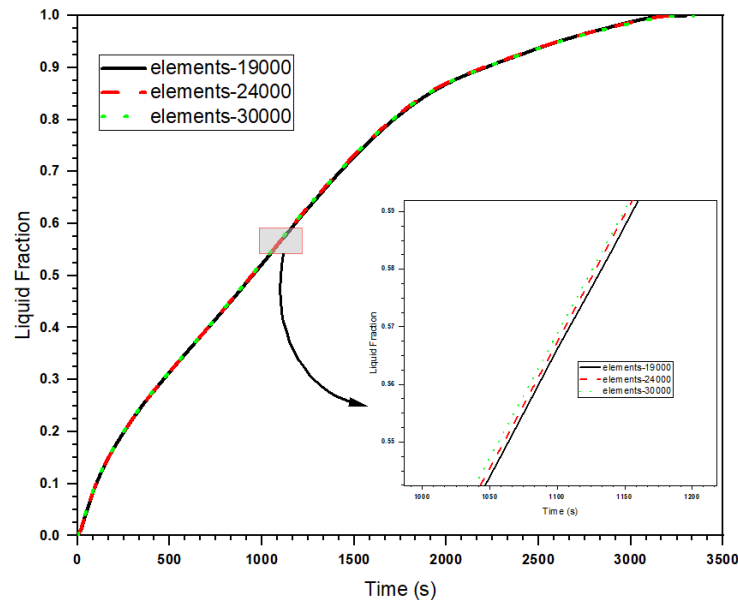


Fig. 5.3. Investigation into mesh independence.

similarity between the current numerical simulation and the published results. The evaluations in Fig. 5.4 (b) indicate that the maximum deviation in the THC time between the present investigation's results and the published simulation study is approximately 1%. Furthermore, the thermal charging outcomes of the heat pipe, fins, and PCM integrated within a rectangular container, as studied by Tiari, Qiu, and Mahdavi [85], have been juxtaposed with our findings in Fig. 5.4 (c). The Maximum difference in thermal charging time between our investigation and the referenced research is less than 1.5%. This validates the credibility of the numerical methodology adopted in our study.

To experimentally validate our current model, we examined the locations of the solid-liquid boundary of Gallium at specific time intervals. A comparative analysis was then conducted, aligning our results with the experimental observations of Gau and Viskanta [115], the numerical analysis by Brent and colleagues [92], and the numerical analysis undertaken by Khodadadi and Hosseinzadeh [45], as depicted in Fig. 5.5. The slight deviation noticed between the predicted melting interface in our model and the experimental observations can be ascribed to two potential factors. Firstly, achieving precise temperature control of the heat and cold walls in the experimental setup poses

challenges. Secondly, the model, being two-dimensional, does not encompass three-dimensional effects, contributing to the observed variation. Significantly, a robust agreement is evident between the outcomes of our simulation and those reported in these earlier studies.

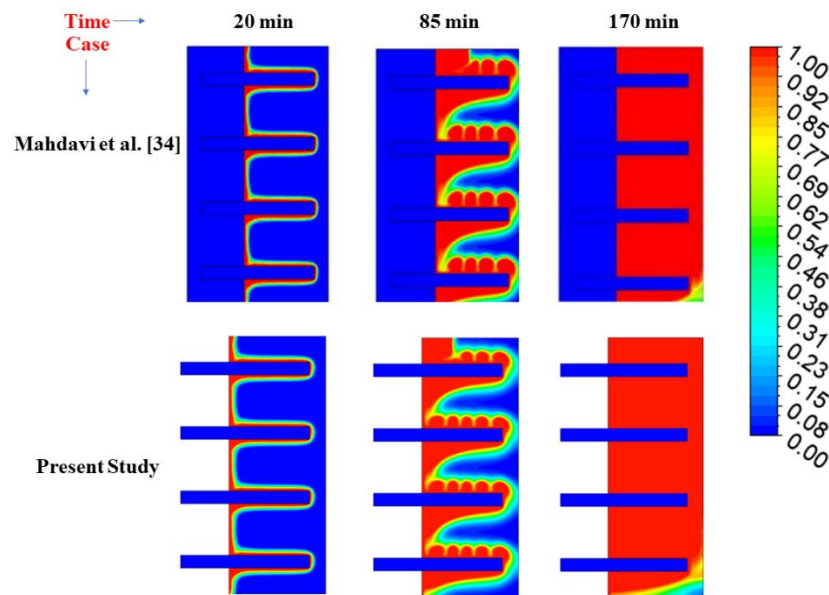


Fig. 5.4(a). Comparative analysis of liquid distribution patterns with those previously reported [40]

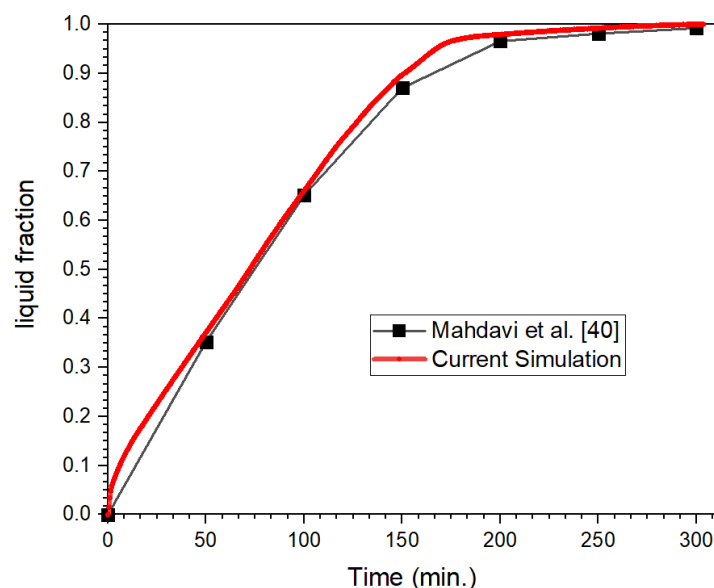


Fig. 5.4(b) Comparative study of the liquid fraction time history in the present research with that of Mahdavi et al. [40]

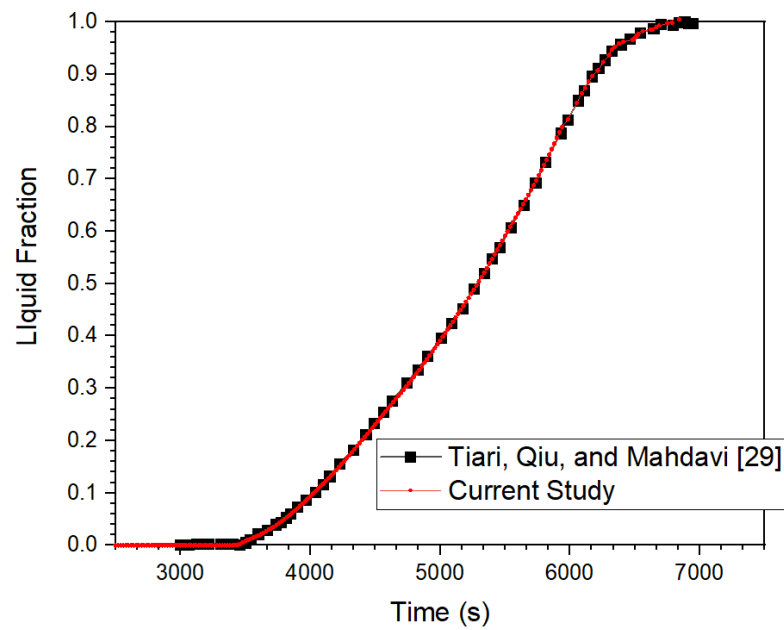


Fig. 5.4(c) Comparative study of the liquid fraction time history in the present research with Tiari, Qiu, and Mahdavi [29]

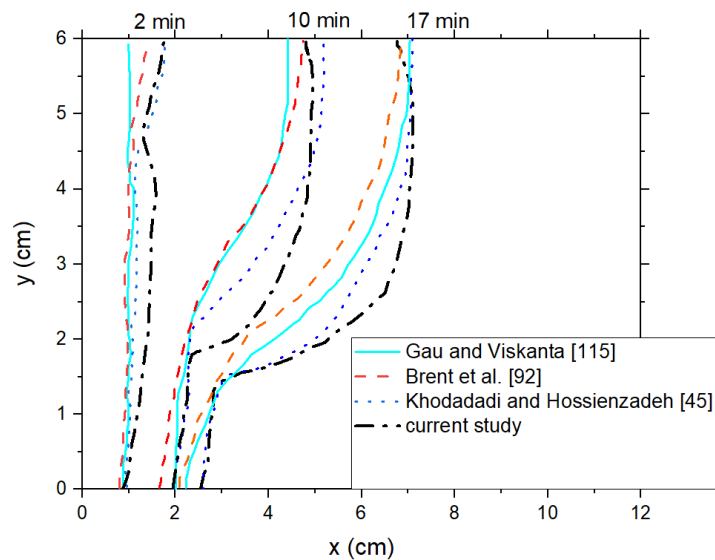


Fig. 5.5 Comparative analysis between our current study and prior research conducted by Gau and Viskanta [115], Brent and colleagues [92], and Khodadadi and Hosseinizadeh [45]

5.5 Results and discussion

The liquid fraction time history of the PCM across various scenarios is depicted in Fig. 5.6. In the initial phase, liquid fraction growth is characterized by a steep, linear melting rate for all cases. Subsequently, this trend undergoes a transition marked by a progressively diminishing slope until the entire melting process concludes. Notably, in cases featuring 12-Al-fins and 12-Cu-fins, the reduction in melting rate becomes apparent after reaching 0.85 liquid fraction. In contrast, for 6-Al-fins and 12-steel-fins cases, this shift occurs at 0.53 and 0.66 liquid fractions, respectively. This observation suggests that configurations with a higher number of fins, especially those composed of high thermal conductivity materials, sustain an elevated rate of THC within the system. Specifically, the 6-Al-fins case exhibits the slowest melting rate, while the 12-Cu-fins case demonstrates the highest. Although initially, the melting curve for 6-Al-fins exhibits a steeper slope than that of 12-steel-fins, it eventually drops below the curve of 12-steel-fins after 2880 seconds and a liquid fraction of 0.66. This underscores the intricate interplay between fin quantity, material conductivity, and the dynamic evolution of PCM melting characteristics within the studied configurations.

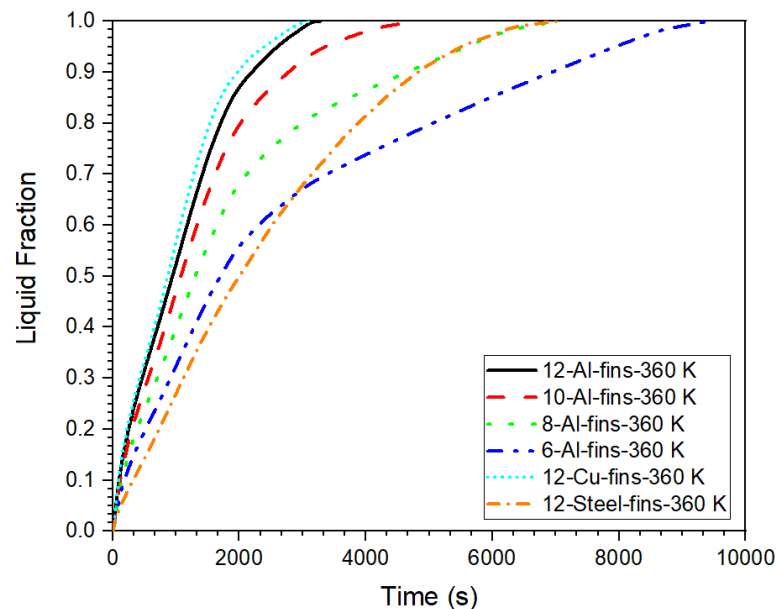


Fig. 5.6. Time history of molten fraction for various numbers and materials of fins embedded with HP.

To delve deeper into the investigation of the melting rate, we introduce an enhancement ratio (e_r) parameter, defined by Eq. (5.2), to quantify the influence of the arrangement of fin length and material on the THC of PCM.

$$e_r = \left[\frac{\lambda}{\lambda_c} - 1 \right] \times 100\% \quad (5.2)$$

Where λ and λ_c are the liquid fraction of the considered and reference cases for the same instant of time. This parameter reflects the aftermath of the fins' number and material on the rate of PCM melting.

Using 6-Al-fins as the reference case, Fig. 5.7 illustrates the temporal variation of e_r . Initially, 12-steel-fins exhibited a negative e_r , designating a slower phase transition rate compared to the base case. However, at a liquid fraction of 0.66, it surpasses the baseline, reaching a maximum of 15% (e_r) at a liquid fraction of 0.93. This phenomenon is attributed to the initially lower thermal conductivity of steel, leading to prolonged heat diffusion times in the fins. In all other cases, except for 12-steel-fins, positive e_r values persist throughout the entire melting duration. The maximum enhancement ratio in these cases occurs between 0.07 and 0.09 liquid fraction, after which that maintains a nearly constant value from 0.14 to 0.82 liquid fraction before starting to decline. Comparatively, 12-Cu-fins exhibit the highest, while 12-steel-fins display the lowest enhancement ratio across all cases. The increasing number of Al fins demonstrates a higher enhancement ratio, but this impact diminishes with an increasing number of fins. These findings underscore that fins with greater thermal conductivity and a higher quantity contribute to a faster PCM melting rate.

Fig. 5.8 and Fig. 5.9 represent the liquid fraction contours of various situations. In Fig. 5.8, during the initial phase ($t \leq 1000$ s), the scenarios with varying numbers of fins display a comparable melting pattern. Molten PCM is primarily concentrated around the fin, bottom wall, and HP region. By the 2000 s, the molten zone is observed to have expanded to the immediate surroundings of fin's, HP's, and bottom's wall. In 6-Al-fins and 8-Al-fins cases, fins unoccupied PCM region remain un-melted after 3000 s. In this un-melted region, heat diffuses from the upper melted region through conduction and by natural convection from the bottom wall. Fig. 5.9 reveals that the melting pattern is similar in the case of Al and Cu fins for an equal number of fins. However,

when using steel fins, a greater extent of melting is observed near the heat pipe and along the lower boundary of the enclosure. Subsequently, this occurs due to the comparatively lower thermal conductivity of steel fins in contrast to Al and Cu. After 5000 s, the last un-melted PCM was found at the upper and towards the side wall of the enclosure. Therefore, the choice of fin number and material significantly dictates the evolution of the solid-liquid boundary in the PCM.

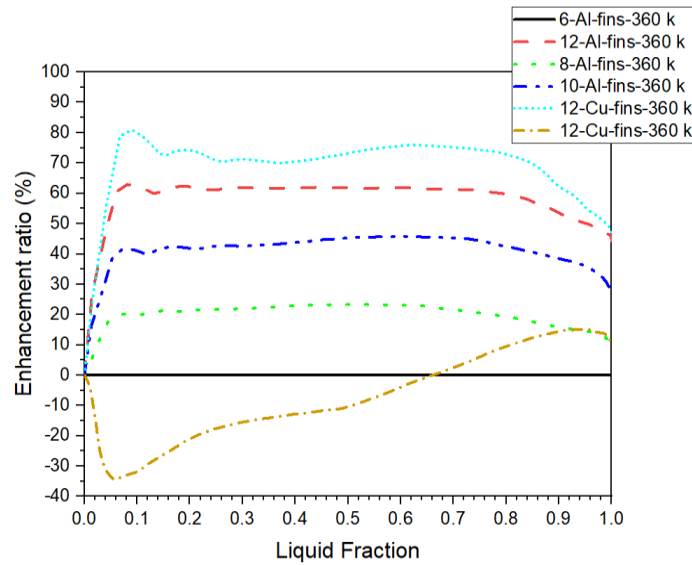


Fig. 5.7. Time history of enhancement ratio for all cases under consideration.

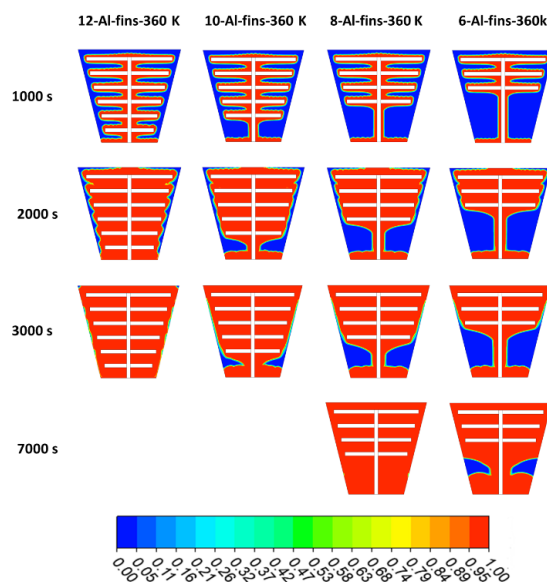


Fig. 5.8. Contour representation of liquid fraction for 12, 10, 8, and 6 fins embedded with HP.

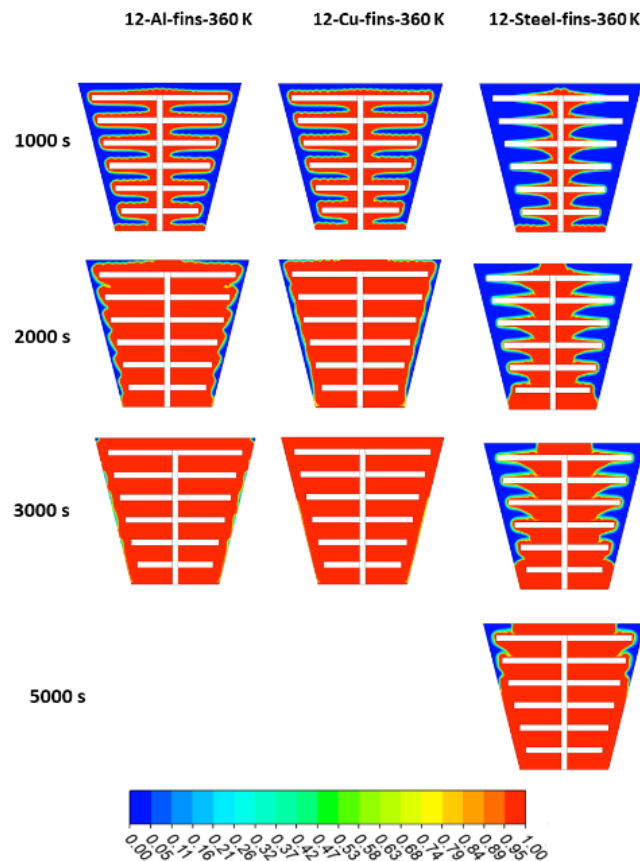


Fig. 5.9. Contours illustrating liquid fraction for fins made of Al, Cu, and Steel embedded with HP.

Fig. 5.10 and Fig. 5.11 depict temperature distribution contours for various cases. In Fig. 5.10, as the number of variable fins increases, heat diffusion within the PCM improves, leading to a more uniform temperature spread. The outcomes reveal that, initially, the presence of a higher number of variable fins facilitates rapid melting due to enhanced heat diffusion. However, as the process advances, the concentration of heat between the fins, driven by natural convection, results in a significant diminish in the rate of melting for scenarios with a lower number of fins.

In Fig. 5.11, the 12-Steel-fins case exhibits a more even temperature distribution, surpassing both the Al and Cu cases. This phenomenon arises from the minimal difference in thermal conductivity between the PCM and steel compared to the other two materials.

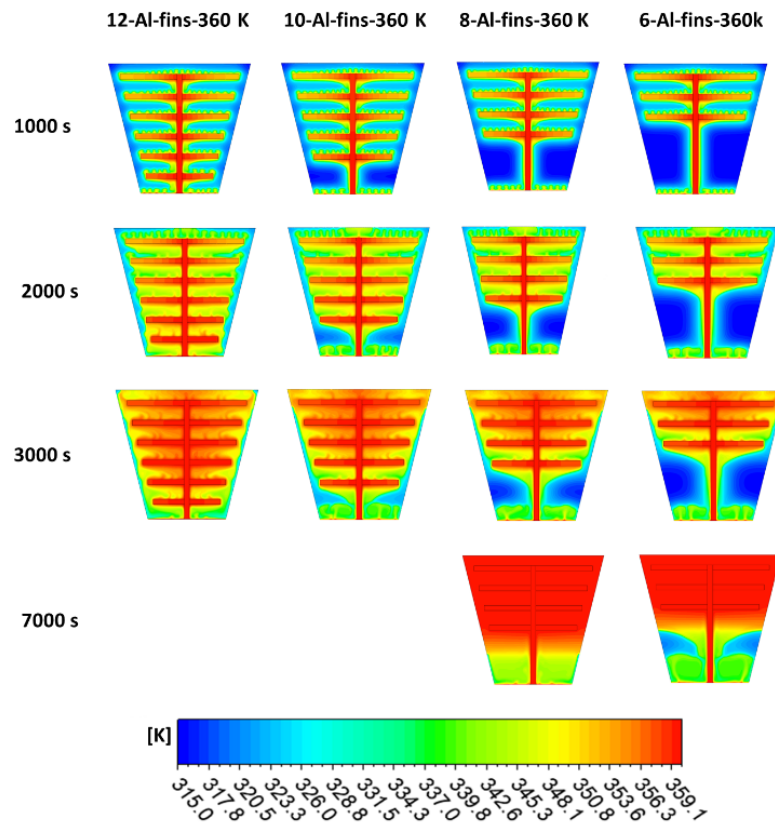


Fig. 5.10. Contour maps of avg temperature for 12, 10, 8, and 6 fins embedded with HP.

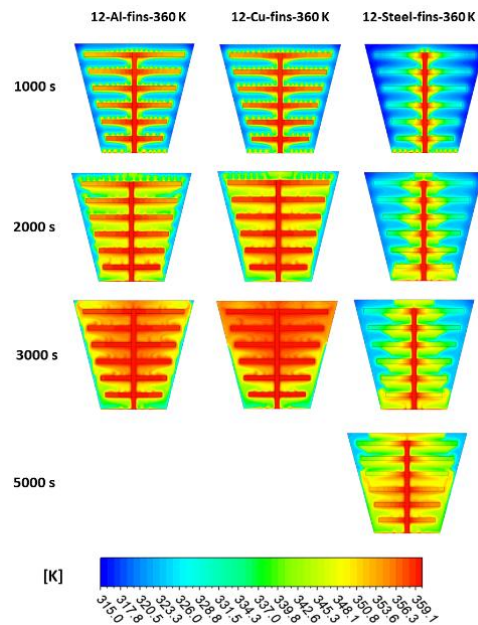


Fig. 5.11. Contour maps of avg temperature for fins made of Al, Cu, and Steel embedded with HP.

➤ Total melting time (t_m)

Using the 12-Al-fins case as the reference, Fig. 5.12 illustrates the t_m . All cases, with the exception of 12-Cu-fins, exhibit a longer t_m compared to the base case. Notably, Cu demonstrates the minimum t_m , succeeded by Al and C-steel cases. This aligns with expectations, considering the superior thermal conductivity of Cu in comparison to steel and Al. The 12-steel-fins and 8-Al-fins cases display nearly identical t_m , underscoring the compensatory impact of raising the number of fins to counterbalance the lower thermal conductivity of the fins. Remarkably, 6-Al-fins and 12-Cu-fins showcase the highest and lowest melting times, representing a 188% increase and a 4% decrease, respectively, compared to the 12-Al-fins case.

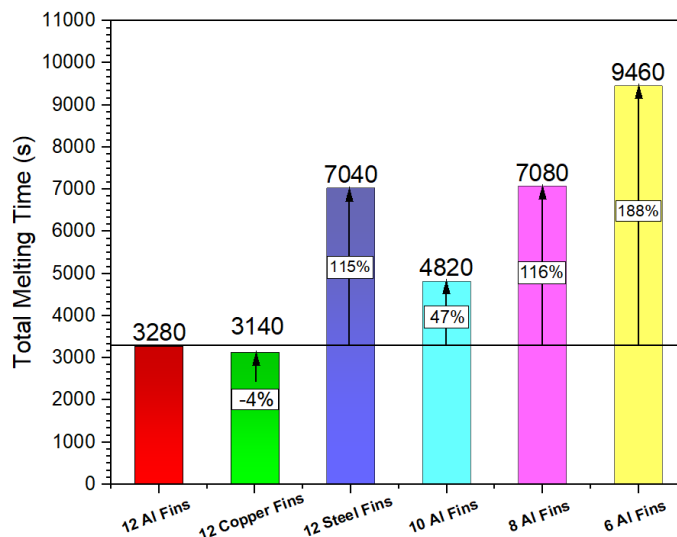


Fig. 5.12 Total melting Time

➤ The avg PCM and fins temperature

Fig. 5.13 displays the avg temperature of the PCM across different situations. Throughout the charging phase, a portion of the heat diffusion contributes to phase change, while the remainder serves to elevate the temperature. Initially, in the early stages of THC, heat propagation predominantly occurs through conduction and natural convection.

Notably, the 12-Al-fins and 12-Cu-fins cases exhibit a similar rate of change in PCM temperature initially. However, as the process advances, the curves begin to diverge, influenced by the differing thermal conductivity of the fin materials. With a lowering in the number of fins, the slope of the curves declines due to a diminished heat transfer

area and non-uniform heat distribution. Interestingly, the 12-steel-fins case initially displays the lowest slope on the temperature-time diagram, followed by the 6-Al-fins case, owing to the relatively low heat transfer rate of steel fins. Nevertheless, at 5760 seconds, the 12-steel-fins curve surpasses that of the 6-Al-fins case, attributed to the extended heat dissipation surface of the fins.

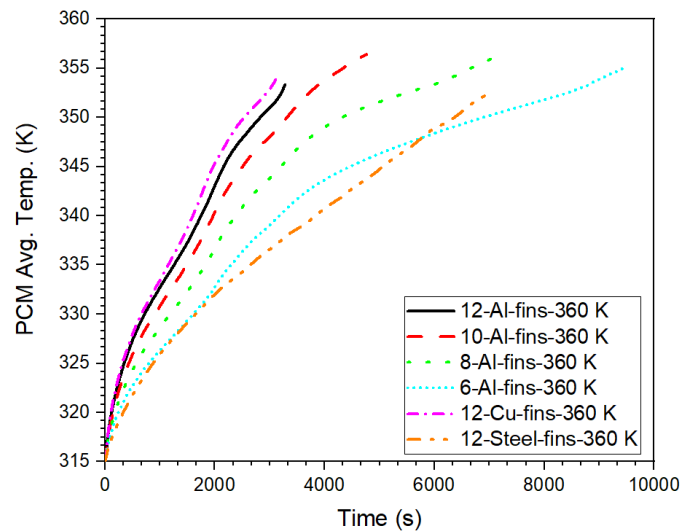


Fig. 5.13. Time history of avg PCM temperature for all cases

The avg temperature of the fins across different cases is illustrated in Fig. 5.14. Initially, the average fin temperature experiences a rapid ascent. Within the first 200 seconds, the avg temperature of the fins reaches its peak value in all cases except for the 12-Steel-fins. The temperature curve for 12-Steel-fins diverges from the others after just 60 seconds, and the curve starts to plateau. This occurrence can be ascribed to the significantly lower thermal conductivity of steel compared to Al and Cu. Consequently, a reduced temperature gradient is available for heat transmission in the PCM in the case of 12-Steel-fins. At 3300 seconds, all cases, excluding 12-Steel-fins, reach the maximum temperature of 359 K, maintaining this level until the attainment of melting completion. In contrast, 12-Steel-fins achieve a maximum temperature of 348 K upon the attainment of melting completion.

➤ Total stored energy (E_s)

The cumulative energy contained by both the PCM and fins within the system constitutes by the E_s . As depicted in Fig. 5.15, all cases exhibit greater energy storage

than the 12-Al-fins Case. Notably, a decrease in the number of variable fins correlates with a boost in the total accumulated energy, owing to the augmented PCM mass within the enclosure. The 6-Al-fins case stores the highest energy, surpassing the 12-Al-fins Case by 7.6%. When the Al fins are replaced with Cu and steel, there is an increment in total energy storage by about 2.2% and 0.2%, respectively.

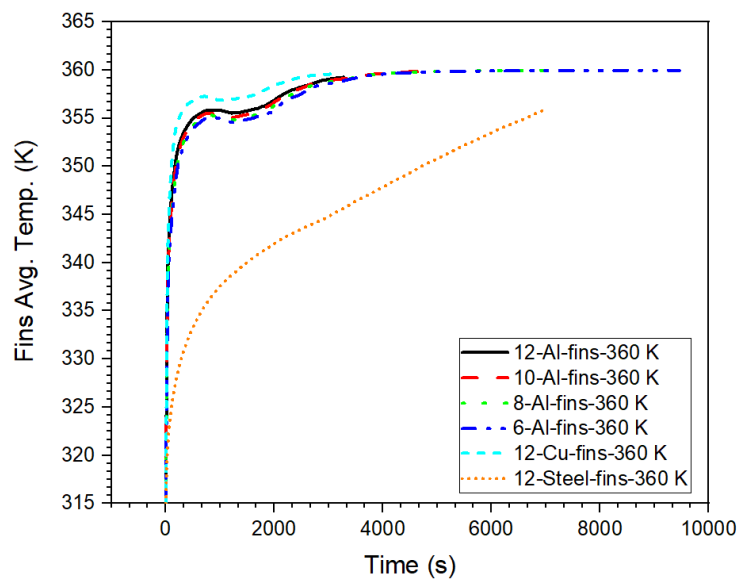


Fig. 5.14. Time history of avg fins temperature for all cases

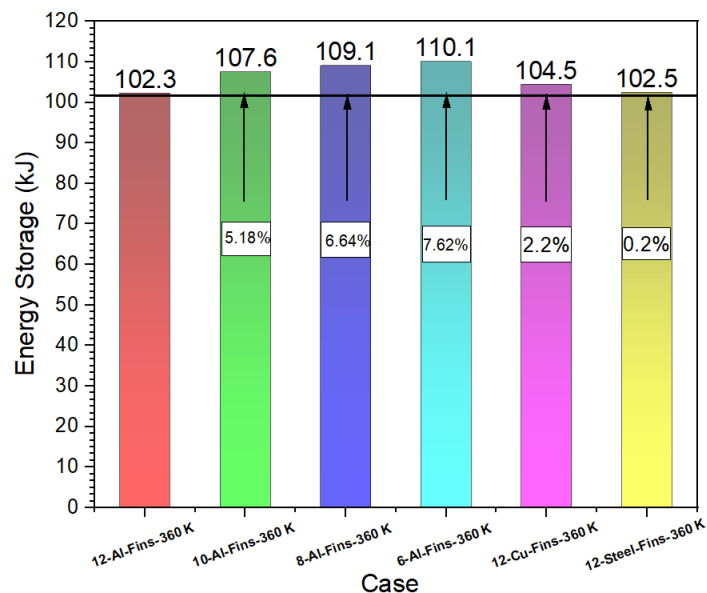


Fig. 5.15. Total energy storage by PCM and fins for all cases

The energy accumulated by the PCM (E_{PCM}) constitutes a substantial fraction of the total stored energy (E_s), encompassing both Q_{latent} and $Q_{sensible}$ imbibed by the PCM. The $Q_{sensible}$ is directly linked to the avg temperature of the PCM ($T_{avg,PCM}$), while the Q_{latent} is associated with the phase transition process (liquid fraction) of the PCM. Therefore, it is imperative to scrutinize the rate of energy accumulation in the PCM, as illustrated in Fig. 5.16. For the 12-Cu-fins case, the rate of energy accumulation is elevated compared to the other cases. Notably, once the PCM has completely liquified, the rate of latent energy absorption tends toward zero in all cases. Concerning the variable fin material, the rate of total heat absorbed is utmost for the Cu fin case, subsequent by the Al and Steel cases, attributed to the substantial rate of sensible heat. The Q_{latent} curve slope for 12-Cu-fins is higher than that of 6-Al-fins at a melting fraction of 0.51. Additionally, as the number of variable fins surges, the impact on the rate of latent and sensible heat becomes more pronounced.

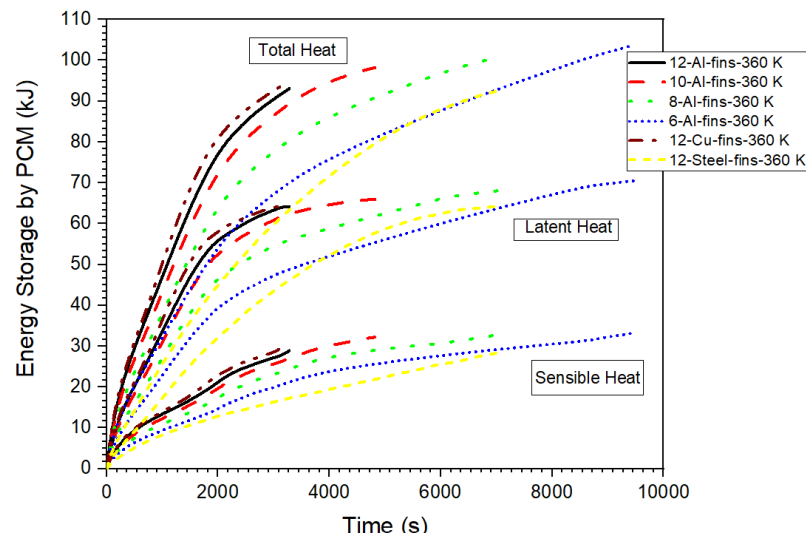


Fig. 5.16. Variation of energy stored by PCM for all cases

➤ Mean power (P_m)

The P_m of the system is defined in the Eqn. (12). In Fig. 5.17, P_m is illustrated for various cases. Remarkably, 12-Cu-fins exhibit the highest P_m , followed by 12-Al-fins and 10-Al-fins. An augment in the number of fins corresponds to an amplification in P_m due to improved heat diffusion, aftermath is a significant minimization in the total melting span compared to the total stored energy. Similarly, when the thermal

conductivity of fins rises with an equal number of fins (12 fins), the mean power also improves, attributed to enhanced heat diffusion within the PCM.

Interestingly, it is perceived that the P_m of the 12-Steel-fins case is lower than that of the 8-Al-fins case. The P_m for 12-Al-fins is 31.2 W, roughly triple the value for 6-Al-fins (11.6 W). These findings underscore the aftermath of the quantity and materials of the fins on the mean power of HP-integrated fins.

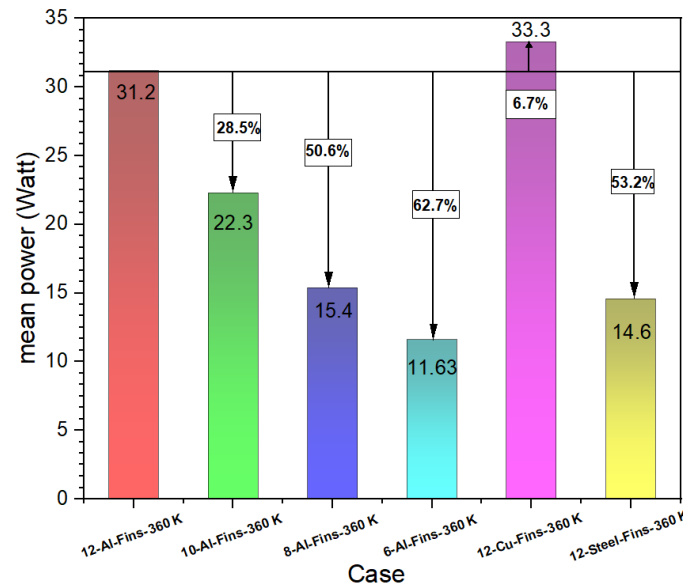


Fig. 5.17. Mean power analysis for all cases

➤ Cost per mean power (C_{cp})

The economic analysis of TESS is pivotal for determining its commercial viability, as its acceptance in the market hinges on cost considerations. Therefore, the cost per mean power (C_{cp}) and the total cost (C_{tt}) of the system are crucial metrics to evaluate the sustainability of TESS in the commercial domain. The C_{cp} and C_{tt} for various scenarios are presented in Fig. 5.18. Notably, the 12-Cu-fins and 12-Al-fins cases exhibit equal and the lowest cost per mean power among all scenarios. This occurs because although 12-Cu-fins have a larger mean power than Al fins, their cost is also higher than that of Al and Steel.

Similarly, the 8-Al-fins and 12-steel-fins cases share an equal C_{cp} but possess values that are 114% higher than the 12-Al-fins case. As the number of fins decreases, C_{cp} also experiences a drastic rise. The 6-Al-fins case, for instance, has a C_{cp} that is 186%

higher than that of the 12-Al-fins and 12-Cu-fins cases. Conversely, the 12-steel-fins case is 114% more expensive than the 12-Al-fins and 12-Cu-fins in terms of C_{cp} . These findings lead to the conclusion that the C_{cp} in the trapezoidal PCM's container can be lowered by escalating the number of variable-length fins with higher thermal conductive material.

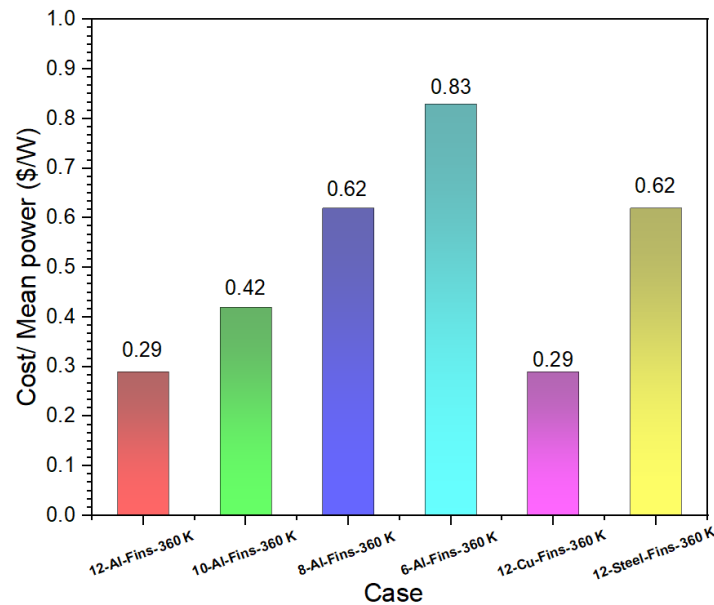


Fig. 5.18. Analysis of the cost per mean power for all cases

Chapter 6

Experimental Investigation of the Impact of Heat Pipes on Latent Heat Thermal Energy Storage Systems

6. Introduction

One promising technique to intensify heat transport efficiency is embedding heat pipes or thermosyphons within the PCM. These components facilitate efficient thermal exchange between a hot or cold external fluid and the PCM phase change interface during melting and freezing. Heat pipes, utilizing vaporization and condensation cycles, operate with extremely low thermal resistance, thereby significantly accelerating the phase change process. Compared to conventional solid fins, heat pipes offer lower thermal mass, further improving the melting and freezing rates of PCMs, making them an attractive solution for overcoming the thermal limitations of LHTES. Mahboobe Mahdavi et al. [40] executed a numerical probe to evaluate the impact of horizontally placed heat pipes within phase change materials on improving thermal efficiency. The results demonstrated that augmenting the number of integrated heat pipes from two to four led to a progressive decrease in thermal charging time by approximately 61.2%, 76%, and 83%, respectively. Moreover, the influence of heat pipes on thermal enhancement was found to be more pronounced than the effect of nanoparticle dispersion in the PCM. Abhat [49] investigated the effectiveness of vertical fins integrated with a single heat pipe (HP) within a PCM enclosure. In this study, the HP was positioned horizontally, while vertical fins were incorporated to boost heat transport. Tiari et al. [85] examined the performance of multiple vertically placed HPs integrated with horizontally oriented fins of varying lengths within a rectangular enclosure. Their outcomes demonstrated that boosting the number of HPs from one to three reduced the thermal charging (THC) time by approximately 10%. However, further increasing the number of HPs beyond three yielded insignificant performance enhancements, suggesting the need to determine an optimal number of HPs based on the PCM mass. Similarly, Sharif et al. [124] analyzed the impact of a

single HP in a vertically positioned PCM enclosure and found that thermal charging efficiency improved with an increase in the container height while maintaining a constant PCM mass. Hai Yang et al. [90] explored the incorporation of HPs in a cylindrical PCM enclosure arranged horizontally. Their study indicated that this configuration led to an 11.2% reduction in THC time compared to cases without HP integration. Motahar et al. [88] experimentally scrutinized the role of HPs in vertical LHTES systems. Their findings revealed that a 15°C amplify in the heat input temperature resulted in a substantial 53% diminish in the thermal charging period, highlighting the significant impact of HPs on accelerating the phase change process. Existing literature has revealed that the melting time in a system (LHTES) can be significantly diminished by embedding heat pipes within the PCM. However, the majority of these investigations have been conducted through numerical simulations or computational modelling. Additionally, heat pipes have predominantly been positioned either vertically or horizontally within the PCM, leaving the effectiveness of inclined heat pipes on the thermal charging rate largely unexplored in experimental studies.

This research is primarily intended to experimentally analyze the impact of inclined heat pipes on the thermal charging rate integrated with a HTF tube within a rectangular shell-and-tube enclosure. To achieve this, three physical models are developed, each incorporating two, four, and six heat pipes. The thermal behavior of the PCM in these configurations is systematically investigated by evaluating total melting time, melting patterns, and PCM temperature distribution.

6.2 Experimental Setup

A photograph of the experimental setup and layout used in the present study is exhibited in Fig. 6.1(a) and Fig. 6.1(b). The heat exchanger consists of a tube-in-shell configuration, where the tube has an outer diameter of 26 mm and a wall thickness of 4 mm. Low-carbon steel is selected as the tube material due to its mechanical strength and good thermal properties. The shell has a rectangular geometry with inner dimensions of 250 mm × 230 mm × 50 mm and is fabricated from polycarbonate. The use of polycarbonate allows clear visualization of the melting and solidification fronts, making it ideal for phase change studies. Additionally, polycarbonate exhibits very low

thermal conductivity, minimizing heat loss during the experiment. To further reduce thermal losses, the shell is designed with a wall thickness of 5 mm, ensuring that heat dissipation through the shell is negligible.

To facilitate the circulation of the HTF (water) and allow for flexible positioning of the heat exchanger, flexible tubes are used for fluid flow. Water is normally used as an HTF as it is low in cost and has a high specific heat. In addition, its properties like the volumetric expansion rate, fluid internal friction, thermal capacity, crystallization point, vaporization temperature and factors like low cost, larger availability, nontoxicity and the absence of expensive pressure equipment for circulation, favour the choice of water as the HTF.

Initially, the HTF temperatures in the hot water baths are set to the desired values. Once the target temperatures are achieved, the HTF is transported through the inner tube of the LHTESS using a pump. The HTF exiting the heat exchanger is then recirculated back to the water bath, ensuring a continuous flow loop and maintaining stable thermal conditions throughout the experiment. Paraffin wax, sourced from Prem Oil Corporation, Delhi, is utilized as the PCM in this study.

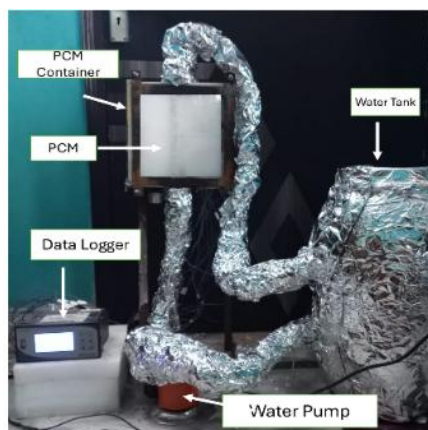


Fig. 6.1 (a)

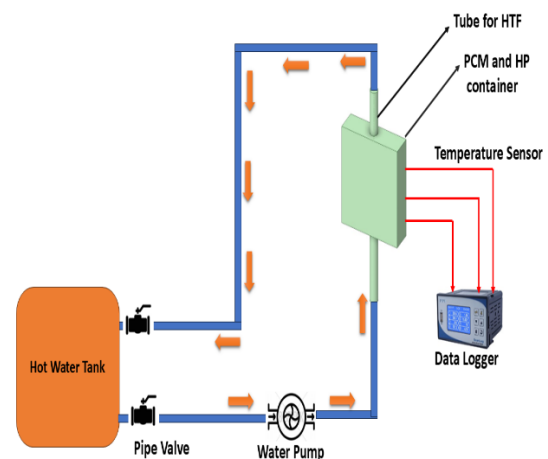


Fig. 6.1 (b)

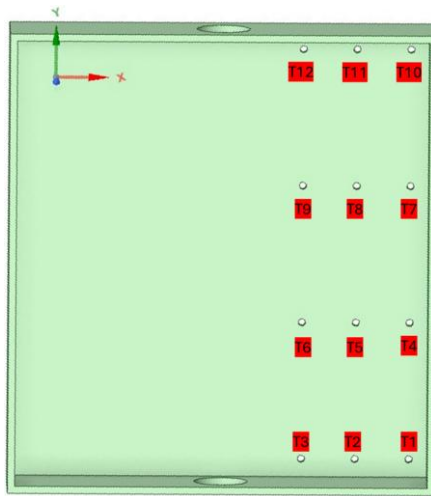


Fig. 6.1 (c)

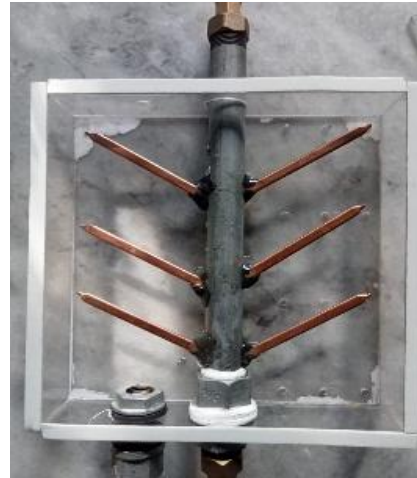


Fig. 6.1 (d)

Fig. 6.1 (a) Experimental setup, Fig. 6.1(b) Experimental setup layout, Fig. 6.1 (c) RTD positions, Fig. 6.1 (d) Heat pipe locations

To ensure uniform distribution, the molten PCM is carefully poured into the heat exchanger, completely occupying the rectangular space between the shell and tube. Prior to commencing the experiments, meticulous checks are performed to confirm that the entire setup is free from leaks. In this study, HTF is introduced from the bottom of the system. For experimental evaluation, the HTF temperature is maintained at 85°C, while the ambient temperature remains at 20°C.

As illustrated in Fig. 1 (c), a total of 12 resistance temperature detectors (RTDs) are strategically positioned to assess the temperature distribution of the PCM. These RTDs are arranged to capture both vertical and horizontal temperature variations, ensuring a comprehensive thermal analysis. Additionally, two RTDs are integrated at the inlet and outlet of the HTF to monitor its temperature variations throughout the process. The specific RTD locations are marked in Fig.1 (c), where T3, T6, and T9 correspond to Vertical positions, while T12, T11, and T10 represent horizontal positions. Temperature readings at all designated points are recorded every three minutes using a PPI data acquisition system, which enables precise monitoring of thermal behaviour. The recorded data is first stored on a pen drive and later transferred to a laptop, where it can be analysed and visualized for further evaluation.

Six copper heat pipes, each measuring 3 mm × 8 mm × 100 mm and having a heat transfer capacity of 70 W, are integrated on both sides of the HTF tube as indicated in Fig. 6.1 (d). The heat pipes are oriented at an angle of 35° with respect to the horizontal axis, based on their central longitudinal axis.

During the charging phase, the HTF-water was preheated to a predetermined temperature in a 30-litre hot water tank. This was achieved using a 2 kW electric immersion heater equipped with externally adjustable thermostats, allowing precise ± 0.1°C temperature control. The heated water was circulated efficiently throughout the system using a Btali centrifugal pump, ensuring uniform thermal distribution. Once the shell unit was filled with PCM, it was maintained at ambient room temperature (20°C) for a minimum of 24 hours to ensure thermal equilibrium. This step allowed the solid PCM to reach a uniform temperature throughout the system, eliminating any initial temperature gradients. By stabilizing the PCM before experimentation, accurate and consistent thermal performance measurements could be achieved. To systematically evaluate and compare the performance of varying thermal storage units, three key parameters were introduced: PCM temperature at every probe, liquid fraction, and melting time.

6.3 Results and Discussion

The experimental study was conducted with water as the HTF at a constant temperature of 85°C, flowing in an upward direction with a constant flow rate. Three different configurations were examined: Case 1 with six inclined heat pipes, Case 2 with four inclined heat pipes, and Case 3 with two inclined heat pipes, to evaluate the consequences of heat pipe quantity on thermal performance under identical operating conditions.

The melt fraction is determined by analysing the surface area of the melted and solid PCM in captured images. In the photographs, the melted portion appears transparent, resembling water, while the solid PCM remains opaque with a white appearance. The surface area of both phases is measured using ImageJ software, which facilitates precise image analysis. This method provides an accurate assessment of the melting

process by distinguishing between liquid and solid regions based on their visual characteristics.

All temperature profiles exhibited a continuous rise with charging time. Initially, the temperature increased steadily, indicating that the PCM was in the solid state and being heated primarily through conduction—an outcome expected due to the PCM's inherently low thermal conductivity. When the temperature at a specific RTD probe location approached the PCM's melting range, the rate of temperature increase began to decline, signifying the onset of the phase change process. Once melting commenced, a steeper rise in temperature was observed, suggesting that the melting front had moved past the RTD probe and heat transfer was now occurring via natural convection in the liquid PCM.

The timing and rate of temperature rise varied across RTDs based on their position relative to the heat pipe and vertical height within the storage system. Typically, RTDs placed at the bottom center—such as the T1 curve in Fig. 6.2 and Fig. 6.3—displayed prolonged periods of gradual heating, implying that conduction remained the dominant mode of heat convey in these regions and that melting occurred later at the bottom. Eventually, the PCM temperature stabilized, approaching the temperature of the HTF. Fig. 6.2 reports the visual progression of PCM melting during the charging process for the configuration with 6 heat pipes (HP), along with corresponding temperature contour plots at selected time intervals. After 40 minutes of charging, melting becomes visible around the HTF tube, particularly in the upper region of the shell, primarily due to conductive heat convey. As charging time progresses, the melting region continues to expand. Due to the amplified thermal conductivity and rapid heat absorption of the heat pipes, localized melting occurs around them. Over time, the shape of the melted region evolves into a triangular form, which becomes clearly visible after 132 minutes. The temperature contour at this point shows that the T12 probe has exceeded the PCM's melting temperature, confirming complete melting at that location. The melting progression is more pronounced in the horizontal direction, especially in the upper region of the storage unit, due to the orientation and influence of the heat pipes. A similar pattern is observed in Fig. 6.3 and Fig. 6.4 for the cases with fewer heat pipes;

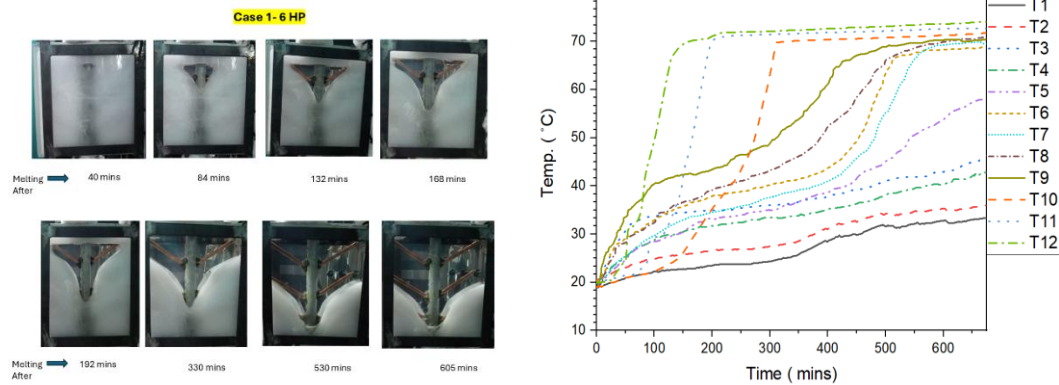


Fig. 6.2. Image of melting of PCM in and temperature time history of all the probes of Case 1 (6-HP)

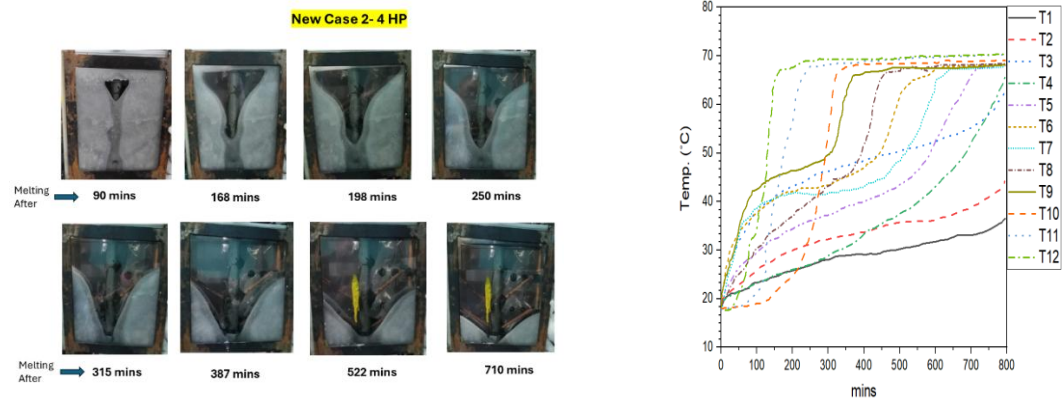


Fig. 6.3. Image of melting of PCM and Temperature time history of all the probes in Case 2 (4-HP)

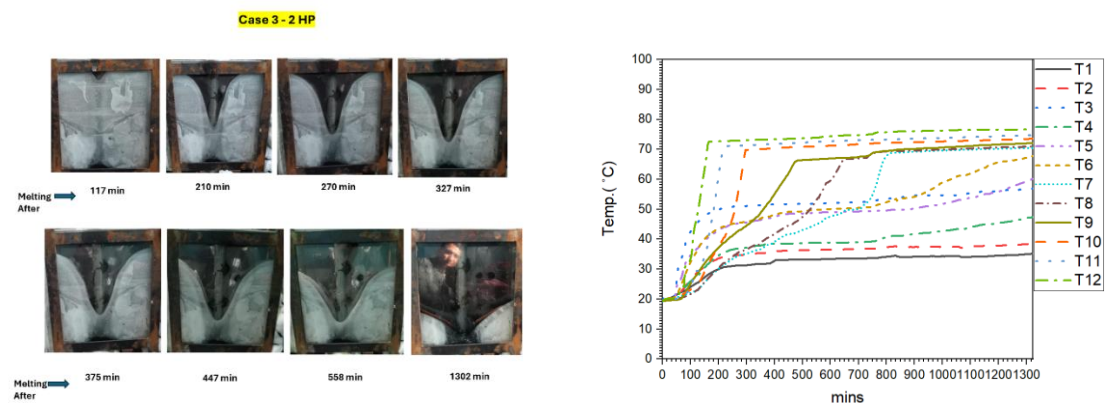


Fig. 6.4. Image of melting of PCM and Temperature time history of all the probes in Case 3 (2-HP)

13 however, the melting occurs over a longer duration due to the reduced number of heat pipes and consequently lower heat transfer effectiveness.

5 For 25% melting of the PCM, Case 2 (4 HP) and Case 3 (2 HP) required approximately 15% and 59% more time, respectively, compared to Case 1 (6 HP). At 50% melting, 9 the additional time required was approximately 17% for Case 2 and 65% for Case 3 relative to Case 1. These results outline that the influence of the number of heat pipes becomes less significant during the melting of the middle region of the PCM. This 69 reduction in impact is attributed to the fact that, once the upper region of the PCM is fully melted, heat begins to transfer through the liquid PCM to the lower solid regions. However, the upper-positioned heat pipes do not effectively contribute to transferring heat downward, resulting in slower melting in the lower section. For achieving 80% melting, Case 2 and Case 3 required approximately 25% and 120% more time, respectively, than Case 1, further emphasizing that Heat pipes located in the upper region become less effective once the PCM around them is fully melted. They contribute minimally to transferring heat to the lower regions, where solid PCM still exists. This highlights the need for the strategic placement of heat pipes throughout the storage unit.

92 The temperature readings from the T12 probe, recorded after 80% melting of the PCM, show that in Case 2 (4 HP) and Case 3 (2 HP), the temperatures are approximately 2.6% and 6.6% lower, respectively, compared to Case 1 (6 HP). This indicates noticeable sensible overheating of the liquid PCM in the upper region for Case 1, caused by the continued heat input from the heat pipes after the local PCM has already fully melted. In LHTES systems, it is preferable to achieve complete melting of the PCM before significant sensible heating of the liquid phase occurs. Premature sensible heating indicates inefficient energy utilization, as it does not contribute to the phase change phenomena. These findings emphasize the importance of strategically distributing heat pipes throughout the storage unit to promote uniform melting and minimize localized overheating, ensuring optimal thermal performance.

The Fig. 6.5 shows the DSC analysis of paraffin, performed at IISER Bhopal, India. The graph displays the heat flow (mW) versus temperature (°C) to characterize the melting behavior of paraffin. The onset temperature of melting is recorded at 56.01°C,

and the endset temperature is 68.67°C, giving a melting range of 12.66°C. The peak melting temperature occurs at 63.69°C, where the maximum phase transition is observed. The enthalpy of fusion (latent heat) is found to be 160.39 J/g, indicating the energy absorbed during melting. A small sample mass of 0.0022 g was used for this measurement, and the area under the peak (29.45 mW·°C) further confirms the melting characteristics.

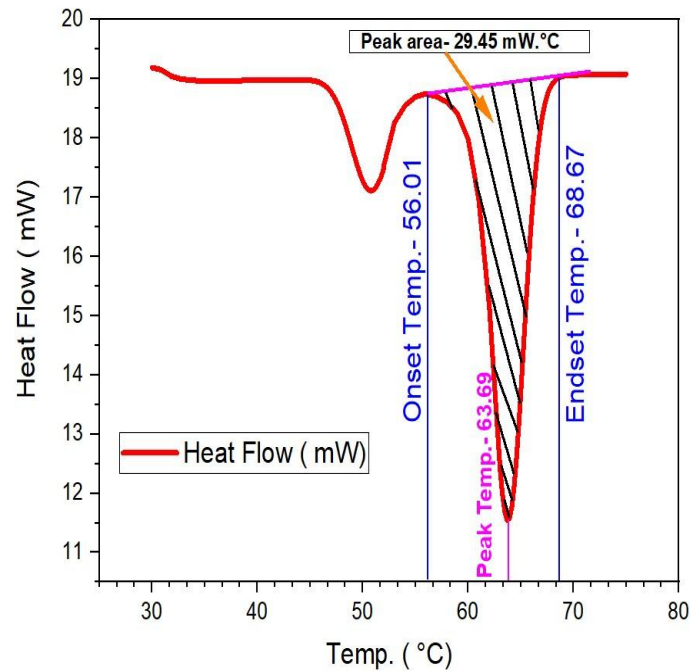


Fig. 6.5 DSC analysis of paraffin

The average temperature of the PCM is derived from experimental data using the weighting method, originally developed by Seddegh et al [129]. In this approach, control volumes are established around each RTD node. Due to the varying placement of RTDs, the size of each control volume differs, affecting the contribution of each temperature measurement. The weighting factor (w) for a given RTD " i " is mathematically defined as:

$$w_i = \frac{v_i}{v_t}$$

Where v_i = Control volume around each RTD

$v_i = V1, V2, V3, \dots, v_{12}$.

v_t = total Volume of the PCM

The average PCM temperature (T_{pcm}) is computed by incorporating the measured local temperature values along with their respective weighting factors.

$$T_{pcm} = \sum w_i T_i$$

The entire PCM region is divided into 12 regions named as V1, V2, V3, ..., and V12 as shown in Fig. 6.6.

V 12	V 11	V 10
V 9	V 8	V 7
V 6	V 5	V 4
V 3	V 2	V 1

Fig. 6.6 control volume around 12 RTD node

The Fig. 6.7 (a) illustrates the variation of average temperature of PCM with time for three configurations incorporating different numbers of heat pipes (HPs) during the charging process. Case 1 (6 HPs) shows the highest temperature rise, followed by Case 2 (4 HPs) and Case 3 (2 HPs), indicating that increasing the number of HPs accelerates the heat transfer and melting process. The average PCM temperature in Case 2 and Case 3 is 3.19% and 2.7% higher, respectively, than in Case 1, suggesting less effective heat distribution in cases with fewer HPs. Initially, all cases follow a similar trend, but with increasing time, the temperature difference becomes more prominent. This trend highlights the role of heat pipes in enhancing thermal charging rates, particularly in the initial melting stages, with diminishing benefits beyond a certain number of heat pipes.

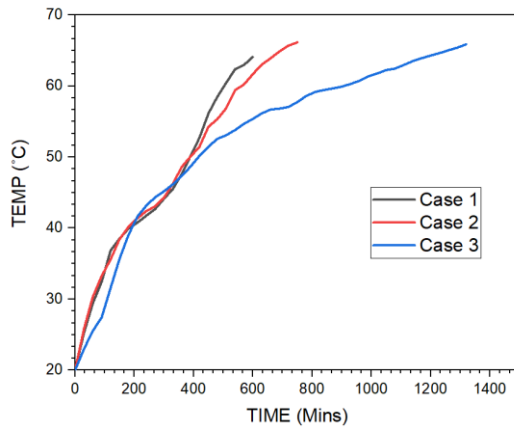


Fig. 6.7 (a)

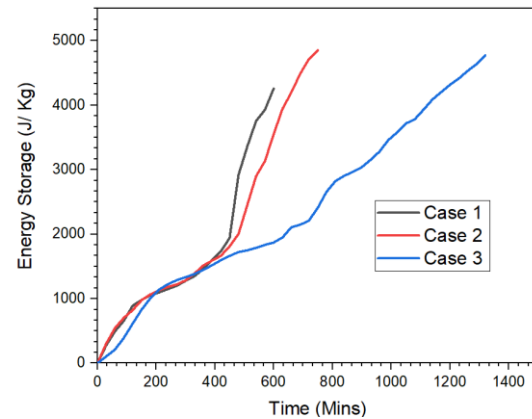


Fig. 6.7 (b)

Fig. 6.7 (a) Avg Temp., and Fig. 6.7 (b) energy Storage in the PCM in cases 1, 2 and

3

The Fig. 6.7 (b) shows the variation of energy storage in PCM over time for three cases with different numbers of heat pipes (HPs). Case 2 (4 HPs) and Case 3 (2 HPs) exhibit higher energy storage compared to Case 1 (6 HPs), with increases of 13.98% and 12.07%, respectively. Initially, all cases follow a similar energy storage trend; however, significant differences appear during the later stages of the charging process. The case with fewer heat pipes stores more energy over time, indicating slower melting but higher accumulated energy due to prolonged charging duration. In contrast, Case 1, with the highest number of heat pipes, shows faster charging but slightly lower overall energy storage, highlighting a trade-off between charging speed and total stored energy. This analysis suggests that optimizing the number of heat pipes is essential for balancing charging rate and energy storage capacity in PCM systems.

The Fig. 6.8 (a) displays the mean power of energy storage in PCM for three different heat pipe (HP) configurations. Case 1 (6 HPs) shows the highest mean power of 7.09 J/kg·s, followed by Case 2 (4 HPs) with 6.46 J/kg·s, and Case 3 (2 HPs) with 3.61 J/kg·s. The mean power of Case 1 is 8.88% higher than Case 2 and 49% higher than Case 3, highlighting the strong influence of increasing the number of heat pipes on enhancing power output. A greater number of HPs accelerates the heat transfer process, resulting in higher power rates during thermal charging. However,

diminishing returns are observed beyond a certain number of HPs, as the percentage increase in power between Case 1 and Case 2 is relatively moderate compared to that between Case 2 and Case 3. This graph emphasizes the importance of optimizing the number of HPs to balance charging speed, energy efficiency, and system cost.

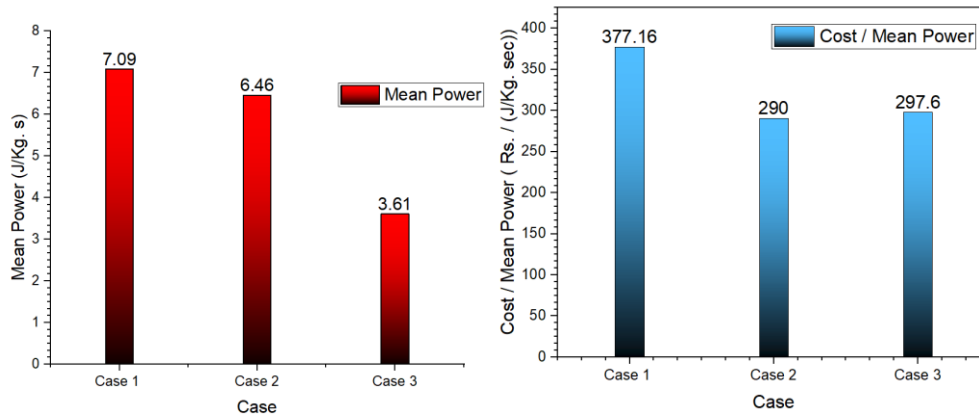


Fig. 6.8 (a)

Fig. 6.8 (b)

Fig. 6.8 (a) Mean power, and Fig. 6.8 (b) cost per mean power of the PCM in cases 1, 2 and 3

The Fig. 6.8 (b) illustrates the cost per mean power of energy storage for three cases with varying numbers of heat pipes (HPs) integrated into the PCM system. Case 1 (6 HPs) exhibits the highest cost per mean power at ₹377.16 per J/kg·s, followed by Case 3 (2 HPs) at ₹297.6, and Case 2 (4 HPs) at ₹290. Both Case 2 and Case 3 are more cost-effective compared to Case 1, with 23.1% and 21% lower cost-to-performance ratios, respectively. Although Case 1 provides the highest mean power, it comes with significantly higher cost, reducing its economic feasibility. Case 2 offers the best cost-to-power balance, suggesting it as a more optimal solution for practical applications where performance and cost must be balanced. This analysis highlights the need for careful techno-economic optimization when designing heat pipe-enhanced PCM storage systems.

Chapter 7

Conclusion and Future Recommendations

7. Conclusions of the Research

This research comprehensively analyzed the thermal charging performance of LHTESS by investigating the effects of heat pipe (HP) integration, tube shape, fin number, and fin material. Both numerical simulations and experimental investigations were carried out, focusing on three types of enclosures—circular shell, trapezoidal shell, and rectangular shell—through three distinct problem cases.

Problem 1: Effect of Eccentric Tube Shapes and Heat Pipe Integration in Circular Shell LHTESS

In the first study, a numerical investigation was conducted to evaluate the thermal charging performance of horizontally-oriented shell-and-tube LHTESS with various eccentric tube shapes, including circular, semi-circular, square, triangular, inverted triangular, and C-shaped tubes. The study also includes the integration of HPs to augment heat transfer between the PCM and the heat source tube wall. The aim is to explore the impact of eccentric tube shape and HP quantity, and locations on the thermal performance of the LHTESS. The insights of this study are presented as follows:

- The C-shape tube significantly diminishes the maximum melting period by 30.3% compared to the circular tube in all considered tube cases. Incorporating one, two, or three HPs into the C-shape tube further reduces the thermal charging time by 45.5%, 57.5%, and 72.2%, respectively.
- The C-shaped tube exhibits the highest e_r value, with an average value of 54.34%, followed by the Inv. triangular, semi-circular, square, and triangular tubes, with an average e_r values of 24.33%, 14.03%, 9.34%, and 3.73%, respectively, using the circular tube as the reference line. The square tube shows consistently superior performance over the largest time span during melting. Incorporating one, two, or three HPs into the C-shape tube further enhances the average e_r value by 23.50%, 52.84%,

and 103.5%, respectively, using the C-shape tube as the reference line. Non-circular tube shapes give their best performance for partial thermal charging or 90% thermal charging of the system.

➤The C-Shape-1HP and semi-circular tube cases exhibit the lowest energy storage, with 10% and 5.5% lower values than the circular tube case, respectively. In contrast, the Inv. triangular, triangular, and square tubes exhibit higher energy storage values of about 1.1%, 0.7%, and 0.3%, respectively, compared to the circular tube. The integration of HPs diminishes the energy accumulation capacity, but this negative impact can be suppressed by surging the number of HPs.

➤All non-circular cases demonstrated better mean power than the circular tube for thermal charging of the system. The C-shape, Inv. triangular, and semi-circular tubes exhibited the highest improvement in mean power by 39%, 24%, and 12%, respectively, when compared to the circular tube. The insertion of one, two, and three HPs has resulted in a further increase in mean power by about 241%, 132%, and 65%, respectively.

Problem 2: Impact of Variable-Length Fins and Fin Material in Trapezoidal LHTESS
In the second investigation, the transient two-dimensional simulation of the charging process in an LHTESS, featuring variable-length fins integrated with HPs within a trapezoidal container enclosing a PCM, has been conducted. This research investigates the aftermath of the quantity of variable-length fins and the material composition of the fins (Al, Cu, and Steel) on the overall system performance. Major outcomes include:

➤The numerical analysis reveals significant impacts of the quantity of variable-length fins on the PCM melting process. While an increased number of Al fins demonstrates a higher enhancement ratio, this effect diminishes with a further rise in the number of fins.

➤The case featuring 12-Steel-fins exhibits the most uniform temperature distribution, surpassing both Al and Cu configurations.

➤Remarkably, the 12-steel-fins and 8-Al-fins cases display nearly identical total melting times, indicating the compensatory effect of raising the number of fins to counterbalance the lower thermal conductivity of the fins. A reduction in the number

of variable fins results in a magnification of the total accumulated energy. Moreover, an augment in the number of fins and their thermal conductivity corresponds to an improvement in mean power due to enhanced heat diffusion. Notably, it is noted that the mean power of the 12-Steel-fins case is lower than that of the 8-Al-fins case.

➤ In terms of cost-effectiveness, the 12-Cu-fins and 12-Al-fins cases demonstrate equal and the lowest C_{cp} among all scenarios. These findings suggest that reducing the C_{cp} in the trapezoidal PCM's container can be accomplished by augmenting the quantity of variable-length fins composed of higher thermal conductive materials.

Problem 3: Experimental Study on Inclined Heat Pipe Integration in Rectangular LHTESS

The third study experimentally investigated the melting behavior of PCM in a rectangular shell-and-tube latent heat storage system integrated with inclined heat pipes. Three configurations—incorporating 2, 4, and 6 heat pipes—were evaluated to compare their thermal performance during the charging process. The analysis was based on temperature profiles, melt fraction evolution, and visual tracking of the melting front. Key findings from the study include:

1. Case 1 (6 heat pipes) demonstrates the 25% and 120% faster melting than Case 2 (4 heat pipes) and Case 3 (2 heat pipes), respectively. It is demonstrating significantly enhanced melting performance with an increased number of heat pipes.
2. While increasing the number of heat pipes enhanced the melting rate, the improvement was not consistently uniform, as overheating was observed in the upper sections of the PCM domain, potentially reducing overall charging efficiency.
3. The average PCM temperature in Case 2 (4 heat pipes) and Case 3 (2 heat pipes) is approximately 3.19% and 2.7% higher, respectively, compared to Case 1 (6 heat pipes).
4. Furthermore, the total energy stored in Case 2 and Case 3 is 13.98% and 12.07% greater than in Case 1. However, Case 1 demonstrates superior performance in terms of mean power output, which is 8.88% and 49% higher than Case 2 and Case 3, respectively. When considering cost-effectiveness (Cost/Mean Power), Case 2 and Case 3 are found to be 23.1% and 21% more economical, respectively, compared to

Case 1. These observations suggest that while Case 1 provides faster thermal response, Case 2 may offer better energy storage efficiency and cost-performance balance.

The studies establish that HPs play a critical role in enhancing the thermal performance of LHTESS. Increasing the number of HPs significantly reduces the melting time and increases the mean power output. However, their placement and number must be optimized to avoid overheating and inefficiencies in the PCM domain.

The experimental results confirmed the simulation findings, showing that increasing the number of HPs improves melting speed, though the improvement is not always linear and can lead to temperature non-uniformity.

In conclusion, the combined use of optimized tube shapes, efficient fin numbers and positions, and strategically placed heat pipes significantly improves the performance of LHTESS. The findings contribute valuable insights for designing cost-effective and high-performance thermal energy storage systems suitable for various thermal management applications.

7.1 Recommendation for future research work

According to the outcomes of the current research, there exist several promising opportunities for extending this research to further enhance the thermal performance of LHTESS integrated with HPs and other thermal enhancement techniques. These future directions can offer deeper insights into optimization strategies for various practical applications.

Firstly, future studies can be extended to investigate the influence of additional heat pipe parameters on the melting and thermal charging behaviours of PCMs. In particular, researchers can focus on the effects of varying the inclination angle of heat pipes beyond the fixed angle used in this study. Studying multiple inclination angles could provide valuable understanding of the optimal positioning required for maximizing natural convection and heat transfer within the PCM domain. Similarly, variation in heat pipe length and diameter offers an unexplored opportunity to optimize the heat transfer rate, as these geometrical factors significantly affect the heat-carrying capacity of the heat pipes. Moreover, the placement or positioning of heat pipes within the PCM container can also be systematically examined to identify the most effective configurations for improving thermal response.

Further, these parameters can be investigated in the context of various container orientations, such as vertical, horizontal, and inclined positions, to understand their combined influence on the system's thermal behaviours. Extending the simulation or experimental work to include different container shapes, such as cylindrical, trapezoidal, and rectangular enclosures, could provide valuable guidelines for optimizing PCM-based storage systems in diverse geometrical setups and spatial constraints.

Additionally, there is a significant research opportunity to analyze combined heat transfer enhancement techniques. Future work could be extended to study the integrated use of heat pipes with fins or other enhancement mechanisms under different container shapes and orientations. Special emphasis could be placed on the positioning of fins relative to the heat pipes, such as locating fins near the evaporator or condenser sections of the heat pipes, to investigate their impact on the overall thermal charging process and to maximize the synergistic effects of these combined techniques.

Further analysis can also be extended by applying heat pipe integration beyond C-shaped tubes to other non-circular tube shapes, such as semi-circular, square, and triangular geometries. Exploring these designs, particularly in vertically oriented systems, may lead to compact solutions by reducing the overall installation footprint, making them attractive for space-constrained applications.

Moreover, the current numerical investigation on the thermal charging performance of trapezoidal LHTESS presents a strong foundation for future experimental validation. Extending this research to practical, experimental setups would help verify simulation results and improve model accuracy. Similarly, the study on the influence of eccentric tube shapes combined with heat pipes on PCM thermal charging can also be extended experimentally. Furthermore, future work can incorporate the full thermal cycle by including the thermal discharging phase, thus offering a complete performance analysis of the LHTESS over successive charging and discharging operations.

In conclusion, the above-mentioned research directions offer valuable opportunities for future investigations, which will contribute to the development of more efficient,

cost-effective, and compact TES systems suitable for real-world thermal management applications.

8. References

- [1] C. K. Jotshi, C. K. Hsieh, D. Y. Goswami, J. F. Klausner, and N. Srinivasan, "Thermal Storage in Ammonium Alum/Ammonium Nitrate Eutectic for Solar Space Heating Applications," *J. Sol. Energy Eng.*, vol. 120, no. 1, p. 20, 1998.
- [2] M. Liu *et al.*, "Review and characterisation of high-temperature phase change material candidates between 500 C and 700°C," *Renew. Sustain. Energy Rev.*, vol. 150, no. June, p. 111528, 2021.
- [3] A. Sharma, V. V. Tyagi, C. R. Chen, and D. Buddhi, "Review on thermal energy storage with phase change materials and applications," *Renew. Sustain. Energy Rev.*, vol. 13, no. 2, pp. 318–345, 2009.
- [4] E. Alptekin and M. A. Ezan, "Performance investigations on a sensible heat thermal energy storage tank with a solar collector under variable climatic conditions," *Appl. Therm. Eng.*, vol. 164, p. 114423, 2020.
- [5] M. Chieruzzi, G. F. Cerritelli, A. Miliozzi, and J. M. Kenny, "Effect of nanoparticles on heat capacity of nanofluids based on molten salts as PCM for thermal energy storage," *Nanoscale Res. Lett.*, vol. 8, no. 1, pp. 1–9, 2013.
- [6] H. Nazir *et al.*, "Recent developments in phase change materials for energy storage applications: A review," *Int. J. Heat Mass Transf.*, vol. 129, pp. 491–523, 2019.
- [7] P. Gadhave, F. Pathan, S. Kore, and C. Prabhune, "Comprehensive review of phase change material based latent heat thermal energy storage system," *Int. J. Ambient Energy*, vol. 43, no. 1, pp. 4181–4206, 2022.
- [8] Y. Lin, Y. Jia, G. Alva, and G. Fang, "Review on thermal conductivity enhancement, thermal properties and applications of phase change materials in thermal energy storage," *Renew. Sustain. Energy Rev.*, vol. 82, no. May 2017, pp. 2730–2742, 2018.
- [9] S. Saha, A. R. M. Ruslan, A. K. M. Monjur Morshed, and M. Hasanuzzaman, "Global prospects and challenges of latent heat thermal energy storage: a review," *Clean Technol. Environ. Policy*, vol. 23, no. 2, pp. 531–559, 2021.
- [10] K. Pielichowska and K. Pielichowski, "Phase change materials for thermal energy storage," *J. Prog. Mater. Sci.*, vol. 65, pp. 67–123, 2014.

- [11] Z. A. Qureshi, H. M. Ali, and S. Khushnood, "Recent advances on thermal conductivity enhancement of phase change materials for energy storage system: A review," *Int. J. Heat Mass Transf.*, vol. 127, pp. 838–856, 2018.
- [12] A. Solé, H. Neumann, S. Niedermaier, I. Martorell, P. Schossig, and L. F. Cabeza, "Stability of sugar alcohols as PCM for thermal energy storage," *Sol. Energy Mater. Sol. Cells*, vol. 126, pp. 125–134, 2014.
- [13] J. Pereira da Cunha and P. Eames, "Thermal energy storage for low and medium temperature applications using phase change materials - A review," *Appl. Energy*, vol. 177, pp. 227–238, 2016.
- [14] A. Abhat, "Low temperature latent heat thermal energy storage: Heat storage materials," *Sol. Energy*, vol. 30, no. 4, pp. 313–332, 1983.
- [15] V. Raj and T. Goswami, "Use of phase change material (PCM) for the improvement of thermal performance of cold storage," vol. 1, no. 2, pp. 49–61, 2018.
- [16] S. Khare, M. Dell'Amico, C. Knight, and S. McGarry, "Selection of materials for high temperature latent heat energy storage," *Sol. Energy Mater. Sol. Cells*, vol. 107, pp. 20–27, 2012.
- [17] M. Kenisarin and K. Mahkamov, "Solar energy storage using phase change materials," *Renew. Sustain. Energy Rev.*, vol. 11, no. 9, pp. 1913–1965, 2007.
- [18] N. I. Ibrahim, F. A. Al-Sulaiman, S. Rahman, B. S. Yilbas, and A. Z. Sahin, "Heat transfer enhancement of phase change materials for thermal energy storage applications: A critical review," *Renew. Sustain. Energy Rev.*, vol. 74, pp. 26–50, 2017.
- [19] S. Höhle, A. König-Haagen, and D. Brüggemann, "Thermophysical characterization of MgCl₂·6H₂O, xylitol and erythritol as phase change materials (PCM) for latent heat thermal energy storage (LHTES)," *Materials (Basel)*, vol. 10, no. 4, 2017.
- [20] S. A. Mohamed *et al.*, "A review on current status and challenges of inorganic phase change materials for thermal energy storage systems," *Renew. Sustain. Energy Rev.*, vol. 70, no. December, pp. 1072–1089, 2017.
- [21] N. Xie, Z. Huang, Z. Luo, X. Gao, and Y. Fang, "Inorganic Salt Hydrate for Thermal Energy Storage," *Appl. Sci.*, vol. 7, no. 1317, pp. 2–18, 2017.

- [22] J. Fukai, M. Kanou, Y. Kodama, and O. Miyatake, "Thermal conductivity enhancement of energy storage media using carbon fibers," *Energy Convers. Manag.*, vol. 41, no. 14, pp. 1543–1556, 2000.
- [23] E. B. S. Mettawee and G. M. R. Assassa, "Thermal conductivity enhancement in a latent heat storage system," *Sol. Energy*, vol. 81, no. 7, pp. 839–845, 2007.
- [24] M. K. Rathod and J. Banerjee, "Thermal stability of phase change materials used in latent heat energy storage systems: A review," *Renew. Sustain. Energy Rev.*, vol. 18, pp. 246–258, 2013.
- [25] W. Sun, Y. Zhou, J. Feng, X. Fang, Z. Ling, and Z. Zhang, "Compounding $\text{MgCl}_2 \cdot 6\text{H}_2\text{O}$ with $\text{NH}_4\text{Al}(\text{SO}_4)_2 \cdot 12\text{H}_2\text{O}$ or $\text{KAl}(\text{SO}_4)_2 \cdot 12\text{H}_2\text{O}$ to obtain binary hydrated salts as high-performance phase change materials," *Molecules*, 2019.
- [26] S. Xie *et al.*, "A thermally stable phase change material with high latent heat based on an oxalic acid dihydrate/boric acid binary eutectic system," *Sol. Energy Mater. Sol. Cells*, vol. 168, no. April, pp. 38–44, 2017.
- [27] N. Sarier and E. Onder, "Organic phase change materials and their textile applications: An overview," *Thermochim. Acta*, vol. 540, pp. 7–60, 2012.
- [28] L. A. Chidambaram, A. S. Ramana, G. Kamaraj, and R. Velraj, "Review of solar cooling methods and thermal storage options," *Renew. Sustain. Energy Rev.*, vol. 15, no. 6, pp. 3220–3228, 2011.
- [29] S. G. Jeong, O. Chung, S. Yu, S. Kim, and S. Kim, "Improvement of the thermal properties of Bio-based PCM using exfoliated graphite nanoplatelets," *Sol. Energy Mater. Sol. Cells*, vol. 117, pp. 87–92, 2013.
- [30] S. Harish, D. Orejon, Y. Takata, and M. Kohno, "Thermal conductivity enhancement of lauric acid phase change nanocomposite with graphene nanoplatelets," *Appl. Therm. Eng.*, vol. 80, pp. 205–211, 2015.
- [31] O. Sanusi, R. Warzoha, and A. S. Fleischer, "Energy storage and solidification of paraffin phase change material embedded with graphite nanofibers," *Int. J. Heat Mass Transf.*, vol. 54, no. 19–20, pp. 4429–4436, 2011.
- [32] P. Ji, H. Sun, Y. Zhong, and W. Feng, "Improvement of the thermal conductivity of a

- phase change material by the functionalized carbon nanotubes,” *Chem. Eng. Sci.*, vol. 81, pp. 140–145, 2012.
- [33] P. Chandrasekaran, M. Cheralathan, V. Kumaresan, and R. Velraj, “Enhanced heat transfer characteristics of water based copper oxide nanofluid PCM (phase change material) in a spherical capsule during solidification for energy efficient cool thermal storage system,” *Energy*, vol. 72, pp. 636–642, 2014.
- [34] J. L. Zeng, Z. Cao, D. W. Yang, L. X. Sun, and L. Zhang, “Thermal conductivity enhancement of Ag nanowires on an organic phase change material,” *J. Therm. Anal. Calorim.*, vol. 101, no. 1, pp. 385–389, 2010.
- [35] X. H. Wu, C. X. Wang, Y. L. Wang, and Y. J. Zhu, “Experimental study of thermo-physical properties and application of paraffin-carbon nanotubes composite phase change materials,” *Int. J. Heat Mass Transf.*, vol. 140, pp. 671–677, 2019.
- [36] N. Kumar, J. Hirschey, T. J. LaClair, K. R. Gluesenkamp, and S. Graham, “Review of stability and thermal conductivity enhancements for salt hydrates,” *J. Energy Storage*, vol. 24, no. May, p. 100794, 2019.
- [37] T. Nomura, K. Tabuchi, C. Zhu, N. Sheng, S. Wang, and T. Akiyama, “High thermal conductivity phase change composite with percolating carbon fiber network,” *Appl. Energy*, vol. 154, pp. 678–685, 2015.
- [38] A. M. Tayeb, “Use of some industrial wastes as energy storage media,” *Energy Convers. Manag.*, vol. 37, no. 2, pp. 127–133, 1996.
- [39] B. Li, H. Zhou, Y. Huo, and Z. Rao, “Investigation of Fractal Fins towards Heat Transfer Properties in Thermal Storage System,” *Heat Transf. Eng.*, pp. 1–17, Mar. 2024.
- [40] M. Mahdavi, S. Tiari, and V. Pawar, “A numerical study on the combined effect of dispersed nanoparticles and embedded heat pipes on melting and solidification of a shell and tube latent heat thermal energy storage system,” *J. Energy Storage*, vol. 27, no. October 2019, p. 101086, 2020.
- [41] L. Kalapala and J. K. Devanuri, “Influence of operational and design parameters on the performance of a PCM based heat exchanger for thermal energy storage – A review,” *J. Energy Storage*, vol. 20, no. September, pp. 497–519, 2018.

- [42] J. M. Maldonado, A. de Gracia, and L. F. Cabeza, "Systematic review on the use of heat pipes in latent heat thermal energy storage tanks," *J. Energy Storage*, vol. 32, no. April, 2020.
- [43] X. Zhang *et al.*, "Polyethylene glycol/Cu/SiO₂ form stable composite phase change materials: Preparation, characterization, and thermal conductivity enhancement," *RSC Adv.*, vol. 6, no. 63, pp. 58740–58748, 2016.
- [44] K. Bhagat, M. Prabhakar, and S. K. Saha, "Estimation of thermal performance and design optimization of finned multitube latent heat thermal energy storage," *J. Energy Storage*, vol. 19, no. June, pp. 135–144, 2018.
- [45] J. M. Khodadadi and S. F. Hosseinzadeh, "Nanoparticle-enhanced phase change materials (NEPCM) with great potential for improved thermal energy storage," *Int. Commun. Heat Mass Transf.*, vol. 34, no. 5, pp. 534–543, 2007.
- [46] A. Kumar, S. K. Saha, K. R. Kumar, and D. Rakshit, "Study of melting of paraffin dispersed with copper nanoparticles in square cavity subjected to external magnetic field," *J. Energy Storage*, vol. 50, no. February, p. 104338, 2022.
- [47] B. Águila V, D. A. Vasco, P. Galvez P, and P. A. Zapata, "Effect of temperature and CuO-nanoparticle concentration on the thermal conductivity and viscosity of an organic phase-change material," *Int. J. Heat Mass Transf.*, vol. 120, pp. 1009–1019, 2018.
- [48] A. Mustaffar, A. Harvey, and D. Reay, "Melting of phase change material assisted by expanded metal mesh," *Appl. Therm. Eng.*, vol. 90, 2015.
- [49] A. Abhat, "PERFORMANCE STUDIES OF A FINNED HEAT PIPE LATENT THERMAL ENERGY STORAGE SYSTEM," *SUN Mankind's Future. Source Energy*, pp. 541–546.
- [50] H. Behi *et al.*, "Enhancement of the thermal energy storage using heat-pipe-assisted phase change material," *Energies*, vol. 14, no. 19, 2021.
- [51] H. Yang, J. Song, B. He, and G. Ding, "Numerical study on charging characteristics of heat pipe-assisted cylindrical capsule for enhancing latent thermal energy storage," *Sol. Energy*, vol. 190, no. August, pp. 147–155, 2019.
- [52] C. Zhang, Y. Fan, M. Yu, X. Zhang, and Y. Zhao, "Performance evaluation and analysis of a vertical heat pipe latent thermal energy storage system with fins-copper foam

- combination,” *Appl. Therm. Eng.*, vol. 165, no. September 2019, p. 114541, 2020.
- [53] B. Lu, Y. Zhang, J. Zhu, J. Zhang, and D. Sun, “Enhancement of the charging and discharging performance of a vertical latent heat thermal energy storage unit via conical shell design,” *Int. J. Heat Mass Transf.*, vol. 185, 2022.
- [54] G. S. Sodhi, A. K. Jaiswal, K. Vigneshwaran, and P. Muthukumar, “Investigation of charging and discharging characteristics of a horizontal conical shell and tube latent thermal energy storage device,” *Energy Convers. Manag.*, vol. 188, no. January, pp. 381–397, 2019.
- [55] F. Iachachene, Z. Haddad, H. F. Oztop, and E. Abu-Nada, “Melting of phase change materials in a trapezoidal cavity: Orientation and nanoparticles effects,” *J. Mol. Liq.*, vol. 292, p. 110592, 2019.
- [56] H. Sattari, A. Mohebbi, M. M. Afsahi, and A. Azimi Yancheshme, “CFD simulation of melting process of phase change materials (PCMs) in a spherical capsule,” *Int. J. Refrig.*, vol. 73, pp. 209–218, 2017.
- [57] S. Khobragade and J. K. Devanuri, “Impact of inclination on the thermal performance of shell and tube latent heat storage system under simultaneous charging and discharging : Numerical investigation,” *Appl. Therm. Eng.*, vol. 214, no. October 2021, p. 118811, 2022.
- [58] I. Al Siyabi, S. Khanna, T. Mallick, and S. Sundaram, “An experimental and numerical study on the effect of inclination angle of phase change materials thermal energy storage system,” *J. Energy Storage*, vol. 23, no. March, pp. 57–68, 2019.
- [59] B. Kamkari, H. Shokouhmand, and F. Bruno, “Experimental investigation of the effect of inclination angle on convection-driven melting of phase change material in a rectangular enclosure,” *Int. J. Heat Mass Transf.*, vol. 72, pp. 186–200, 2014.
- [60] M. S. Mahdi, H. B. Mahood, A. F. Hasan, A. A. Khadom, and A. N. Campbell, “Numerical study on the effect of the location of the phase change material in a concentric double pipe latent heat thermal energy storage unit,” *Therm. Sci. Eng. Prog.*, vol. 11, pp. 40–49, 2019.
- [61] J. Kumar, P. Singh, R. Kumar, and M. Sciences, “The Effect of Geometric Parameters

of a Container on Thermal Charging of Latent Heat Thermal Energy Storage System : A Review,” vol. c, pp. 1–11, 2022.

- [62] S. H. Kim, S. Pandey, S. H. Park, and M. Y. Ha, “A numerical investigation of the effect of fin inclination angle on the thermal energy storage performance of a phase change material in a rectangular latent heat thermal energy storage unit,” *J. Energy Storage*, vol. 47, 2022.
- [63] J. Kumar, P. Singh, and R. Kumar, “A numerical study on the influence of fin numbers and material embedded with heat pipe for thermal charging in a trapezoidal container,” *Numer. Heat Transf. Part A Appl.*, vol. 0, no. 0, pp. 1–22, 2024.
- [64] F. L. Tan, “Constrained and unconstrained melting inside a sphere,” *Int. Commun. Heat Mass Transf.*, vol. 35, no. 4, pp. 466–475, 2008.
- [65] W. Li, S. G. Li, S. Guan, Y. Wang, X. Zhang, and X. Liu, “Numerical study on melt fraction during melting of phase change material inside a sphere,” *Int. J. Hydrogen Energy*, vol. 42, no. 29, pp. 18232–18239, 2017.
- [66] M. Fadhil and P. C. Eames, “A comparative study of the effect of varying wall heat flux on melting characteristics of phase change material RT44HC in rectangular test cells,” *Int. J. Heat Mass Transf.*, vol. 141, pp. 731–747, 2019.
- [67] B. Zivkovic and I. Fujii, “An Analysis of Isothermal Phase Change of Phase Change material within rectangular and cylindrical containers,” *Sol. Energy*, vol. 70, no. 1, pp. 51–61, 2001.
- [68] A. Kumar Yadav, T. Donepudi, and S. Bhargav Sriram, “Numerical and Experimental Investigation of Melting Characteristics of Phase Change Material-RT58,” *Therm. Sci. Eng. Prog.*, p. 100378, 2019.
- [69] M. Bechiri and K. Mansouri, “Study of heat and fluid flow during melting of PCM inside vertical cylindrical tube,” *Int. J. Therm. Sci.*, vol. 135, no. September 2018, pp. 235–246, 2019.
- [70] Z. J. Zheng, Y. Xu, and M. J. Li, “Eccentricity optimization of a horizontal shell-and-tube latent-heat thermal energy storage unit based on melting and melting-solidifying performance,” *Appl. Energy*, vol. 220, pp. 447–454, 2018.

- [71] A. Abderrahmane *et al.*, “Enhancing the Melting Process of Shell-and-Tube PCM Thermal Energy Storage Unit Using Modified Tube Design,” *Nanomaterials*, vol. 12, no. 17, pp. 1–18, 2022.
- [72] S. H. Park, Y. G. Park, and M. Y. Ha, “A numerical study on the effect of the number and arrangement of tubes on the melting performance of phase change material in a multi-tube latent thermal energy storage system,” *J. Energy Storage*, vol. 32, p. 101780, 2020.
- [73] A. Kumar and S. K. Saha, “Performance study of a novel funnel shaped shell and tube latent heat thermal energy storage system,” *Renew. Energy*, vol. 165, pp. 731–747, 2021.
- [74] A. Shafiei Ghazani and A. Gholamzadeh, “The effect of conical shell and converging/diverging tube on the charging performance of shell and tube latent heat thermal energy storage system,” *J. Energy Storage*, vol. 65, p. 107262, Aug. 2023.
- [75] K. A. A. Mahdi Mustafa S. , Mahood Hameed B. , Campbell Alasdair N., “Experimental Study on the Melting Behavior of a Phase Change Material in a Conical Coil Latent Heat Thermal Energy Storage Unit Mustafa,” *Appl. Therm. Eng.*, vol. 11, pp. 40–49, 2019.
- [76] X. Cao, Y. Yuan, B. Xiang, and F. Highlight, “Effect of natural convection on melting performance of eccentric horizontal shell and tube latent heat storage unit,” *Sustain. Cities Soc.*, vol. 38, no. December 2017, pp. 571–581, 2018.
- [77] İ. G. Demirkıran and E. Cetkin, “Emergence of rectangular shell shape in thermal energy storage applications: Fitting melted phase changing material in a fixed space,” *J. Energy Storage*, vol. 37, no. February, 2021.
- [78] V. Safari, B. Kamkari, and H. Abolghasemi, “Investigation of the effects of shell geometry and tube eccentricity on thermal energy storage in shell and tube heat exchangers,” *J. Energy Storage*, vol. 52, p. 104978, Aug. 2022.
- [79] S. Seddegh, S. S. M. Tehrani, X. Wang, and F. Cao, “Comparison of heat transfer between cylindrical and conical vertical shell-and-tube latent heat thermal energy storage systems,” *Appl. Therm. Eng.*, vol. 130, pp. 1349–1362, 2018.

- [80] Q. Mao, N. Liu, L. Peng, and D. Liu, "A novel shell-and-tube thermal energy storage tank: Modeling and investigations of thermal performance," *Appl. Therm. Eng.*, vol. 159, no. February 2018, p. 113964, 2019.
- [81] R. P. Singh, H. Xu, S. C. Kaushik, D. Rakshit, and A. Romagnoli, "Charging performance evaluation of finned conical thermal storage system encapsulated with nano-enhanced phase change material," *Appl. Therm. Eng.*, vol. 151, no. September 2018, pp. 176–190, 2019.
- [82] L. Kalapala and J. K. Devanuri, "Parametric investigation to assess the melt fraction and melting time for a latent heat storage material based vertical shell and tube heat exchanger," *Sol. Energy*, vol. 193, no. March, pp. 360–371, 2019.
- [83] H. B. Mahood, M. S. Mahdi, A. A. Monjezi, A. A. Khadom, and A. N. Campbell, "Numerical investigation on the effect of fin design on the melting of phase change material in a horizontal shell and tube thermal energy storage," *J. Energy Storage*, vol. 29, no. February, p. 101331, 2020.
- [84] N. R. Vyshak and G. Jilani, "Numerical analysis of latent heat thermal energy storage system," *Energy Convers. Manag.*, vol. 48, no. 7, pp. 2161–2168, 2007.
- [85] S. Tiari, S. Qiu, and M. Mahdavi, "Numerical study of finned heat pipe-assisted thermal energy storage system with high temperature phase change material," *Energy Convers. Manag.*, vol. 89, pp. 833–842, 2015.
- [86] A. Saraswat, R. Bhattacharjee, A. Verma, M. K. Das, and S. Khandekar, "' SI : ISHMT-ASFE HMTC- 2015 ' Revised Submission : June 27 , 2016 Investigation of Diffusional Transport of Heat and its Enhancement," *Appl. Therm. Eng.*, 2016.
- [87] S. Tiari and S. Qiu, "Three-dimensional simulation of high temperature latent heat thermal energy storage system assisted by finned heat pipes," *Energy Convers. Manag.*, vol. 105, pp. 260–271, 2015.
- [88] S. Motahar and R. Khodabandeh, "Experimental study on the melting and solidification of a phase change material enhanced by heat pipe," *Int. Commun. Heat Mass Transf.*, vol. 73, pp. 1–6, 2016.
- [89] C. Zhang, M. Yu, Y. Fan, X. Zhang, Y. Zhao, and L. Qiu, "Numerical study on heat

transfer enhancement of PCM using three combined methods based on heat pipe,” *Energy*, vol. 195, p. 116809, 2020.

- [90] H. Yang, J. Song, B. He, and G. Ding, “Numerical study on charging characteristics of heat pipe-assisted cylindrical capsule for enhancing latent thermal energy storage,” *Sol. Energy*, vol. 190, no. August, pp. 147–155, 2019.
- [91] S. Seddegh, X. Wang, and A. D. Henderson, “A comparative study of thermal behaviour of a horizontal and vertical shell-and-tube energy storage using phase change materials,” *Appl. Therm. Eng.*, vol. 93, pp. 348–358, 2016.
- [92] A. D. Brent, V. R. Voller, K. J. Reid, V. R. Voller, and K. J. R. Enthalpy-porosity, “Enthalpy-porosity technique for modeling convection-diffusion phase change: application to the melting of a pure metal,” *Numer. heat transfer*, vol. 13, pp. 297–318, 1988.
- [93] P. C. E. & F. B. A. Andrew J. Parry, “Modeling of Thermal Energy Storage Shell-and-Tube Heat Exchanger,” *Heat Transf. Eng.*, vol. 35, no. 1, pp. 1–14, 2014.
- [94] S. Tiari, S. Qiu, and M. Mahdavi, “Discharging process of a finned heat pipe – assisted thermal energy storage system with high temperature phase change material,” *Energy Convers. Manag.*, vol. 118, pp. 426–437, 2016.
- [95] M. Mahdavi, S. Tiari, and V. Pawar, “Heat transfer analysis of a low-temperature heat pipe-assisted latent heat thermal energy storage system with nano-enhanced PCM,” *ASME Int. Mech. Eng. Congr. Expo. Proc.*, vol. 6B-2018, pp. 1–9, 2018.
- [96] J. Guo, B. Yang, Y. Li, X. Yang, Y. L. He, and B. Sundén, “Thermal energy storage characteristics of finned tubes with different gradients of fin heights,” *Numer. Heat Transf. Part A Appl.*, vol. 0, no. 0, pp. 1–30, 2023.
- [97] S. M. C. & B. F. Francesco Fornarelli, “Convective Effects in a Latent Heat Thermal Energy Storage,” *Heat Transf. Eng.*, vol. 42, no. 1, pp. 1–22, 2021.
- [98] P. Rawat and A. Faizan, “International Journal of Heat and Mass Transfer A numerical study on the impact of fin length arrangement and material on the melting of PCM in a rectangular enclosure,” vol. 205, 2023.
- [99] M. J. Hosseini, M. Rahimi, and R. Bahrampoury, “Experimental and computational

evolution of a shell and tube heat exchanger as a PCM thermal storage system,” *Int. Commun. Heat Mass Transf.*, vol. 50, pp. 128–136, 2014.

- [100] O. B. & H. Y. M. D. Muhammad, “Validation of a CFD Melting and Solidification Model for Phase Change in Vertical Cylinders,” *Numer. Heat Transf. Part A Appl.*, vol. 68, no. 5, pp. 501–511, 2015.
- [101] H. Soltani, M. Soltani, H. Karimi, and J. Nathwani, “International Journal of Heat and Mass Transfer Heat transfer enhancement in latent heat thermal energy storage unit using a combination of fins and rotational mechanisms,” *Int. J. Heat Mass Transf.*, vol. 179, p. 121667, 2021.
- [102] A. Hossein *et al.*, “A new design to enhance the conductive and convective heat transfer of latent heat thermal energy storage units,” *Appl. Therm. Eng.*, vol. 215, no. March, p. 118955, 2022.
- [103] Y. Dutil, D. R. Rousse, N. Ben Salah, S. Lassue, and L. Zalewski, “A review on phase-change materials: Mathematical modeling and simulations,” *Renew. Sustain. Energy Rev.*, vol. 15, no. 1, pp. 112–130, 2011.
- [104] J. Vogel and A. Thess, “Validation of a numerical model with a benchmark experiment for melting governed by natural convection in latent thermal energy storage,” *Appl. Therm. Eng.*, vol. 148, pp. 147–159, 2019.
- [105] S. Jegadheeswaran and S. D. Pohekar, “Performance enhancement in latent heat thermal storage system: A review,” *Renew. Sustain. Energy Rev.*, vol. 13, no. 9, pp. 2225–2244, 2009.
- [106] Y. L. & Y. Z. Shuli Liu, “Review on Heat Transfer Mechanisms and Characteristics in Encapsulated PCMs, Heat Transfer Engineering,” *Heat Transf. Eng.*, vol. 36, no. 10, pp. 880–901, 2015.
- [107] O. M. & S. N. B. B. Davide Ercole, “Numerical Analysis on a Latent Thermal Energy Storage System with Phase Change Materials and Aluminum Foam,” *Heat Transf. Eng.*, vol. 41, no. 12, pp. 1075–1084, 2020.
- [108] A. H. N. Al-Mudhafar, A. F. Nowakowski, and F. C. G. A. Nicolleau, “Enhancing the thermal performance of PCM in a shell and tube latent heat energy storage system

by utilizing innovative fins,” *Energy Reports*, vol. 7, pp. 120–126, 2021.

- [109] M. H. Hekmat, M. H. K. Haghani, E. Izadpanah, and H. Sadeghi, “The influence of energy storage container geometry on the melting and solidification of PCM,” *Int. Commun. Heat Mass Transf.*, vol. 137, p. 106237, Oct. 2022.
- [110] H. A. Hasan and K. H. Suffer, “Thermal performance enhancement of energy storage system using spiral-wired tube heat exchanger,” *Energy Sources, Part A Recover. Util. Environ. Eff.*, vol. 45, no. 3, pp. 7280–7293, 2023.
- [111] S. E. Ghasemi and A. A. Ranjbar, “A novel numerical study on the melting process of phase change materials in a heat exchanger for energy storage,” *Numer. Heat Transf. Part A Appl.*, vol. 85, no. 2, pp. 237–249, 2024.
- [112] Y. H. Diao, L. Liang, Y. H. Zhao, Z. Y. Wang, and F. W. Bai, “Numerical investigation of the thermal performance enhancement of latent heat thermal energy storage using longitudinal rectangular fins and flat micro-heat pipe arrays,” *Appl. Energy*, vol. 233–234, no. 100, pp. 894–905, 2019.
- [113] S. Ebadi, S. H. Tasnim, A. A. Aliabadi, and S. Mahmud, “Melting of nano-PCM inside a cylindrical thermal energy storage system : Numerical study with experimental verification,” *Energy Convers. Manag.*, vol. 166, no. April, pp. 241–259, 2018.
- [114] C. Nie, S. Deng, and J. Liu, “Numerical investigation of PCM in a thermal energy storage unit with fins: Consecutive charging and discharging,” *J. Energy Storage*, vol. 29, p. 101319, 2020.
- [115] R. Gau, C and Viskanta, “melting and Solidification of a Pure Metal on a Vertical Wall,” *J. Heat Transfer*, vol. 108, no. February, pp. 174–181, 1986.
- [116] A. Najafian, F. Haghighat, and A. Moreau, “Integration of PCM in domestic hot water tanks: Optimization for shifting peak demand,” *Energy Build.*, vol. 106, pp. 59–64, 2015.
- [117] G. Alva, L. Liu, X. Huang, and G. Fang, “Thermal energy storage materials and systems for solar energy applications,” *Renew. Sustain. Energy Rev.*, vol. 68, no. October 2016, pp. 693–706, 2017.
- [118] M. Hoseini Rahdar, A. Emamzadeh, and A. Ataei, “A comparative study on PCM and

- ice thermal energy storage tank for air-conditioning systems in office buildings,” *Appl. Therm. Eng.*, vol. 96, pp. 391–399, 2016.
- [119] A. De Gracia and L. F. Cabeza, “Phase Change Materials and Thermal Energy Storage for Buildings,” *Energy Build.*, 2015.
- [120] M. Mumtaz, A. Khan, R. Saidur, and F. A. Al-sulaiman, “A review for phase change materials (PCMs) in solar absorption refrigeration systems,” *Renew. Sustain. Energy Rev.*, vol. 76, no. February, pp. 105–137, 2017.
- [121] M. Zhao, L. Yao, W. Ye, and Q. Fang, “Structural optimization of a latent heat storage unit with the fractal fin,” *Numer. Heat Transf. Part A Appl.*, vol. 84, no. 8, pp. 921–939, 2023.
- [122] S. Rahmanian, H. Rahmanian-Koushkaki, M. Moein-Jahromi, and M. Setareh, “Numerical thermal performance assessment of phase change process in a PCM/foam-fins enclosure under various thermal conditions,” *Energy Sources, Part A Recover. Util. Environ. Eff.*, vol. 46, no. 1, pp. 2360–2376, Dec. 2024.
- [123] J. Khan, I. Kaur, Y. Aider, H. Cho, S. Choi, and P. Singh, “Transient thermal performance enhancement of phase change material (RT82) through novel pin arrangements under varied gravity conditions,” *Numer. Heat Transf. Part A Appl.*, vol. 0, no. 0, pp. 1–15, 2023.
- [124] N. Sharifi, A. Faghri, T. L. Bergman, and C. E. Andraka, “Simulation of heat pipe-assisted latent heat thermal energy storage with simultaneous charging and discharging,” *Int. J. Heat Mass Transf.*, vol. 80, pp. 170–179, 2015.
- [125] W. Q. Li, K. Cao, Q. L. Song, P. F. Zhu, and Y. Ba, “Enhancements of heat transfer and thermoelectric performances using finned heat-pipe array,” *Appl. Therm. Eng.*, vol. 230, no. April, 2023.
- [126] S. Tiari, A. Hockins, and M. Mahdavi, “Case Studies in Thermal Engineering Numerical study of a latent heat thermal energy storage system enhanced by varying fin configurations,” *Case Stud. Therm. Eng.*, vol. 25, no. March, p. 100999, 2021.
- [127] “ANSYS fluent 22 R1, Material Data Base.” 2022.
- [128] A. S. I. Irbai’ and Y. S. H. Najjar, “Enhancement of the melting process in the thermal

energy storage system by using novel geometry,” *Numer. Heat Transf. Part A Appl.*, vol. 76, no. 12, pp. 1006–1022, 2019.

- [129] S. Seddegh, X. Wang, M. M. Joybari, and F. Haghighat, “Investigation of the effect of geometric and operating parameters on thermal behavior of vertical shell-and-tube latent heat energy storage systems,” *Energy*, vol. 137, pp. 69–82, 2017.

BIO-DATA

Name: Mr. Jayesh Kumar

Current Designation: Assistant Professor, Department of Mechanical Engineering

Institution: Maharaja Surajmal Institute of Technology (MSIT), Delhi

Research Scholar: Delhi Technological University (DTU), Delhi

I am currently pursuing his Ph.D. in Mechanical Engineering at Delhi Technological University (DTU), with a research focus on latent heat thermal energy storage systems.

I hold a B. Tech in Mechanical Engineering and an M. Tech in Manufacturing Technology and Automation, both completed with First Division.

I have qualified the GATE examination in Mechanical Engineering in the years 2008 and 2012. With over fourteen years of teaching experience, I am currently serving as

an Assistant Professor at Maharaja Surajmal Institute of Technology, Delhi. My

research interests include thermal energy storage, phase change materials (PCMs), latent heat storage, and computational fluid dynamics (CFD).

In recognition of my academic contributions and dedication, I have received an Appreciation Letter from Maharaja Surajmal Institute of Technology.